Tampere University

Emmanuel Nana Boadu Aidoo

A COMPARATIVE ANALYSIS OF ELECTRO-HYDROSTATIC ACTUATORS AND A CONVENTIONAL VALVE-CONTROLLED ACTUATOR FOR HEAVY-DUTY MOBILE APPLICATIONS

Master's Thesis
Faculty of Engineering and Natural Sciences
Prof. Tatiana Minav
November 2020

ABSTRACT

Emmanuel N.B. Aidoo: A Comparative Analysis of Electro-Hydrostatic Actuators and a Conventional Valve-Controlled Actuator for Heavy-Duty Mobile Machines
Masters' Thesis
Tampere University
Master in Factory Automation and Robotics
November 2020

Significant throttling losses in valve-controlled hydraulic actuators offer a potential for energy saving and efficiency improvement in heavy-duty mobile machines. Coupled with the stringent regulations on emissions, industry and the research community are faced with the challenge to introduce energy efficient systems while maintaining cost savings. Pump-controlled hydraulic actuators have been proposed as a solution to reducing emissions and improving energy efficiency of heavy-duty mobile machines.

The electro-hydrostatic actuator system, a variant of pump control, has been studied in this thesis to analyse its motion performance and energy efficiency. Two different concepts of the electro-hydrostatic actuator system: single-pump and two-pump, have been studied and placed side-by-side against a conventional valve-controlled actuator system for comparison.

The three actuator systems were implemented based on the parameters of a mobile boom crane experimental rig with certain modifications. The systems were then modelled and simulated in Simcenter AMESIM. A closed-loop control of a 3-phase permanent magnet synchronous motor was also modelled in AMESIM as an electric drive to the hydraulic setup.

It was found that, all three systems attained satisfactory motion performance with minimal position tracking errors. The pressure dynamics in the valve-controlled and single-pump electro-hydrostatic systems experienced high spikes and oscillations due to the asymmetry of the differential cylinder. In contrast, the pressure spikes and oscillations were significantly reduced by the introduction of the secondary pump in the two-pump electro-hydrostatic system.

Energy efficiency analyses of the three systems showed an improved efficiency in both electro-hydrostatic actuators compared to their valve-controlled counterpart. The results also demonstrated that the prime mover can be significantly downsized in the case of the electro-hydrostatic actuators, leading to remarkable cost savings since their total energy consumption over the test working cycle was about three times less. The two electro-hydrostatic systems also showed a potential for energy regeneration during the lowering of the load, thus greatly reducing the total energy consumption and the installed prime mover capacity.

Keywords: Linear hydraulic actuator, valve-controlled actuator, pump-controlled actuator, electro-hydrostatic actuator, direct-driven hydraulics, differential cylinder, modelling and simulation, energy efficiency, mobile machines

PREFACE

In agreement with the saying, “great things are not done by impulse, but by a series of small things brought together”, this work has been the culmination of many years of studies and effort. Alone, I could only have done little, and I would express my profound gratitude to all those who have helped me in diverse ways till this point.

This research was carried out using the resources of the Innovative Hydraulics and Automation (IHA) research unit of Tampere University. As such, my heartfelt gratitude goes to Professor Tatiana Minav for giving me the opportunity to join this group and for the supervision and advice on getting this work done. I quite remember her words “you don’t need to know about hydraulics before you start, you can always learn”. I have learnt a great deal from this experience considering I had no background knowledge before I ventured this research.

I would also like to specially thank Dr. Xu Han, for the help granted as a thesis advisor, and David Fassbender for his invaluable comments on this work. Thanks to all members of the IHA team for the various forms of support, feedback and knowledge acquired from our meetings and presentations. It was a privilege to share an office with some of you, and others, meeting you online. Under different circumstances, I believe we would have had a great time in the office together, but unfortunately, the COVID-19 pandemic had a different plan for us.

Finally, I would not have gotten this far in my life without my family. I am highly indebted to my mothers, yes mothers – Anna and Hanna, and also to my brothers and sister for their relentless support and love. There are not enough words to express my appreciation for them, so this work is dedicated to my family, I love you all.

Tampere, 26 November 2020

Emmanuel Nana Boadu Aidoo

CONTENTS

LIST OF FIGURES

LIST OF SYMBOLS AND ABBREVIATIONS

AEA	All-electric aircraft
CO_2	Carbon dioxide
DDH	Direct-driven hydraulic
EHA	Electro-hydrostatic actuator
EMA	Electromechanical actuator
FOC	Field-oriented control
ICE	Internal combustion engine
HDMM	Heavy-duty mobile machine
LS	Load sensing
MEA	More electric aircraft
MOS	Metering out system
NRMM	Non-road mobile machine
PMSM	Permanent magnet synchronous motor
A_o	Orifice cross-sectional area
A_1	Piston-side chamber area
A_2	Rod-side chamber area
C_f	Flow coefficient
D_1	Displacement of main pump
D_2	Displacement of secondary pump
d_h	Hydraulic diameter
d_p	Piston diameter
d_r	Rod diameter
$e(t)$	Error signal
E	Energy
E_{in}	Input energy
E_{out}	Output energy
F	Force
F_L	Load force
F_{max}	Maximum force
I	Current
i_d	Motor d-axis current
i_q	Motor q-axis current
i_s	Motor stator current
J	Inertia
K_p	Proportional gain
L_d	Motor d-axis inductance
L_q	Motor q-axis inductance
p	Pole pairs of motor
p_L	Load pressure
p_{max}	Maximum pressure
P	Power
P_{cyl}	Cylinder power
P_{elec}	Electrical power
P_h	Hydraulic power of pump
P_{mech}	Mechanical power
Q	Flow rate
Q_{max}	Maximum flow rate
R_A	Cylinder chamber area ratio
R_e	Reynold's number

R_s	Motor stator resistance
T_d	Derivative time constant
T_e	Electromagnetic torque of motor
T_i	Integrator time constant
T_L	Load torque
$u(t)$	Control signal
v	Fluid kinematic viscosity
v_f	Flow speed
v_{max}	Piston velocity
v_p	Piston velocity
V	Voltage
η	Efficiency
φ	Motor magnetic flux linkage
ρ	Fluid density
τ_p	Pump shaft torque
ω	Rotational speed

1. INTRODUCTION

Hydraulic systems have been widely deployed in many applications, be it stationary (example: in production, lift, military, amusement applications), or mobile (example: in construction, aerospace, automobile, agriculture industry). They rely on fluids to generate, transmit and control power demanded by the application needs. Hydraulic actuators are common for generating linear movements and have become a mainstay since their practical applications appeared on the market in the early 1900s. Their continuance in practical applications have partly been a result of their ruggedness, relative ease of speed and position control and their ability to provide compact systems with high power density [1].

Hydraulic actuation has been heavily deployed in construction, mining and agricultural machines, otherwise referred collectively in this thesis as heavy-duty mobile machines (HDMM). Over the years, the architecture of hydraulic actuation systems has undergone changes and improvements due to the constant work of the research community to improve system dynamics, efficiency and performance. The high demand for technology in hydraulic applications can be attributed to the large production numbers of these machines and a competitive market. In HDMM applications, where space is a limiting factor, hydraulic drives are expected to be compact and yet, powerful to be resilient to varying loads.

The most common and technology-matured hydraulic actuation system used in HDMM applications is the valve-controlled actuator system. This conventional concept involves hydraulic consumer units (hydraulic cylinders, hydraulic motors, etc.) driven by pumps which are supplied by a prime mover – most commonly a diesel-powered internal combustion engine (ICE) (**Figure 1.1**). High power consumption, high energy losses and low efficiency associated with this conventional system, due to throttling losses in hydraulic components, have led to electric-powered solutions. The incentive of cost savings and increasingly strict environmental emission policies also heighten the need for electric-powered solutions.

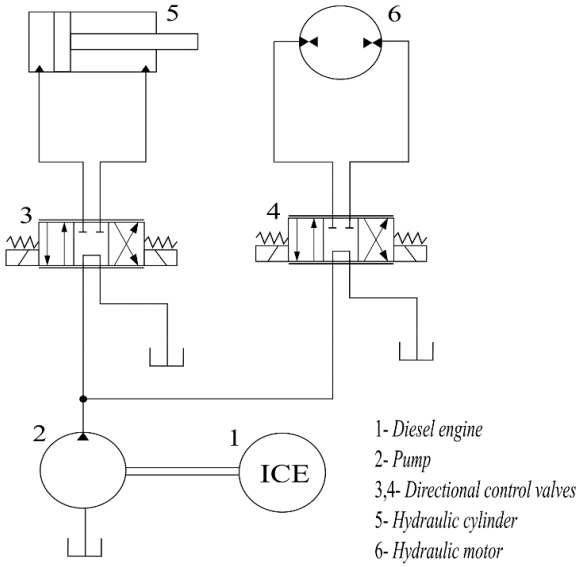

Figure 1.1: *Schematic of a conventional valve-controlled hydraulic actuator*

Electric-powered solutions involve a replacement of the conventional diesel-powered ICE with a high-efficiency electric machine to drive the pump (**Figure 1.2**). The absence of diesel tank and exhaust system (ICE-related system) in electric-powered HDMMs contributes to optimal use of limited space. This results in a more efficient and compact system, compared to the ICE-driven system, without having to compensate for the classic counterweight since the weight of the batteries make up for the counterweight. [1]

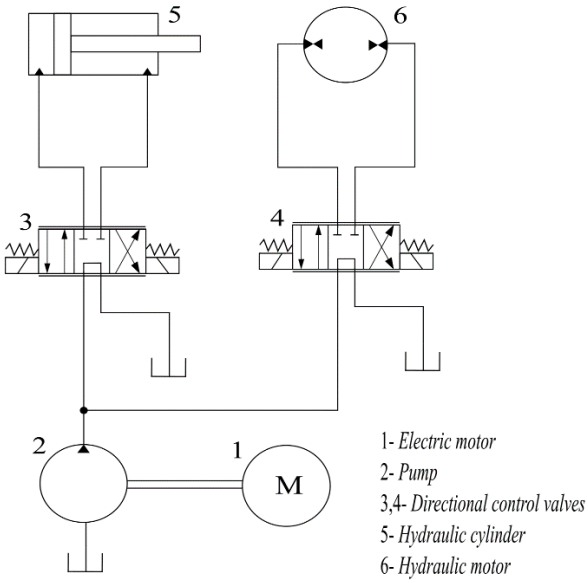

Figure 1.2: *Schematic of a valve-controlled system with electric drive*

Further from these valve-controlled systems, progressive research seeks to find improved solutions and more efficient systems by reducing or eliminating the high throttling

losses in valve-controlled systems. Throttling losses offer a potential for energy savings, dependent on finding solutions that can regenerate energy from these losses. Researchers have proposed pump-controlled actuation systems as a remedy to the problems faced with valve-controlled actuators. With the aerospace industry leading the way in actuation systems research, the motivation of emission reduction and cost savings introduced the development and implementation of electro-hydrostatic actuators (EHA), a form of pump-controlled actuator, for practical applications in aircrafts with the benefits of flexible speed control, weight and noise reduction [2], [3]. EHA solution is a compact system that delivers the advantages of the conventional valve-controlled hydraulic actuator, whiles improving energy efficiency significantly by providing power on demand.

An electro-hydrostatic actuator system is defined by Caliskan et al. as an 'integrated electric and hydraulic system where a bi-directional pump, directly driven by an electric motor, is connected to the two chambers of a hydraulic cylinder' (**Figure 1.3**) [4].

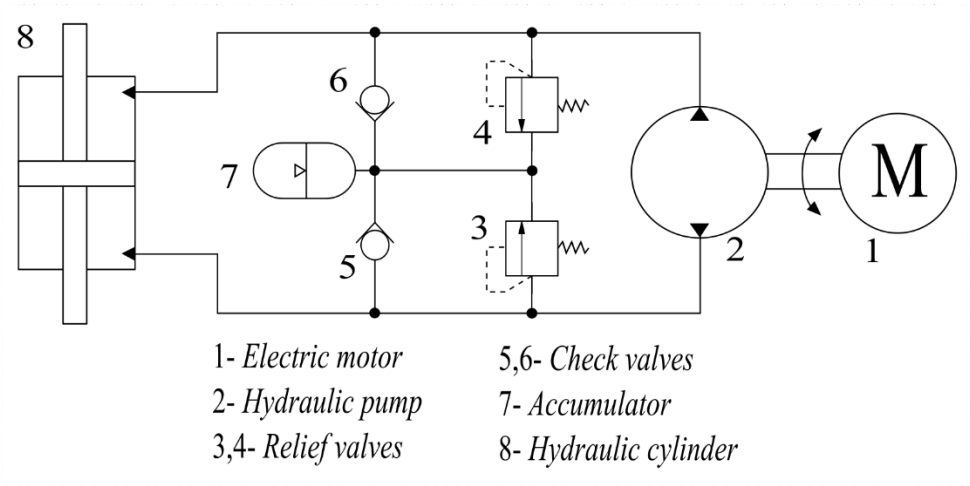

Figure 1.3: *Schematic of an electro-hydrostatic actuator*

The notable absence of the proportional directional control valve in **Figure 1.3** sets the premise for improved efficiency since the throttling losses associated with the valve component is eliminated. On this ground, the research community has channeled much attention to EHA with regards to safety, performance and market-readiness toward the anticipated implementation of this technology in HDMMs. The aim of this thesis, therefore, is to assess and compare the performance and efficiency of the electro-hydrostatic actuator against the conventional valve-controlled actuator.

It is also worthy of note, that in the bid to drastically diminish or even fully eliminate environmental footprint of system emissions, research is leaning toward a future oil-less actuation system. Electromechanical actuators (EMA) have been touted as a potential technology toward a zero-emission future. Developments in the aerospace industry,

which birthed the “More Electric Aircraft (MEA)” concept, attempts to meet expectations of safety, cost reduction and reduced environmental footprint by replacing mechanical, hydraulic and pneumatic systems with electrical systems. This gradual transition involves the research and practical integration of EHA and EMA into aircraft systems, toward an ultimate future goal of All Electric Aircraft (AEA). [2]

With regards to EMA applications in HDMM, electromechanical linear actuators have been incorporated into a compact excavator prototype (EX02) built by Volvo Construction Equipment as a research project [5]. So far, EMA technology has been used for low-power and low-force applications in aircraft. Their lighter weight improves fuel economy and aerodynamics, thus making them appealing for applications in the aerospace industry. Commercially, EMA has been applied in aircrafts for landing gear doors and secondary flight control surfaces. The aim is to gradually adopt EMA technology for large actuation application when they are considered to be highly safe and reliable after thorough research. [6], [7]

As governments and standards push for greener solutions, it is only a matter of time before EMAs become the predominant actuation technology. However, this thesis focuses only on the hydraulic actuation systems briefly explored in this introduction since it is currently the most-demanded technology due to its advantages and technical maturity, making them suitable for applications in HDMM. Until EMA technology is developed to match the power density of hydraulic systems, it remains years behind to being implemented for high-power HDMM applications and shall therefore not be considered in this work.

1.1 Comparison of Actuators

In light of enhancing system efficiency, conventional valve-controlled actuators have been replaced by electro-mechanical actuators especially for low-power applications [3], [8], [9]. Proposals to replace conventional actuators and EMAs with EHAs postulate that, EHAs have the ability to overcome the limitations of the EMA whiles maintaining the advantages of conventional hydraulic actuation [8], [9]. This section probes the advantages and disadvantages of commercially applied actuation systems and current focus of research into actuation systems from literature review. A comparison is drawn among the three actuation system and summarized in **Table 1.1**. This comparison sets forth the emphasis of this thesis which shall be defined in the following section **1.2**.

Table 1.1: *Comparison of different actuation systems* [1]–[4], [10]–[13]

	Electro-hydrostatic Actuators	**Electromechanical Actuators**	**Valve-controlled Actuators**
Advantages	Provide high power in compact size	Offer better positioning precision	High power density
	High force/torque	High speed dynamics	High force/torque
	Flexible layout and reduced hydraulic tubing	Simplified assembly	Rugged design
	Moderate noise and vibrations	Reduction in CO_2 and noise emissions	Higher payload capacity
	Reliable and requires less maintenance	Very low maintenance costs	Matured technology and reliable
	Higher energy efficiency than conventional hydraulic actuators	Significantly improved system efficiency	
		Fuel economy/savings	
	Electro-hydrostatic Actuators	**Electromechanical Actuators**	**Valve-controlled Actuators**
Disadvantages	Short cycle oil circuit leading to temperature rise	Restricted to low-power and low-force applications	Complex systems/ incorporates many components
	Limited heat radiating area	Huge reflected inertia to load	Requires extensive maintenance of wearing parts and seals
	Safety regarding flammable hydraulic fluids	Unreliable because they are susceptible to jamming and free-run faults	Safety regarding flammable hydraulic fluids, high temperatures and pressure
		Safety and criteria not fully evaluated	

1.2 Scope

Researchers have proposed pump-controlled systems to replace the inefficient conventional valve-controlled actuator in HDMMs industry. Due to the unmatched power densities of hydraulic actuators, they are still preferred over electro-mechanical actuators for many applications and as such this thesis focuses on hydraulic actuation.

For that matter, two different concepts of the EHA system were selected to be compared against conventional valve-controlled actuators in this thesis: single-pump EHA and two-pump EHA systems, which utilize pilot-operated check valves and secondary pump, respectively, for flow balancing. For a clear distinction between the two different EHA configurations in this thesis, the single-pump EHA shall henceforth be often referred to as classic EHA.

The aim of this thesis, therefore, is to investigate and compare the motion performance and energy efficiency of three hydraulic actuator solutions for applications in mobile machines: the conventional valve-controlled actuator, classic EHA and two-pump EHA systems. To achieve the goal of this thesis, the actuator systems are modelled and simulated in Simcenter AMESIM. The simulated models were implemented for a mobile crane application and the results were compared in terms of motion performance and energy efficiency.

With reference to motion performance, the employed control strategy was not designed to achieve position precision but rather, maintaining the actuator positions within tolerable limits was considered acceptable to assess the pressure dynamics.

1.3 Outline

The outline of this thesis is as follows:

Chapter 2 considers recent developments and state-of-the-art research in the field of HDMMs.

The three system architectures selected and presented in this thesis are discussed in Chapter 3. A further overview of the concepts is addressed in chapter 3.

The simulation models for the three actuator systems are developed in Simcenter AMESIM and discussed in chapter 4. The component selection process is explained, and the model validation is presented in the same chapter.

Chapter 5 discusses the motion performance and energy efficiency results from the simulations and conclusions and further work are presented in chapter 6.

2. STATE OF THE ART REVIEW

As stricter policies concerning CO_2 emissions are being imposed and the rising need for industries to stay ahead of the market, the research community and industry have geared their efforts towards the direction of finding more efficient and sustainable solutions. With regards to innovative actuation methods, the aircraft industry leads the state-of-the-art research. Several tests with electro-hydrostatic actuators have been performed and implemented in aircrafts proving this method as feasible and matured [2], [3], [8], [10]. It is intuitive to draw inspiration from the aircraft industry to apply these new technologies to heavy-duty machinery in order to reap the benefits of such technologies. Currently, electro-hydrostatic actuators have been proposed by the research community to succeed conventional valve-controlled hydraulic actuation systems in control equipment and machinery. The next section 2.1 discusses state of the art valve-controlled actuation methods.

2.1 Valve-Controlled Hydraulic Actuator

The ongoing paradigm of valve-controlled hydraulics actuators involves a replacement of diesel drives by electric power drives, usually consisting of battery-powered electric motor drives. The transition adds many advantages to conventional hydraulic systems and improves the efficiency. Moreover, there is the added advantage of reduced noise and emissions, which is necessary as emission regulations become stricter.

Lodewyks et al. [1] points out the faster response of electric motor, significant energy savings due to better efficiency of electric motor, increased system operation time and energy regeneration possibilities by replacing the diesel engine of an excavator with a frequency-controlled electric motor. These advantages were achieved without the need to optimize the hydraulic system. The energy flow diagram and average power of an excavator boom cylinder (**Figure 2.1**) highlights the benefits of replacing the diesel engine with an electric drive – without considering the possibility of energy regeneration.

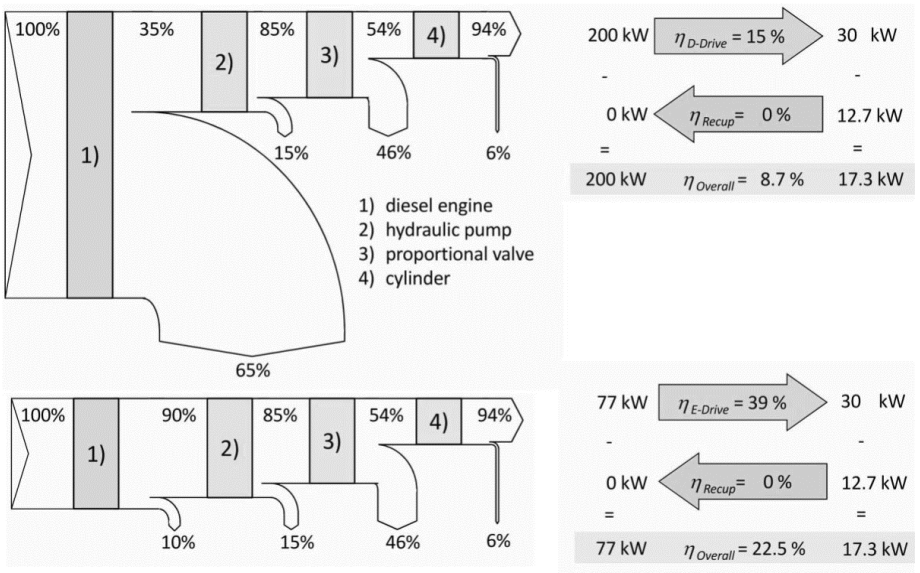

Figure 2.1 *Comparing efficiencies of diesel-driven and electric-driven valve-controlled hydraulic system* [1]

However, diesel engines are still much in use due to low prices of fuel and high cost of fully electric hydraulic machines [14]–[16]. Efforts have been made to improve the ICE-driven hydraulic system by regenerating energy from the return flow. A hydraulic oil regeneration system that retrieves the potential energy, from lowering the boom of an excavator, and kinetic energy of the swing was proposed in a patent application submitted by Imura et al. [17]. The recovered energy is used effectively to drive a second hydraulic pump for the purpose of supplementing energy from the main hydraulic pump. The driving power from the prime mover is reduced, thus reducing overall fuel consumption of the excavator.

Besides the efficiency improvement observed by changing the diesel engine prime mover to an electric motor, huge throttling losses render the valve-controlled concept inefficient. To address this challenge, researchers propose various solutions and architectures of the conventional concept. The selected architecture of the hydraulic system can affect the energy efficiency. For improved system performance and guaranteed pressure drop characteristics with varying loads, some architectures proposed by researchers incorporate additional components with special properties and integrated control. These components are commercial and used in many industrial applications. For instance, a benchmark valve-controlled actuator setup used by Hagen et al. applies a state-of-the-art pressure-compensated, proportional directional control valve for the cylinder motion [9].

Another contribution to the inefficiency of conventional hydraulic actuators is the amount of power wasted under low loads since the system is sized according to the maximum

load. The common solution for this problem, widely applied in mobile machines, is the load sensing (LS) technique which consists of a fixed/variable displacement load sensing unit, load sensing directional valve and compensator block [18]. This technique involves the adjustment of pump pressure and flow rate to meet the demands of the consumer load pressure, avoiding excess flow from the pump. However, load sensing systems become very inefficient for varying load conditions and an increased number of actuators subjected to different loads. This is because the system supplies power according to the maximum load requirement and thus there is huge pressure drop across the valves supplying lower loads. Consequently, there is high cumulative energy losses and heat generated across the valves.

To address the common disadvantages of the traditional LS in valve-controlled actuators, researchers have developed systems with multi pressure networks (or rails), where pressure levels are adapted to the load requirements. Huova et al introduced a concept which involves feeding the cylinder chambers from different pressure sources, each having a unique pressure level, via on-off valves [19]. Even though their results showed increased power losses, a practical number of different pressure sources could reduce losses by 73% compared to a load sensing proportional valve.

Another recent introduction to mobile machines is the meter out sensing (MOS) system for flow rate regulation and overrunning load control by adjusting the pressure drop of a meter-out valve. This system is capable of compensating pressure differences in multiple-actuator systems and keeping a constant pressure for overrunning loads. The advantages of this system over the LS technique is better energy management, energy savings due to regeneration and control of overrunning loads. [18]

Finally, digital hydraulic technology presents a way out by reducing most of the throttling losses due to the complete opening of the valve by switching control mode. Efficiency is improved by realizing intelligent hydraulic energy supply using digital hydraulic technology. Unfortunately, current application of high-speed switching hydraulic technology is limited by noise and durability of high frequency components. The increased number of components and substantial increase in size and cost limits the practical application of parallel digital hydraulic technology. Overall, the different categories of digital hydraulics, namely high-speed switching, parallel and stepping digital hydraulic technologies, require complex control strategies in their applications. [20]

2.2 Electro-hydrostatic Actuators

Electro-hydrostatic actuators (EHA) have exploited the advantages of both electrical and hydraulic systems and have been widely used in various industrial and commercial applications. Their applications are very common in the aircraft industry [2], [3] and proposed by researchers as successors to conventional valve-controlled actuators, which are currently used for mobile machine applications [8], [10], [18]. To realize this, EHA systems need to have comparable or even possess better characteristics than the conventional systems in terms of applicability, reliability, durability and safety. Electro-hydrostatic actuators have been shown by research to enhance energy efficiency of hydraulic systems, whiles maintaining the high-power density of conventional hydraulics, albeit in compact systems [8], [9].

Furthermore, the research community has focused efforts on developing pump-controlled system architectures that maximize the advantages of conventional valve-controlled systems for varied applications. Many concepts and topologies have been proposed, with emphasis on compensating the asymmetrical flow observed in differential cylinders [21]. This type of cylinder is preferred for applications in mobile hydraulic systems because of their high output force density and compact size for optimized installation space [9], [22], [23]. About 80% of electro-hydraulic actuator systems adopt the differential cylinder for its force and size advantage [10].

With regards to differential cylinders, various EHA solutions seek to compensate flow imbalance associated with this type of cylinders, which causes undesired pressure instabilities and occasional cavitation in the cylinder chambers [4], [14], [21]. These imbalanced flow compensation methods include using a secondary pump system [21], [24], hydraulic transformer [25], 3-port axial piston pump system [22], and valve solutions. Under the valve solutions, some researchers have proposed using pilot-operated check valves [26] and shuttle valves [4], to compensate the flow imbalances. Another solution proposed by Schmidt et al. is the redesign of the secondary pump system by introducing a third gear pump to compensate flow in one direction of motion [14].

On the other hand, different topologies have been realized depending on different combinations of components: for example, the type of displacement unit, prime mover or compensation methods employed [8]. Efficient systems based on variable displacement units, which can adjust fluid flow to load pressure requirements, have been realized. But on the downside, variable displacement units tend to increase system cost and complex-

ity [21]. For that matter, research has turned to studying systems based on fixed displacement units [14]. There is no straightforward comparison that can be made for different topologies as each topology is optimized for specific applications.

The energy efficiency of EHAs are further improved by their energy regeneration capabilities. Lowering of lifting systems and braking action of rotary actuators in HDMMs offer potential and kinetic energy, respectively, which could be recuperated and reused in the system. Open-circuit energy recovery systems have been researched adequately, but their inherent losses due to throttling in employed valves require in-depth research of closed-circuit recover systems to optimize energy recovery, especially for differential cylinder systems [10].

Even though many advantages have been realized with pump-controlled systems over valve-controlled systems, pump-controlled systems are associated with non-linearities and system uncertainties which demand robust and flexible control methods [10], [27]. [11] reports that energy efficiency and position accuracy of EHAs are affected by the control design and improvements can be achieved depending on the selected control strategy. Research efforts have turned to finding and implementing advanced control structures to enhance controllability and achieve a good balance between efficiency and performance of EHAs. [10]

Another notable trend in electro-hydrostatic system architecture in HDMMs is the decentralization of the system which involves distributing EHA systems throughout the HDMM system. This approach implies that hydraulic power source is readily available at different zones in the system to provide power-on-demand, acquiring the term zonal hydraulics. The advantages of this zonal architecture include reduced hydraulic tubing, ease of integration and simplified structure by eliminating valves and fixtures. However, the limitation to this zonal system is the increased number of electric component to be fitted in a compact HDMM. [13]

A notable advantage of the EHA system quoted by researchers is the reduced hydraulic tubing. With this comes the challenge of short cycle oil circuit, leading to temperature rise in the system. Thermal analyses conducted on a thermo-electro-hydraulic model of DDH operating continuously in [28] predicted heat dissipation was largely concentrated in the electrical motor. Heat generation in hydraulic systems is attributed to power losses and heat transfer in the hydraulic components is by means of the hydraulic oil. Temperature affects the operating performance, safety and service life of the actuator. Furthermore, the effects of heat distribution on the oil and the system is critical to the safe and

reliable operation and as such, necessitate a thorough study of the thermal behaviour of EHAs. [28], [29]

Recent EHA research adopt pressurized hydraulic accumulators in place of conventional oil tanks to enhance compactness [1], [4], [9], [13], [30]. Lodewyks in [1] reports a 10% increase in energy efficiency, 5% initial cost savings and power regeneration capabilities with an a hydraulic accumulator. According to [30], the implementation of a hydraulic accumulator in a direct driven hydraulic (DDH) system improved the efficiency by 30%. Notwithstanding, these architectures utilizing hydraulic accumulators result in increased oil temperatures, emphasizing the need for further thermal analysis to address the thermal issues [8].

The maturation of EHAs for implementation in HDMMs also requires a thorough analysis of failure modes, fault tolerance and system reliability. As a multi-domain system, EHAs are prone to failures of different components which make diagnosis complex. The common failure modes are related to hydraulic and electric systems due to various factors including harsh environmental conditions, contamination, wearing, excessive loading and electromagnetic noise from control failure modes [31], [32]. According to [31], system redundancy is a costly solution for fault-tolerant HDMMs which are already limited by space. Even though there are no general methods for fault detection, [31] proposed the utilization of sensors, a target component and virtual sensors for condition monitoring and fault detection to prevent costly downtimes of mobile machines.

To ensure the economic feasibility of EHAs, [33] reviews sensorless operation of EHAs especially for position control. This method requires information from system components (motor, pump or cylinder) to estimate position and achieve position control. Implementation of sensorless methods eliminates the application of state-of the-art sensors, thereby reducing system cost. It also enhances system redundancy by applying low-cost sensors. However, research of sensorless control in hydraulic systems and electro-hydraulic systems is limited as compared to the more extensive sensorless control studies available for electrical motors. Further research is required if sensorless control is to be realized in EHAs. [33]

Commercially, implementation of EHAs has been realized in Airbus 380 and A350 as a backup actuator for fail-safe mode [3]. The technology is also adopted on the Lockheed Martin's F-35 lightning II combat aircraft for flight control and for thrust vector control on NASA's 2nd Generation Reusable Launch Vehicle program [34].

As modern research trends in industrialization call for electrification, the next section briefly highlights the steps taken towards the electrification of mobile machines.

2.3 Recent Progress in Electrification of Mobile Machines

The roll-out of fully electric HDMMs remains a technology for the future despite the much-advertised needs and advantages of electrification. Diesel drives are still heavily used currently, partly because diesel fuel is cheaper compared to their electric-motor counterparts. Other factors hindering electrification includes high cost of power electronic components, cost of energy storage systems and compliance with safety standards. [15]

As the world pushes for greener and cleaner systems, industries are expected to rise to the challenge and match that demand by introducing new solutions to the market. Yet, there have been only few fully electric heavy-duty machines which have been commercialized or demonstrated to the market and stakeholders. Case in point, Mecalac has unveiled its fully electric e12 compact excavator with commercial availability anticipated [35]. The Volvo EX02 is also another case of fully electric excavator which has been demonstrated to stakeholders even though the company states that there are no plans for industrialization yet [5]. One more interesting project is Yanmar's eFuzion Concept – an autonomous construction machinery [36]. The eFuzion Concept integrates key technologies like all-electric operations, autonomous driving and robotics and particularly targeted for the future of industry and production.

Even though electrification of HDMM has been a slow development, a more realistic approach and ongoing trend to meet the expectations of improved system energy and fuel efficiency and emission reduction is hybridization. This involves integration of electric drives for assisting power demands and energy regeneration possibilities, enabling downsizing of the ICE [16]. This implies that consumer loads in the system can be supplied by the hydraulic drive, electric drive or both (hybrid), thus increasing flexibility and optimizing energy consumption.

Commercial solutions of hybrid construction machinery have been available over a decade now and they represent a significant share of the global market [37]. The stages of their development on the market over the years are presented in **Figure 2.2**. Hybrid construction machines demonstrate improved fuel efficiency and reduced emissions. Studies are being performed on existing designs to find ways to improve energy storage, fuel efficiency, control strategies, among others. [38], [39]

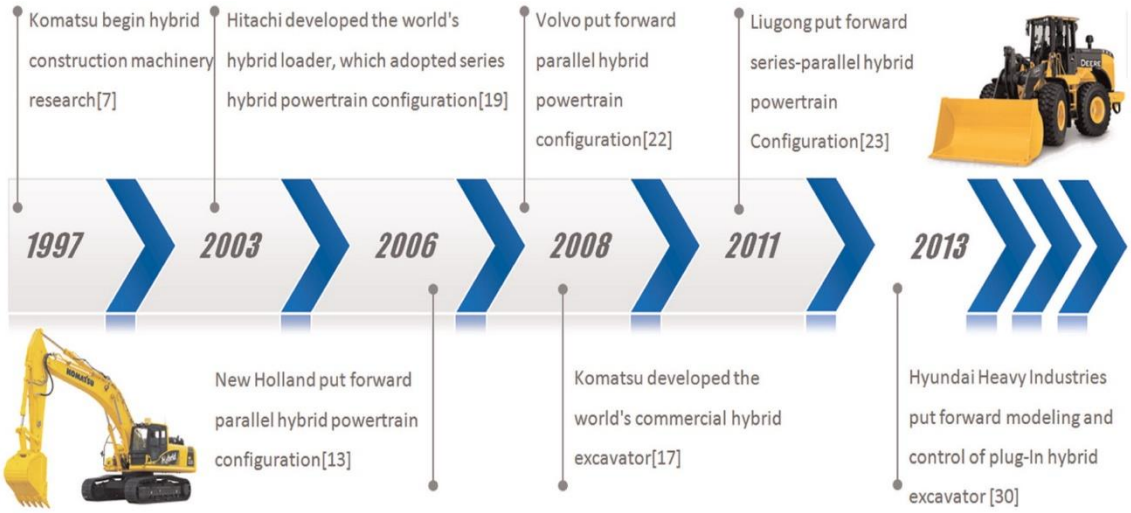

Figure 2.2: *Stages of hybrid construction machines development* [37]

EHA will play a major role in the electrification and hybridization project as they have been shown in the preceding chapter to provide better efficiencies. Also, they can be integrated into electric or hybrid HDMMs since an electric powertrain is available. Even though the practical applications of EHA on the market are limited to prototypes and custom designs [9], the technology is very promising for the future trend of green and sustainable solutions.

3. ARCHITECTURE OF THE PROPOSED SOLUTIONS

The system architectures selected in section **1.2** and simulated in this thesis are presented in this chapter. The referred mobile crane setup is introduced in section **3.1**. The chapter follows with the architecture of the conventional valve-controlled actuator, classic EHA and two-pump EHA presented in sections **3.2**, **3.3** and **3.4**, respectively.

3.1 Study Case

The selected systems are modelled and integrated with a 1.2-ton Masters FC 1100 mobile boom crane test rig studied by Bonato [40] and Järf [41], in their thesis. The test rig, illustrated in **Figure 3.1**, is referred for its practical mobile machine application and for component selection. The setup design utilizes the two-pump electro-hydrostatic actuator configuration and the reader is referred to the referenced theses for a detailed description of the actual test setup. The components selected for the actuator models in this thesis were designed based on the mechanical structure of the boom crane test rig and the components' manufacturers data. There were no practical tests performed with the referred setup and thus, all results reported in this thesis were simulated.

Figure 3.1: *Test setup referred in this thesis*

3.2 Conventional Valve-Controlled Hydraulic Actuator System

Consistent with current state-of-the-art research, the ‘conventional’ valve-controlled hydraulic system model used in this thesis shall be driven by an electric motor, in contrast to the commonly used ICE-driven system. Accordingly, the term ‘conventional valve-controlled system’, used henceforth in this thesis, shall refer to an electric-powered setup for clarity. It is the benchmark for industry, offshore and mobile machine applications. Although the setup considered, demonstrated in ***Figure* 3.2,** does not represent the state-of-art in industrial solutions, the configuration follows a similar pattern void of the industry-standard components. The architecture employs a fixed displacement pump because these units are simple-structured with low-cost, high reliability and require low control complexity [8], [12].

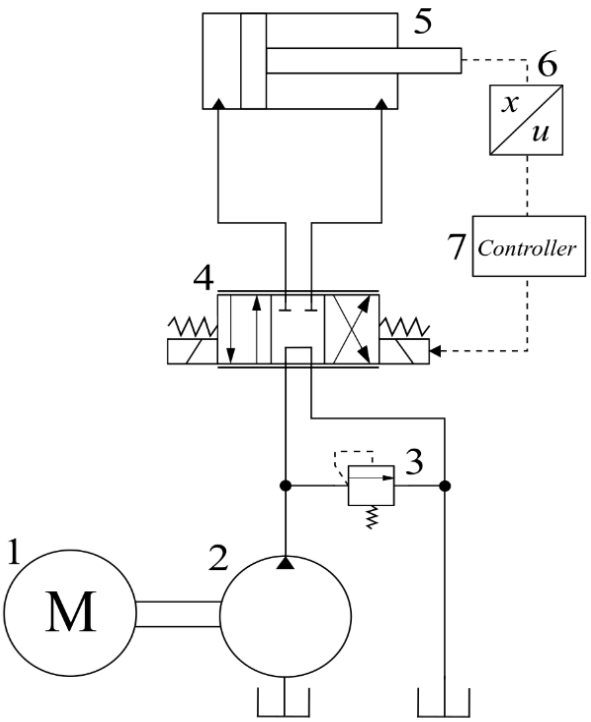

Figure 3.2: *Schematic of valve-controlled hydraulic actuator system simulation model*

The setup constitutes an electric motor (1) running at constant speed to drive the fixed displacement pump (2). Fluid flow to the hydraulic cylinder (5), and thus its motion, is controlled by the 4-way-3-position proportional directional control valve (4). The spool position of the 4/3 proportional valve is electrically controlled by a controller (7) and a control input signal from the position sensor (6). The relief valve (3) is installed for system safety.

3.3 Classic Electro-hydrostatic Actuator System

The single-pump EHA configuration follows the definition of EHAs given in the introduction. The classic EHA is a pump-controlled hydraulic system involving a single reversible fixed displacement hydraulic pump/motor directly connected to the two ports of the cylinder. This configuration allows a closed cycle of fluid flow from the pump's outlet to drive the cylinder (during lifting cycle), with the return fluid from the cylinder going back to the pump through the pump's inlet. The closed-circuit configuration used in this thesis is adapted from a self-contained electro-hydraulic cylinder model used by Hagen et al. [9], illustrated in ***Figure* 3.3**. Hagen's model is further simplified in this thesis to omit some auxiliary hydraulic components, and then modified for simulation in this thesis.

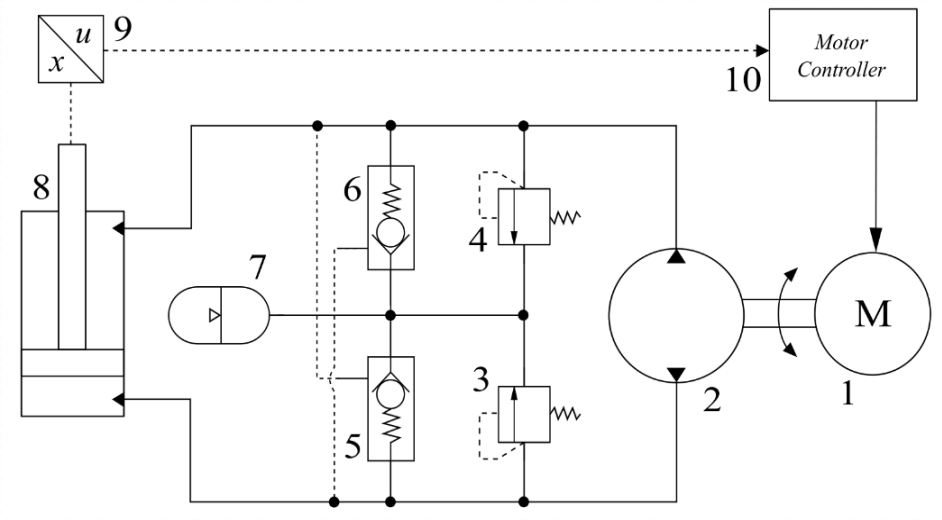

Figure 3.3: *Schematic of classic EHA system simulation model*

The setup consists of an electric motor (1) which drives the hydraulic pump/motor unit (2). The pilot-opertated check valves (5,6) balance the differential flow to the asymmetric cylinder (8). The pilot valves also double as anti-cavitation valves to avoid cavitation in the cylinder. The hydraulic accumulator (7) serves as a sealed reservoir and compliments the flow to the respective cylinder chamber when needed. Relief-valves (3,4) provide safety and prevent over-pressurization of the system. The position sensor (9) and motor controller (10) control the displacement of the cylinder in a closed loop by sending control signal from the sensor to the controller.

3.4 Two-pump Electro-hydrostatic Actuator System

This pump-controlled architecture utilizes two reversible fixed displacement hydraulic pumps to compensate the flow imbalance caused by the cylinder asymmetry. The displacement units are connected to the same shaft of the electric motor, but in opposite directions, and operate as both pump and motor interchangeably, depending on the shaft

rotation direction and the pressure differences. The simulated model for this configuration is inspired by an experimental direct-driven hydraulic (DDH) unit studied in [28], [30], [42]. The experimental setup is modified to develop the model of two-pump EHA system used in this thesis, demonstrated in ***Figure* 3.4**.

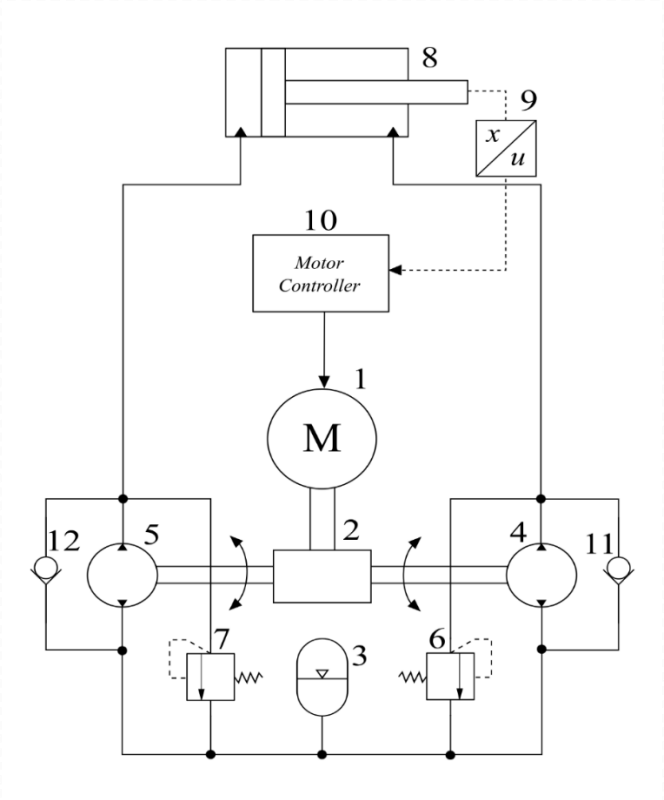

Figure 3.4: *Schematic of two-pump EHA system simulation model*

In ***Figure* 3.4,** the two fixed displacement units (4,5) are confined to the same rotational speed generated by the electric motor (1). They are interconnected by the mechanical gearbox (2) which delivers motion from the electric motor and inverts the direction of one pump depending on the desired displacement of the actuator (8). An anti-cavitation system, represented by check valves (11,12) was adopted and modified from a model designed in [14] to avoid cavitation and ensure continuous flow of fluid in the pumps. The hydraulic accumulator (3) serves as a reservoir and relief valves (6,7) prevent over-pressurization in the system. The position sensor (9) and motor controller (10) are implemented as a closed-loop control of the actuator.

Having laid out the system configurations, the thesis proceeds to develop the simulation models of these proposed configurations in the succeeding chapter.

4. SIMULATION MODEL

This chapter describes the simulation model developed to examine the motion performance and energy efficiency of the system configurations introduced in chapter 3.

The chapter begins by explaining the selection and parameterization of the simulation model in section **4.1**. Sections **4.2** and **4.3** discuss the mutual characteristics of the system models and control model implementation. The simulated load is given in section **4.4** and section **4.5** presents the complete simulation model as developed in AMESIM for this thesis. Finally, these simulation models are verified in section **4.6**.

4.1 Selection of System Components

This section describes the mathematical deductions conducted for the selection of key components of the hydraulic circuit. These components shall be sized such that the three actuators will have comparable characteristics for the analysis.

This thesis merely refers to the mechanical setup of the boom crane described in section **3.1** and the components' manufacturers selected in building the test rig. The reason for this was to simplify the selection of components from known sources and perform simulations with a practical load that reflect practical conditions. The manufacturers for critical components to be used in this thesis are therefore:

1. Vivoil Oleodinamica for the hydraulic pump manufacturer [43]
2. Emerson Control techniques for the electric motor [44]
3. Pikapaja Oyj for the hydraulic cylinder [45]

For clarity, this thesis is purely a simulation-based investigation and as such, no practical tests were carried out for this thesis.

4.1.1 Hydraulic Cylinder

Bonato in [40] modelled the physical system configuration of the boom crane to determine the total force acting on the hydraulic cylinder due to the lack of technical data on the boom crane. The analysis yielded the required piston force and pressure during static conditions, which were found to be almost constant at *5.44-kN* and *1.92-MPa*, respectively. Knowledge of the piston force and pressure means that the required piston area of the cylinder can be calculated as:

$$A_1 = \frac{F_{max}}{p_{max}}, \quad (4.1)$$

where F_{max} is the maximum force and p_{max} is the maximum pressure. The resulting area is *2.83·10^{-3} m^2*. The area of the piston is related to the piston diameter by the equation:

$$A_1 = \frac{\pi \cdot d_p^2}{4}, \quad (4.2)$$

The piston diameter can then be derived as

$$d_p = \sqrt{\frac{4 \cdot A_1}{\pi}}, \quad (4.3)$$

where A_1 is the piston area, d_p is piston diameter and π is a constant. The piston diameter is computed as *60.03 · 10^{-3} m*. The rod-end area of the cylinder is not equal to piston area of a single-rod cylinder since a part of the piston is occupied by the rod. The rod-end chamber area can be determined by the following equation:

$$A_2 = \frac{\pi}{4}(d_p^2 - d_r^2), \quad (4.4)$$

ISO-6020-2-standard double-acting single-rod hydraulic cylinder manufacturers quote standard piston-end and rod-end chamber area ratio as *1.25:1* [46], [47]. The rod-end area is, therefore, calculated as *2.26 · 10^{-3} m^2*. Hence the rod diameter can be calculated by rearranging Equation (**4.4**) as:

$$d_r = \sqrt{d_p^2 - \frac{4 \cdot A_2}{\pi}}, \quad (4.5)$$

where d_r is the diameter of the rod and d_p is the diameter of the piston. Finally, the rod diameter is calculated as *26.88 · 10^{-3} m*.

The next largest cylinder provided in Pikapaja's cylinder datasheet [45] was selected to correspond to the calculated values for the application since these calculated sizes are not standard commercial sizes. The piston and rod diameters of the selected MIRO cylinder were *0.06 m* and *0.03 m,* respectively, with a stroke of *0.4 m* according to the crane requirements. The manufacturer datasheet is summarized in **APPENDIX A**.

Given the selected cylinder parameters, with a full stroke extension per second of *0.40 m/s*, the required flow to ensure the system extends with this speed is calculated as:

$$Q_{max} = v_{max} \cdot A_1, \quad (4.6)$$

where Q_{max} are v_{max} are required maximum flow rate and piston velocity at full load capacity, respectively. Equation (**4.6**) yields a maximum flow of *67.92 L/min*.

4.1.2 Hydraulic Pump/motor

Knowledge of the required flow rate sets the premise for pump selection. The volumetric displacement of the required pump can be determined with known flow rate and pump rotational speed from the equation:

$$\boldsymbol{D_1 = \frac{Q_{max}}{\omega_{max}}}, \qquad \textbf{(4.7)}$$

where D_1, Q_{max} and ω_{max} are displacement, maximum flow rate and maximum rotational speed of the pump. The selected XV-2M series of hydraulic pump/motor can provide rotational speeds in the range of *2500 rpm* to *3500 rpm* as stated as in the manufacturer's datasheet [43]. With a midpoint rotational speed of *3000 rpm*, the required pump displacement is then evaluated as *22.6 cm^3/rev*. In accordance with the manufacturer's standard specifications, the next largest motor to provide the calculated displacement was found at *22.8 cm^3/rev*. The manufacturer datasheet of the hydraulic pump is provided in **APPENDIX A - I**.

To determine the size of the secondary pump in the two-pump EHA system, the chamber ratio for the double-acting single-rod hydraulic cylinder is first deduced.

From the selected cylinder manufacturer datasheet, the chamber areas can be calculated from Equation (**4.2**). The piston-side and rod-side chamber areas were found to be *$2.83 \cdot 10^{-3}$ m^2* and *$2.12 \cdot 10^{-3}$ m^2*, respectively. The chamber area ratio R_A, is then derived as:

$$\boldsymbol{R_A = \frac{A_2}{A_1} \cong 0,75}, \qquad \textbf{(4.8)}$$

where A_1 and A_2 are piston-side and rod-side chamber areas, respectively.

With the main pump displacement (D_1) determined and selected, the displacement of the secondary pump can be determined to match the ratio of Equation (**4.8**). Hence, the displacement can be deduced as follows:

$$\boldsymbol{D_2 = D_1 \cdot 0.75} \qquad \textbf{(4.9)}$$

The closest XV-2M-series hydraulic pump/motor, provided by the same manufacturer, to the calculated secondary pump displacement is specified in the datasheet at 1*6.8 cm^3/rev* [43]. The technical specifications of the selected secondary pump provided in

the manufacturer datasheet is summarized in **APPENDIX A - I**. A displacement ratio of *0.74* was achieved with the selected pumps.

This assumption was introduced in the simulation model to eliminate pressure spikes caused by pump-cylinder mismatch. The two pumps are driven by a common electric drive interconnected with a gear box. This ensures that the pumps are rotating at the same speed but in different directions for both pumping and motoring modes.

4.1.3 Electric Motor

In order to proceed to the final selection of the required electric motor for the system, the maximum torque allowed on the pump shaft must be known. Torque absorbed by the pump shaft can be calculated as:

$$\boldsymbol{\tau_p = \frac{P_h}{\omega_{max}}}, \qquad \textbf{(4.10)}$$

where τ_p is the pump shaft torque, P_h is hydraulic power delivered by the pump and ω_{max} is the maximum rotational speed of the pump. Furthermore, hydraulic power is calculated by the equation:

$$\boldsymbol{P_h = p_{max} \cdot Q_{max}}, \qquad \textbf{(4.11)}$$

where p_{max} and Q_{max} are maximum pressure of the pump and maximum flow rate. Nevertheless, the torque rating of the selected pump is stated as *30.84-Nm* by the manufacturer.

A Control Techniques Unimotor FM 115U2C was selected to meet the requirements of this design. The selected motor has peak torque of *28.2-Nm* as stated in the manufacturer's datasheet [44]. This peak value is lower than required pump shaft torque. However, this value is acceptable since the hydraulic pump is not expected to run at full shaft torque for continuous periods. Other parameters of the servo motor are listed in **APPENDIX A - I**

The AMESIM PMSM motor model required magnetic flux density for parameterization and simulation in AMESIM. This specification was not stated in the manufacturer datasheet and thus, it is calculated here. The motor electromagnetic torque and magnetic flux linkage are related by the following simplified equation to provide maximum torque per ampere armature current:

$$\boldsymbol{T_e = \frac{3}{2} \cdot p \cdot \varphi_m \cdot i_q}, \qquad \textbf{(4.12)}$$

where T_e is the electromagnetic torque, p is the number of pole pairs in the PMSM machine, φ_m is the magnetic flux linkage between stator and rotor and i_q is the q-axis current. From the manufacturer datasheet, the continuous stall torque and current are provided, hence the flux linkage is calculated by:

$$\boldsymbol{\varphi_m = \frac{2 \cdot T_e}{3 \cdot p \cdot i_q}} \qquad \textbf{(4.13)}$$

Once the component parameters have been determined, the next section briefly discusses the simulation method in AMESIM and model considerations.

4.2 System Modelling of Mutual Characteristics

System models were built using standard blocks from the hydraulics, electrical and signal library of AMESIM. Parameterization of the AMESIM models is carried out based on the determined components' manufacturer datasheets (**APPENDIX A** - I) after the design calculations in section **4.1**.

The simulation model followed the assumptions below:

1. Frictional, heat transfer and leakage losses were neglected except where stated
2. The dynamics of the check valves and hoses were not taken into account
3. Pressure effects on the fluid properties were ignored
4. Effects of temperature have not been considered in the entire model

The final models used to obtain simulation results are presented in section **4.5**.

In this section and section **4.3**, considerations adopted during system modelling are explained. Section **4.2.1** describes the leakage model implemented in the simulation model. The leakage model was implemented to account for the system leakages since ideal standard blocks were selected for modelling.

4.2.1 System Leakages Modelling

To ensure a more practical simulation model, the pump's internal and external leakages were considered together with the cylinder leakages. The leakages were modelled by introducing orifices that allow fluid flow to the hydraulic reference/reservoir (tank or hydraulic accumulator) as a result of pressure difference across the orifice. The flow through the orifice depends on factors such as the speed and kinematic viscosity of the fluid and orifice geometry (cross-sectional area and hydraulic diameter). The nature of

flow can be determined by using the Reynold's number, which relates the factors by the equation:

$$\boldsymbol{R_e = \frac{v_f \cdot d_h}{v}}, \tag{4.14}$$

where R_e is the Reynold's number, v_f is the flow speed, d_h is the hydraulic diameter and v is the fluid kinematic viscosity.

The parameters of the orifice are set such that volumetric flow through the leakage orifices constitute less than *8%* of the total pump flow. The orifice cross-sectional area and flow rate are related by the equation:

$$\boldsymbol{A_o = \frac{Q}{C_f \cdot \sqrt{\frac{2 \cdot \Delta p}{\rho}}}}, \tag{4.15}$$

where A_o is the cross-sectional area of the orifice, Q is the flow rate through the orifice, C_f is the flow coefficient, Δp is the pressure difference across the orifice and ρ is the fluid density. With the area known, the diameter of the circular orifice can be evaluated with Equation (**4.3**).

4.2.2 Dynamic Modelling of PMSM

PMSM is characterized by high power and torque density, high reliability and high efficiency. It has been deployed for industrial applications and EHA systems in aircraft applications because of its advantages [2], [12], [48].

The Permanent Magnet Synchronous Motor (PMSM) employed in the system models is of the salient type, therefore the d- and q- inductances are not equal. The values of d- and q- inductances used in the simulation have been determined experimentally in in-built AMESIM analysis of PMSM models. Modelling is done in the rotor reference frame with the d-axis parallel to the flux linkage produced by the permanent magnets. Inductances and stator flux stay constant in the rotor reference frame. The power is supplied from a DC source.

The speed of the motor is adjusted in a closed-loop control by the vector control/Field-oriented control (FOC) method. This method has been used to attain high performance and fast torque response.

The stator voltage equations of the PMSM are presented as follows:

$$\boldsymbol{u_{sd} = R_s i_d + \frac{d\varphi_d}{dt} - \omega\varphi_q}, \tag{4.16}$$

$$u_{sq} = R_s i_q + \frac{d\varphi_q}{dt} + \omega\varphi_d \quad (4.17)$$

where R_s is the stator resistance, i_s is stator current, φ_s is the stator flux linkage and ω is the rotor electrical angular speed. The flux linkages are related to the inductances as:

$$\varphi_d = L_d i_d + \varphi_{PM}, \quad (4.18)$$

$$\varphi_q = L_q i_q. \quad (4.19)$$

The electrical torque of the motor is then defined as:

$$T_e = \frac{3}{2} \cdot p \cdot (\varphi_d i_q - \varphi_q i_d) = \frac{3}{2} \cdot p \cdot (L_d i_d i_q - L_q i_d i_q + \varphi_{PM} i_q), \quad (4.20)$$

where p is the number of pole pairs of the motor and L_d and L_q are the d-axis and q-axis inductances, respectively.

The PMSM equation of motion can finally be presented as:

$$T_e - T_L = J\frac{d\omega_{mech}}{dt} + B\omega_{mech}, \quad (4.21)$$

where T_L is load torque, J is inertia, B is frictional constant and ω_{mech} is mechanical rotor angular speed.

4.3 Control System Modelling

Two different control strategies implemented for the conventional actuator and EHA are presented in sections **4.3.1** and **4.3.2**. The tuning method employed for the controller is briefly explained in **4.3.3**.

4.3.1 Speed Control of PMSM

A common control strategy based on closed-loop vector control of PMSM using PI controllers was adopted to ensure a fair comparison among the three systems implemented. All three systems were position-controlled, although the controls were applied differently. The common speed control strategy was implemented for the servomotor with rotor velocity feedback (w_r), illustrated in the block diagram of **Figure 4.1**.

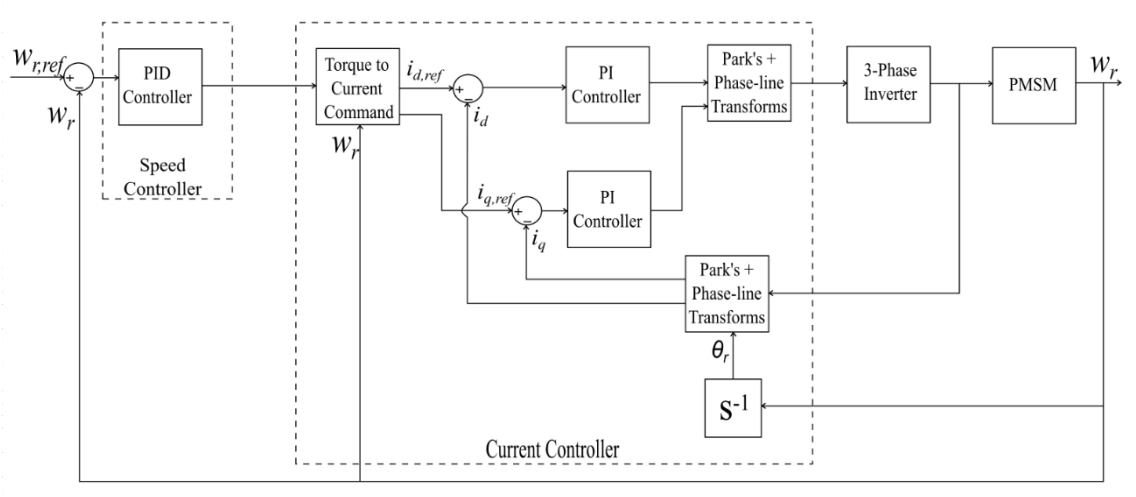

Figure 4.1: *Block diagram model of PMSM speed control*

4.3.2 Position Control of Hydraulic System

For the valve-controlled system, two separate control circuits were implemented to achieve position control of the actuator system. The initial speed control of the servo motor (**Figure 4.1**) was implemented to drive the servo motor at constant speed. The input signal to the speed controller ($w_{r,ref}$) represented the desired rotational speed of the servomotor. A separate piston motion controller, using PID controllers, was implemented to provide reference signal ($x_{c,ref}$) for the desired valve spool opening, and consequently the cylinder piston position. This extra position control loop applied to the electro-hydraulic directional valve is demonstrated in **Figure 4.2**: Block diagram model of valve-controlled system position control.

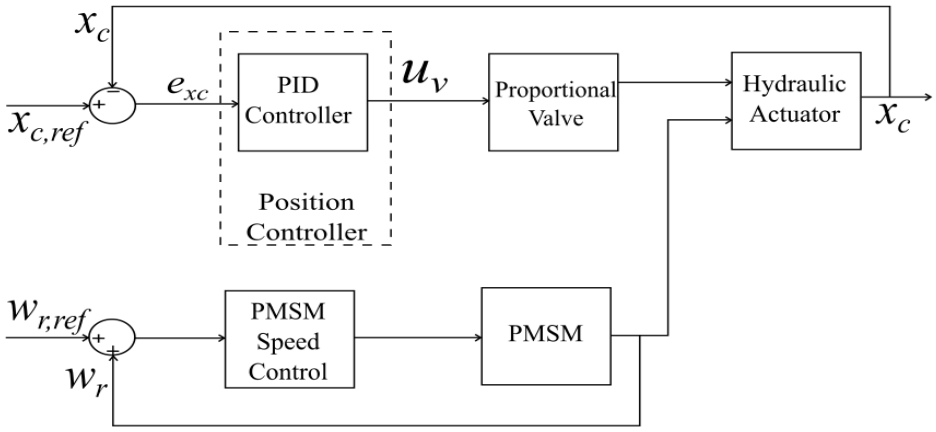

Figure 4.2: *Block diagram model of valve-controlled system position control*

In effect, the valve-controlled system uses two separate reference signals – a speed reference signal ($w_{r,ref}$) applied to servo motor control and a position reference signal ($x_{c,ref}$) applied to the proportional valve.

A slightly different control algorithm was implemented for the EHA systems. In addition to the speed control loop, an outer PID control loop was implemented as position control using feedback from the piston displacement. The block diagram for the control algorithm is demonstrated in **Figure 4.3**: Block diagram model of EHA position control.

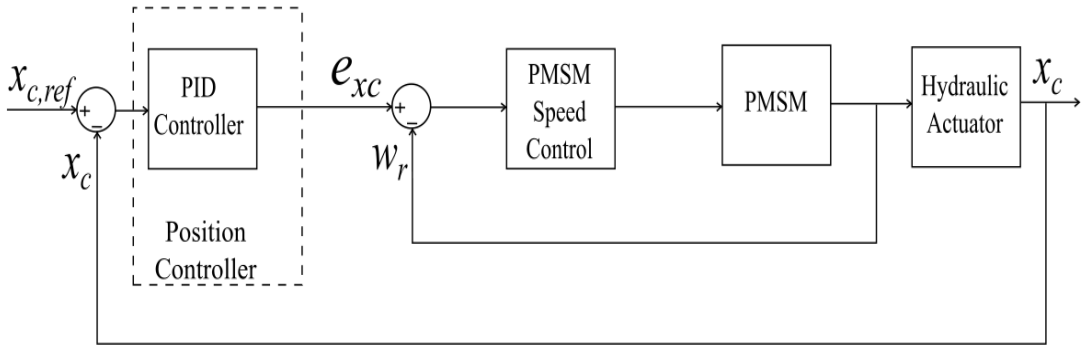

Figure 4.3: *Block diagram model of EHA position control*

In contrast to the control algorithm of the valve-controlled system, one reference signal ($x_{c,ref}$) to the control was used in the EHA system, representing the desired piston position. The summation of the reference signal and position feedback signal (e_{xc}) sets the parameters for the speed control loop.

The implementation of the control model in AMESIM is shown in **APPENDIX B**.

4.3.3 Controller Tuning

The method employed for tuning the PID controllers was the Ziegler-Nichols' heuristic method. This method is not optimal for achieving accuracy but it provides a satisfactory performance for ensuring minimum rise time, overshoot and settling time [49]–[51].

The controller output is established by the equation:

$$\boldsymbol{u(t) = K_p \left(e(t) + \frac{1}{T_i} \int_0^t e(t)\, dt + T_d \frac{de(t)}{dt} \right)}, \qquad \textbf{(4.22)}$$

where $u(t)$ and $e(t)$ are the control and error signals of the controller, respectively. K_p is the proportional gain, T_i is the integrator time constant and T_d is the derivative time constant.

4.4 Payload Simulation

For the load representation, the model uses a constant force and variable mass. The constant force component of the load represents the boom force, which was analyzed by Bonato [40] and determined to have an average value of *5440-N*.

With the positive force applied to the actuator, the boom crane application presented here only operates in two-quadrants. **Figure 4.4**: Four-quadrant operation of hydraulic actuators (with two-quadrant operation of boom crane highlighted) demonstrates a four-quadrant operation of hydraulic actuators with the two-quadrants operation of the boom crane highlighted. These two highlighted quadrants shall be the main focus of this thesis for analysis. The load (F_L) is resistive during extension (Q_1) of the cylinder, and assistive during retraction (Q_2). For this reason, the piston-side chamber of the cylinder is always subjected to a high pressure (represented by the thicker lines in **Figure 4.4**: Four-quadrant operation of hydraulic actuators (with two-quadrant operation of boom crane highlighted)). The rod-side on the other hand, is connected to the low-pressure hydraulic accumulator, which is required to supply the differential to the rod-side chamber during extension.

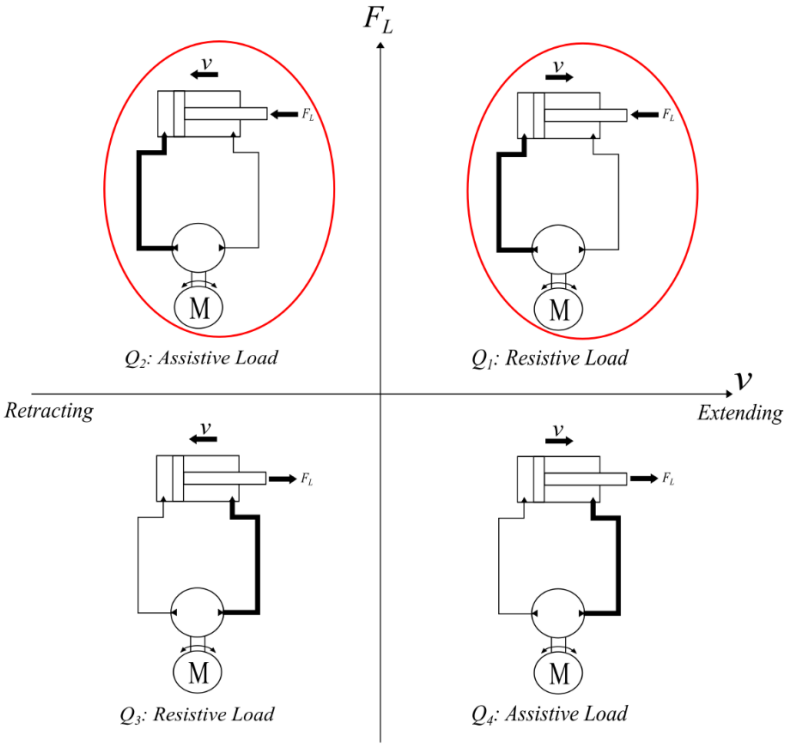

Figure 4.4: *Four-quadrant operation of hydraulic actuators (with two-quadrant operation of boom crane highlighted)*

The maximum load requirement of the Master FC boom crane is given by the manufacturer as *1100 kg* at the shortest boom extension position. The fully extended boom position has a maximum load specification of *300 kg* and this value at full extension of boom is adopted for simulations in this thesis.

4.5 Complete System Models Realized in AMESIM

The overall models of the three proposed configurations can be established based on the component sizing and modelling results. The multidisciplinary coupling of the system components can be illustrated in **Figure 4.5**. The overall models and parameters are presented in **APPENDIX B** - I and **APPENDIX C** - I, respectively. Following sections **4.5.1**, **4.5.2** and **4.5.3** will demonstrate the system models built in AMESIM.

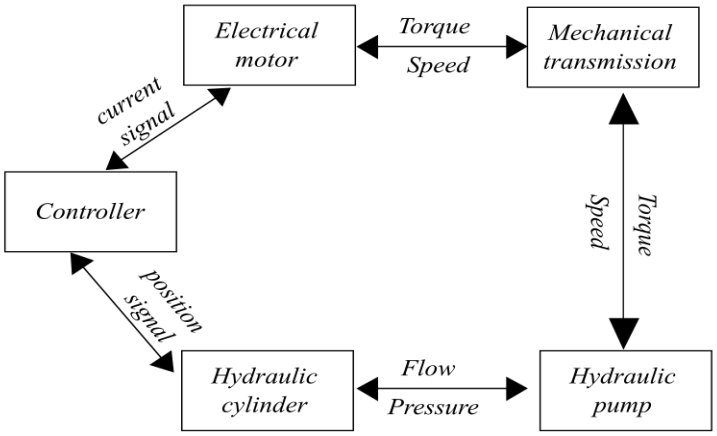

Figure 4.5: *Multidisciplinary coupling of actuator system*

4.5.1 Valve-controlled Actuator System Model

The model architecture of the valve-controlled configuration is illustrated in **Figure 4.6**. The orifices represent the internal leakage caused by fluid flow from the pressurized side to the low-pressure side of the pump as a result of gaps/clearances in the pump assembly, and the external leakage. The pump is modelled with an ideal fixed displacement pump since flow is required in only one direction from the pump

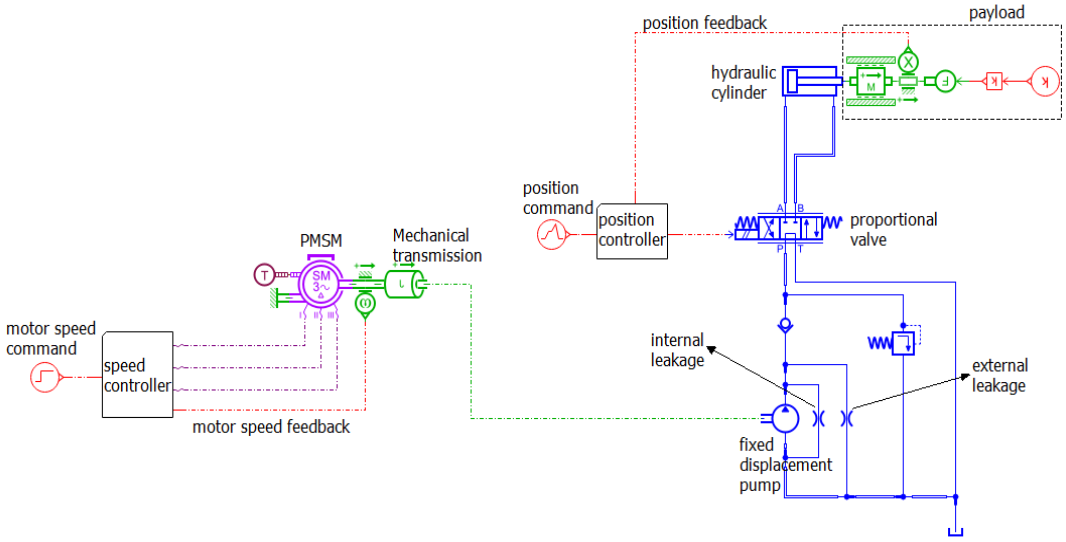

Figure 4.6: *Valve-controlled system model*

4.5.2 Classic EHA System Model

The internal and external leakages are included in the EHA systems as was the case of the conventional system. The two external leakage orifices take into account the pumping and motoring modes of the fixed displacement motor/pump. The ideal hydraulic motor/pump was required in the model for its reversible operation for extension and retraction of the cylinder. The system model is represented in **Figure 4.7**.

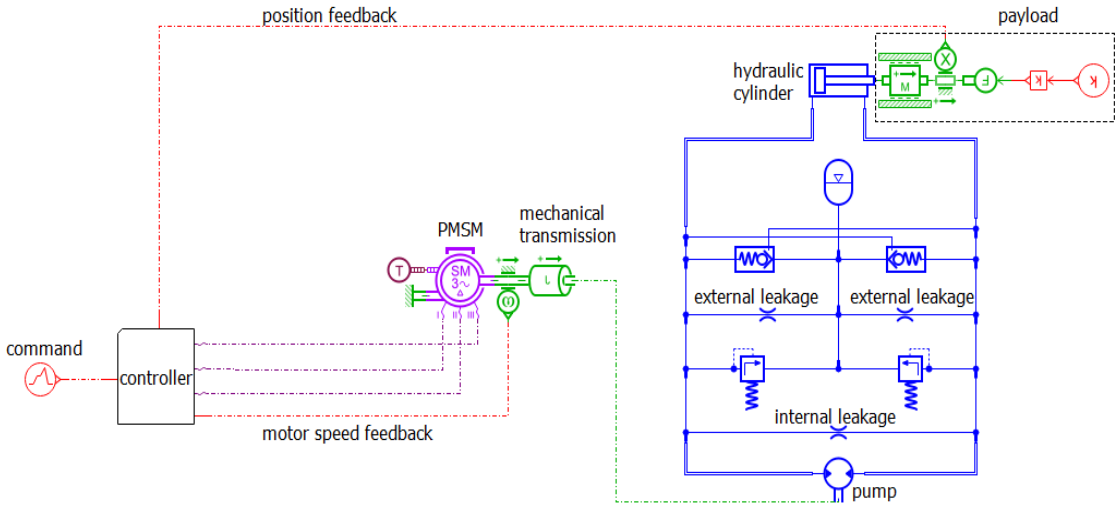

Figure 4.7: *Classic EHA system model*

4.5.3 Two-pump EHA System Model

For the two-pump EHA model demonstrated in **Figure 4.8**, the internal and external leakages were modelled to constitute the leakages of each pump. The gearbox was modelled with a lossless rotary mechanical node.

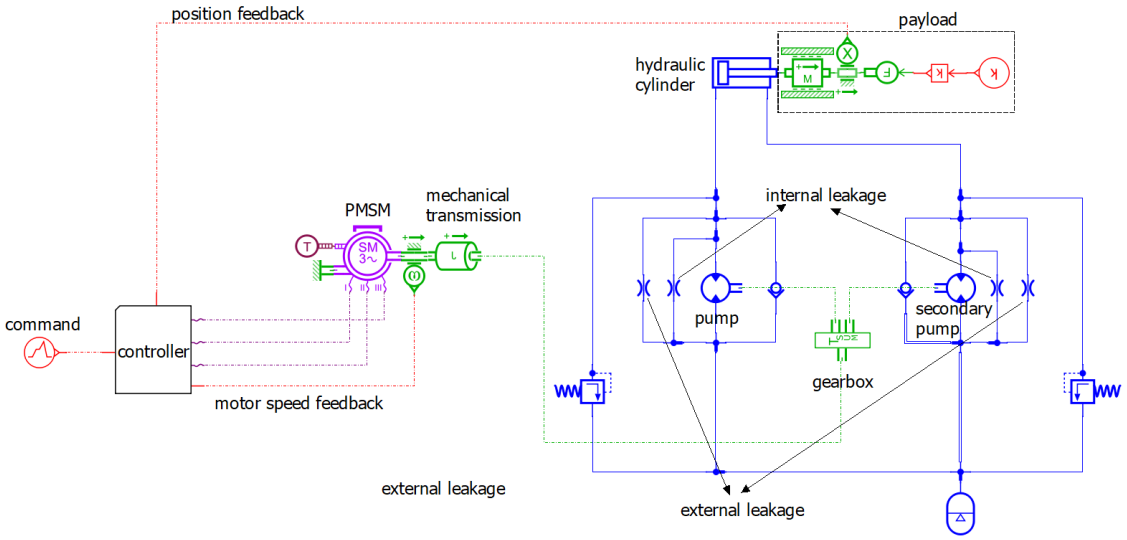

Figure 4.8: *Two-pump EHA system model*

4.6 Model Verification

A simple mathematical calculation was considered to validate the ideal behavior of the system model simulated. This methodology was since no experiments were performed with the referred test setup in section **3.1**.

The validation was performed by running the pump at a constant speed for 10 seconds in an open loop position control. The validation model was simulated with the boom force (*5440-N*) acting on the cylinder. The opening of the proportional valve was commanded with a signal to achieve full opening of the valve spool for extension and retraction of the piston in three complete cycles (**Figure 4.9**). One complete cycle constitutes the valve moving through three spool positions for piston extension, holding and retraction.

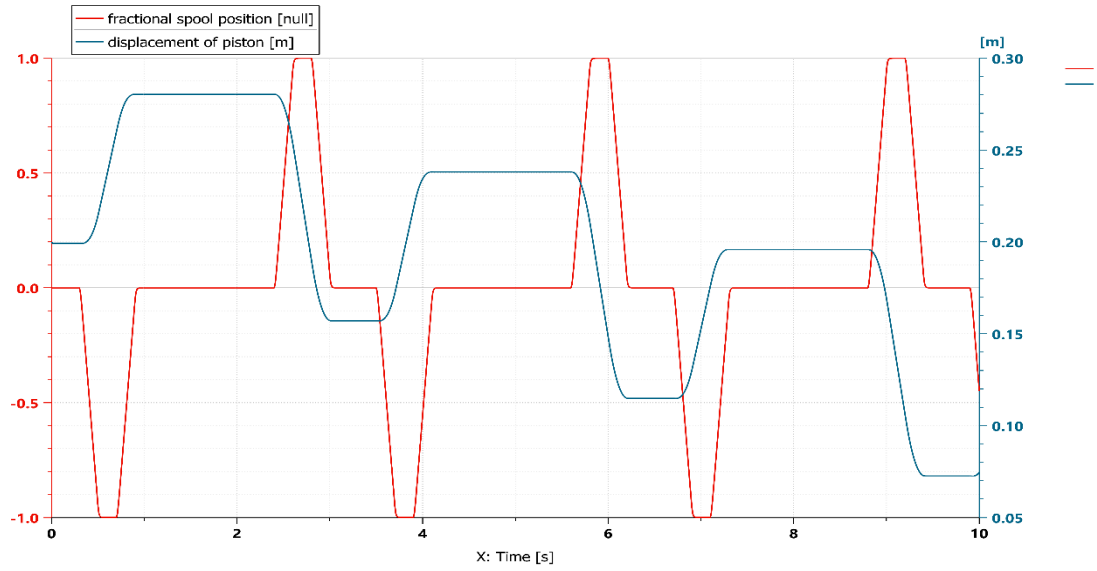

Figure 4.9: *Model Verification- valve spool position and piston displacement*

It follows that the static pressure exerted by the piston head can be calculated according to Pascal's Principle as:

$$p_L = \frac{F_L}{A_1}, \tag{4.23}$$

where F_L is the force applied to the actuator and A_1 is the area of the piston as derived in Equation (**4.1**).

Substituting the known values of F_L and A_1 into Equation (**4.23**) yields a static pressure of *19.22-bar*. This value is close to that obtained in the results of validation model for the piston-side chamber pressure when the valve is closed between *1 to 2.5 seconds*, *4.2 to 5.7 seconds* or *7.4 to 8.9 seconds* (**Figure 4.10**).

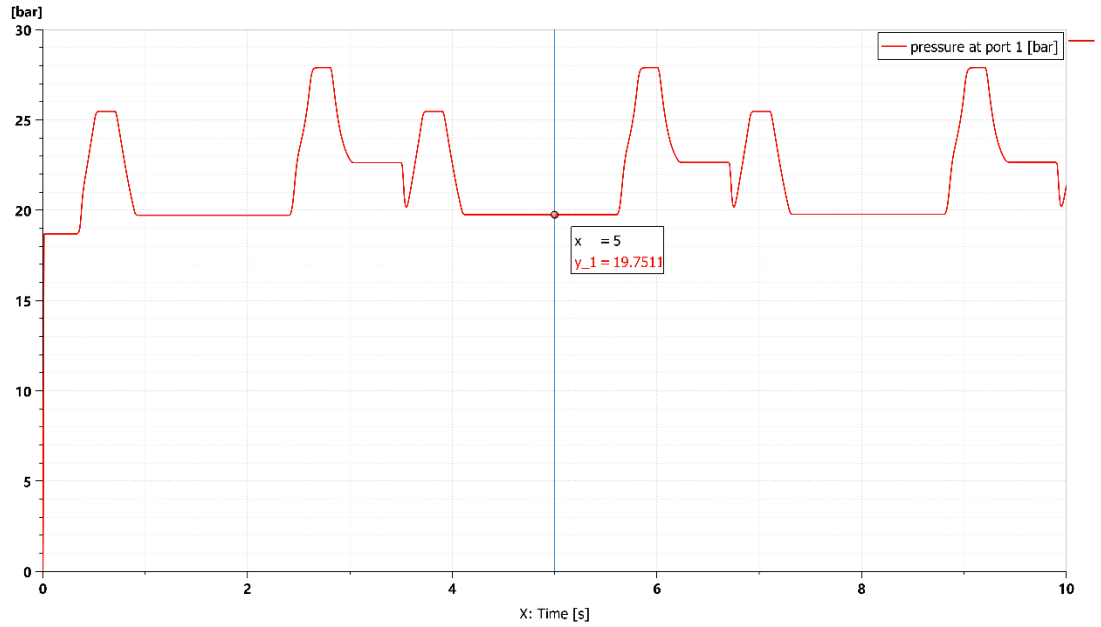

Figure 4.10: *Model verification - piston-side chamber pressure*

As expounded already in Chapter 3, the uncertainties and unpredictability of the pressure dynamics in EHA systems do not allow a well-founded theoretical validation for the simulation method. Since all three configurations explored in this thesis adopt the same hydraulic components and electric motor model, without any changes, we will safely assume the system as valid based on the validation of the conventional valve-controlled model.

5. RESULTS AND ANALYSIS

This chapter analyses the simulation results of the verified models from the previous chapter. The position tracking performance of the three systems are compared under different payload conditions and working cycles. First, the closed-loop responses of the actuators are evaluated with a step signal at maximum payload. The configurations are then tested with a working cycle under no-load, half-load and maximum load conditions, to assess the position tracking error. Position tracking error here refers to the difference between the commanded position (reference) and the simulated position of the cylinder piston. This shall be used in this thesis as the critical quantity to assess position tracking performance.

Since it was not possible to perform simulations in AMESIM with zero-mass for no-load conditions, a negligible mass was considered as the no-load mass. The loading conditions are defined in **Table 5.1** as follows:

Table 5.1: *Definition of loading conditions*

Loading Condition	Representative mass (kg)
No-load	10^{-6}
Half-load	150
Maximum-load	300

For conciseness and clarification, the legend used for the graphs and names adopted for system comparison are summarized in **Table 5.2**:

Table 5.2: *Naming system for graphs*

System	Legend
Valve-controlled Actuator	VC
Classic Electro-hydrostatic Actuator	EHA-classic
Two-pump Electro-hydrostatic Actuator	EHA-2

Section **5.1** of this chapter describes the working cycle of the simulation model and the general presentation of figures in this chapter. A step response performance is conducted for the actuators in section **5.2**. Using the defined working cycle, position tracking and cylinder chamber pressure dynamics are analyzed in section **5.3** and **5.4**, respectively. The efficiency analysis and discussions are performed for the systems under maximum load in sections **5.5** and **5.6**. Finally, further analysis is conducted for the EHA systems at the end of this chapter in section **0**.

5.1 Representative Working Cycle

To compare the position tracking performance in an actual working scenario, a working cycle was defined as the position reference for the piston for lifting and lowering of load (**Figure 5.1**). The extension of piston and lifting of load happens between 1 to 5 seconds. The load is held at maximum position between 5 to 9 seconds and then lowered during retraction of the piston between 9 to 13 seconds. The trajectory is started and completed with a holding position at minimum piston stroke, between 0 to 1 seconds and 13 to 15 seconds, respectively.

The working cycle is repeated for three cycles in the simulation run for a total time of 45 seconds. The reason behind this was that, the first cycle does not represent practical operations since the simulation system is started from initial conditions of 0-pressure. After the first cycle, the system is initialized and stabilized for the second and third cycles.

Analysis is conducted for only one cycle since the second and third cycles have similar dynamics, as will be seen in the step response dynamic analysis in section **5.2**. The time period in the step response results of section **5.2** will show the three complete cycles, to prove that the second and third cycles are similar. Figures in section **5.3** onwards will show the time period between 30 and 45-seconds, representing only the third cycle.

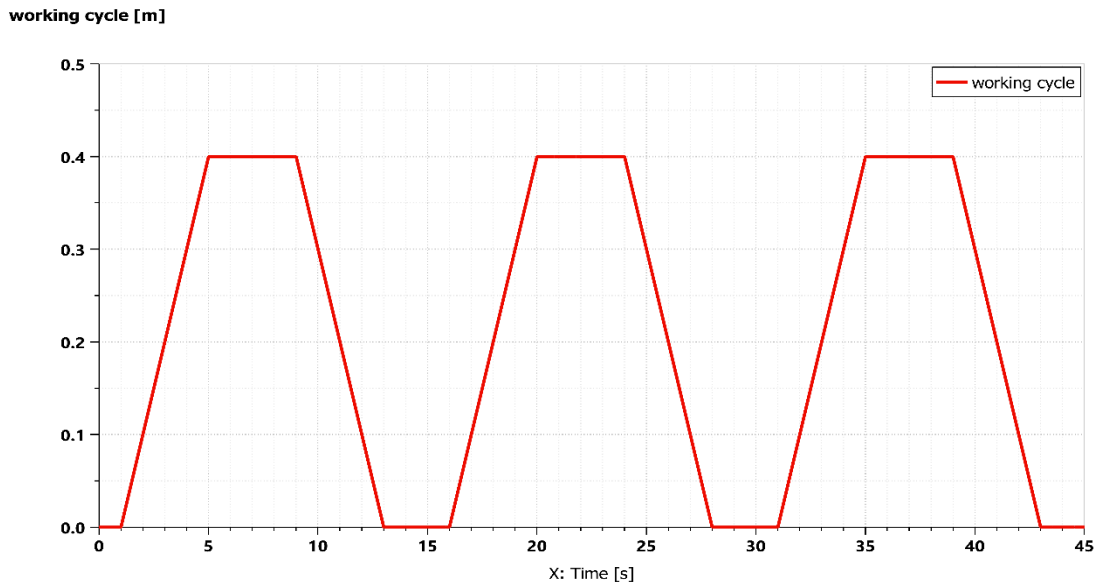

Figure 5.1: *Repeated working cycle (position reference)*

5.2 Position Tracking with Step Response

A small position step from *0.1* to *0.2-m* was commanded with maximum payload to evaluate the closed-loop step response time of the systems. The results of the step response are reported in **Figure 5.2**. Position tracking performance is similar for the three cycles in all the systems (**Figure 5.2**).

Considering the third cycle (10 to 15 seconds), the EHAs have faster rise time (time taken for the response to rise from 10% to 90% of steady-state value), and yet over *6%* slower settling time (time taken for response error to settle within 2% of final steady-state value) than the valve-controlled (Figure 5.2**(a)**). Obviously, the valve-controlled (VC) system has the best steady-state performance even though it records an overshoot (Figure 5.2**(a)**). Nevertheless, all three systems prove to have satisfactory steady-state performance since their steady-state errors are less than 2% of the steady-state value. Also, there is almost no oscillations about the final steady-state value which proves that control system performs acceptably and is robust. The exact values of the step response test are provided in **Table 5.3**.

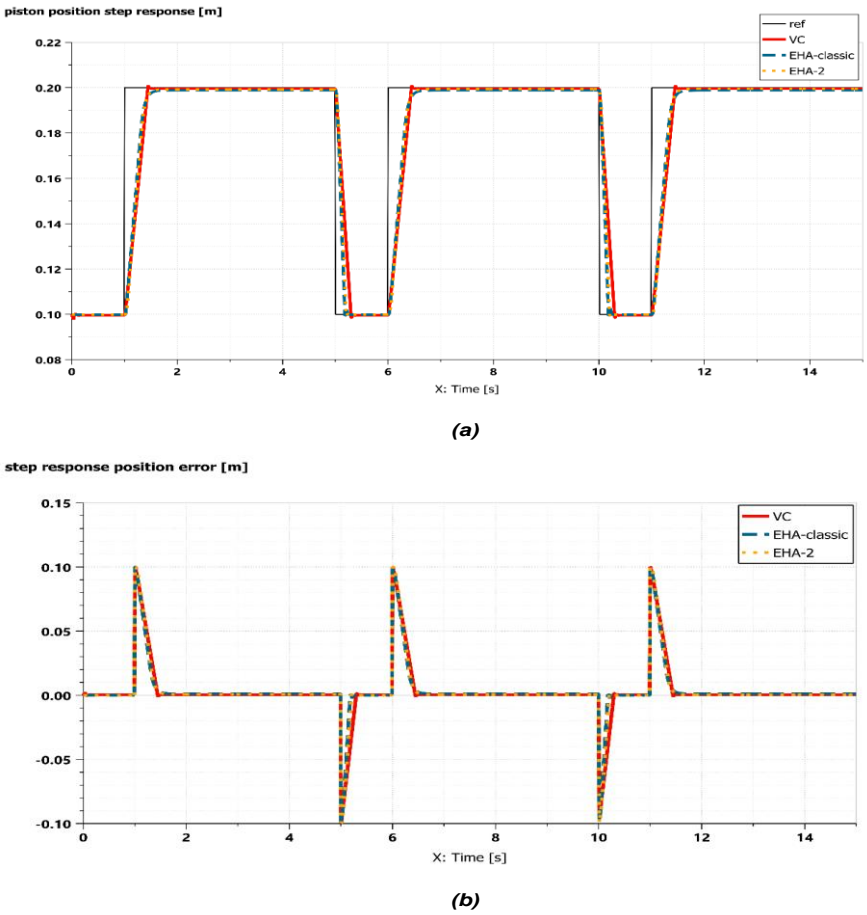

Figure 5.2: *Closed-loop step response position tracking performance for valve controlled actuator (VC), classic EHA actuator (EHA-classic), and two-pump EHA (EHA-2)* ***(a)*** *commanded and simulated positions* ***(b)*** *position tracking errors*

Table 5.3: *Closed-loop position step response results*

System	Rise Time (s)	Settling Time (s)	Overshoot (%)
VC	0,35	1,44	0,53
EHA-classic	0,30	1,53	-
EHA-2	0,30	1,49	-

As seen from Figure 5.3**(a)**, there are oscillations and spikes in the piston-side chamber pressures of the valve-controlled system and even more pronounced in the classic EHA system. The oscillations and spikes are repeated for the classic EHA in the rod-side chamber pressure but not evident for the rod-side chamber pressure of the valve-controlled system (Figure 5.3**(b)**). The two-pump EHA system does not experience significant oscillations, even though high spikes are observed close to the minimum position

mark, in both chamber pressures. The lower oscillations observed in the two-pump EHA is partly due to the flow balancing property of the secondary pump. Steady-state pressure is lowest in the valve-controlled system (*29-bar* at piston-side and *0.1-bar* at rod-side) and higher in the EHAs (*33-bar* at piston-side and *4-bar* at rod-side) for both chambers.

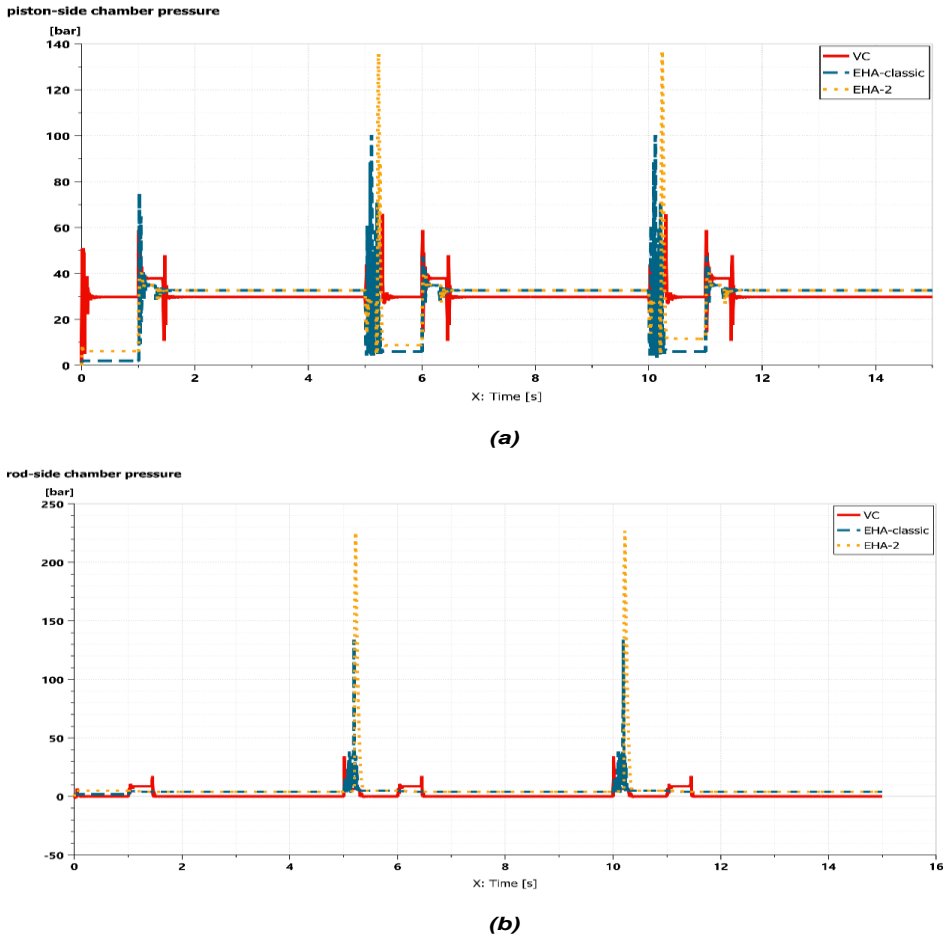

Figure 5.3: *Closed-loop position step response chamber pressure comparison* ***(a)*** *piston-side chamber pressures* ***(b)*** *rod-side chamber pressures*

5.3 Position Tracking with Working Cycle

The systems are subjected to different payloads under the defined working cycle to investigate the effects of load variation on the systems. Three different mass loads, as defined at the beginning of this chapter, are simulated and the results are as presented in this section. The exact values are shown in tables and represent the final value of the error at the end of the different stages of the working cycle – lifting, holding and lowering.

5.3.1 No payload

Figure 5.4 shows the position tracking performance of the systems at no load. Position tracking appears to be identical for all three systems in Figure 5.4**(a)**. The maximum

position error of the systems falls within an acceptable range of 2% of full stroke (Figure 5.4**(b)**).

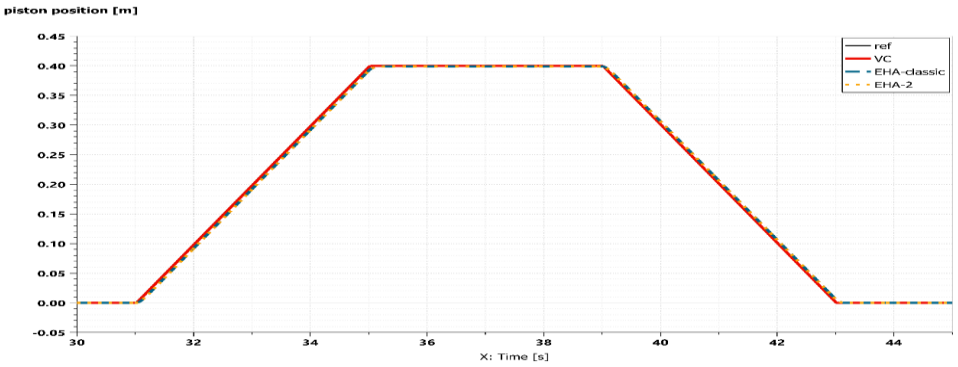

(a)

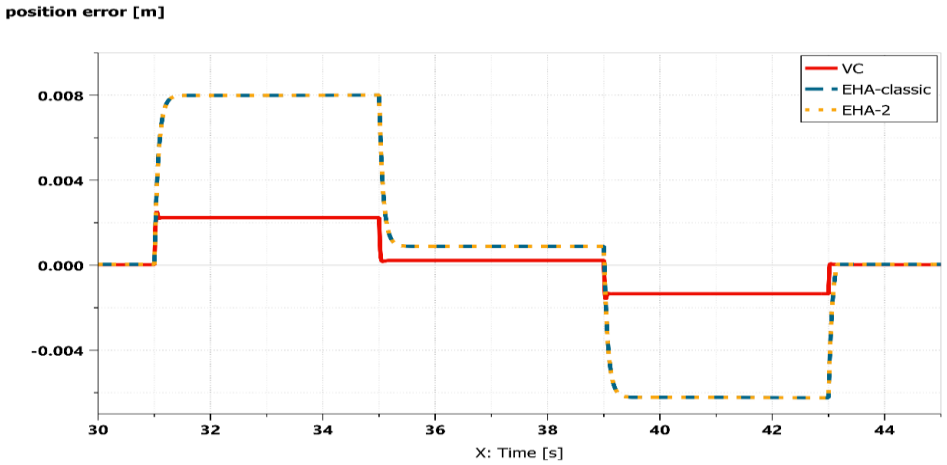

(b)

Figure 5.4: *Position tracking performance comparison at no load* ***(a)*** *commanded and simulated position* ***(b)*** *tracking error*

The simulation values at the end of the different stages of the trajectory are provided in the **Table 5.4** .

Table 5.4: *No-load absolute position error results*

System	**Absolute position error at different stages (mm)**		
	Lifting	**Holding**	**Lowering**
VC	2,25	0,23	1,34
EHA-classic	8,01	0,90	6,23
EHA-2	8,01	0,90	6,24

5.3.2 150 kg payload

Position tracking performance analysis is repeated for the systems at half-load capacity and the results are displayed in **Figure 5.5**. Here again, the simulated position appears to be tracking the reference position quite well for all the systems (Figure 5.5**(a)**). Maximum position error is close to 2% of full stroke even though the final simulation values at the end of the different stages (provided in **Table 5.5**) show that the no-load errors are *3%* better during lifting and holding stage for the conventional and classic EHA systems (Figure 5.5**(b)**). For the lowering stage, the half-load error shows an improvement of 6*%* from the no-load errors for the conventional and classic EHA systems, attributed to the assistive nature of the payload acting under gravity. Position errors in the two-pump EHA for the three stages show no change between no-load and half-load conditions.

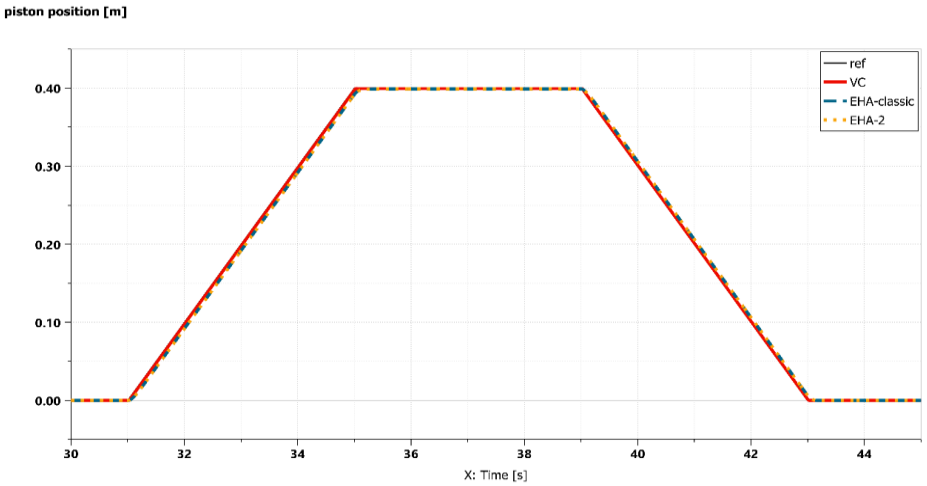

(a)

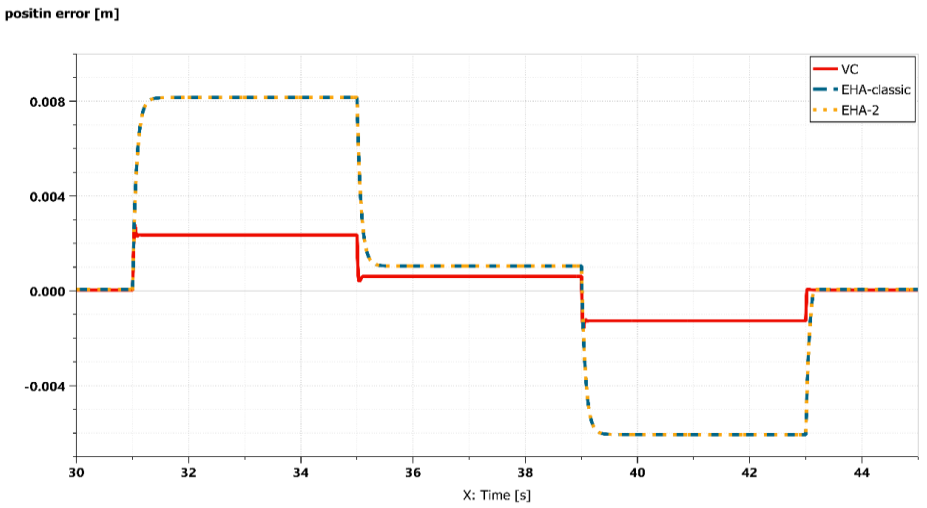

(b)

Figure 5.5: *Position tracking performance comparison at half load* ***(a)*** *commanded and simulated position* ***(b)*** *tracking error*

Table 5.5: *Half-load absolute position error results*

System	Absolute position error at different stages (mm)		
	Lifting	**Holding**	**Lowering**
VC	2,36	0,61	1,26
EHA-classic	8,17	1,05	6,07
EHA-2	8,17	1,05	6,07

5.3.3 300 kg payload

The final position tracking analysis is performed at maximum load for the actuator systems. The simulation results are provided in **Figure 5.6**. Similar to the previous load conditions, position tracking of the reference position is satisfactory and identical for the three systems (Figure 5.6**(a)**). Figure 5.6**(b)** displays an improvement in the lowering position error of the systems compared to the half-load condition. This is explained by the heavier mass assisting the piston lowering. Overall, the errors at maximum conditions are not significantly different from the no-load and half-load conditions.

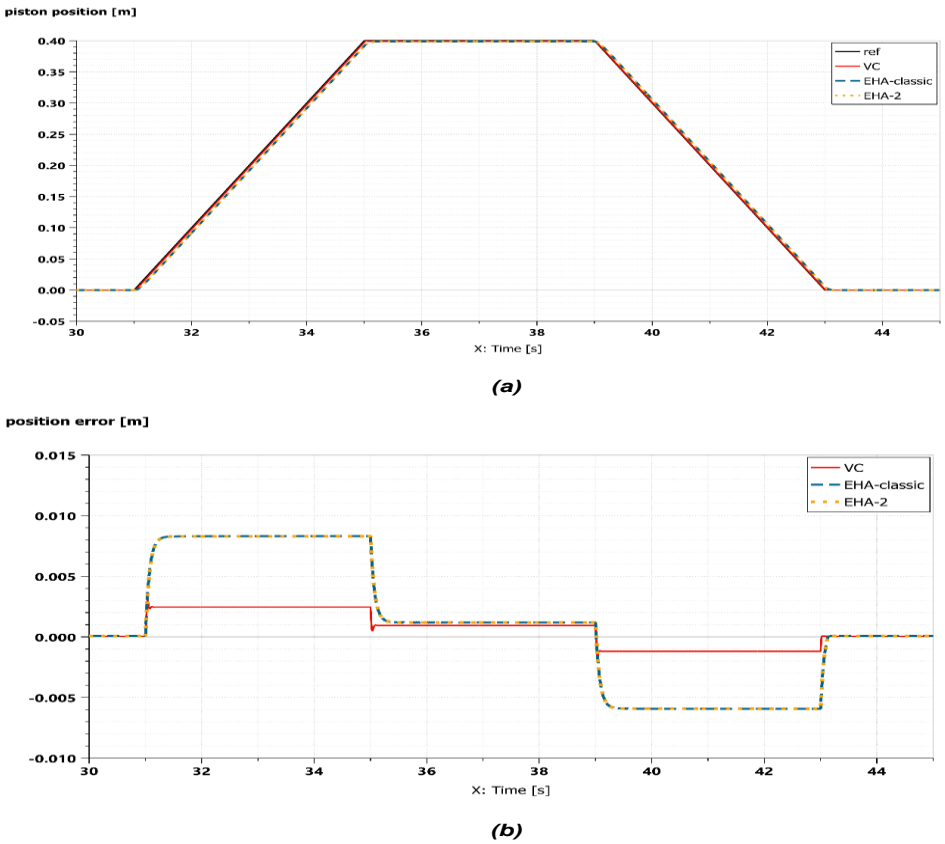

Figure 5.6: *Position tracking performance comparison at maximum load* ***(a)*** *commanded and simulated position* ***(b)*** *tracking error*

The position error numerical results are presented in **Table 5.6** as follows:

Table 5.6: *Maximum-load absolute position error results*

System	Absolute position error at different stages (mm)		
	Lifting	**Holding**	**Lowering**
VC	2,46	0,94	1,19
EHA-classic	8,31	1,19	5,93
EHA-2	8,31	1,19	5,93

5.4 Cylinder pressure

5.4.1 No payload

The cylinder chamber pressures are studied during the working cycle with zero-payload condition and illustrated in **Figure 5.7**. Pressure dynamics vary for different phases of the working cycle as shown in **Figure 5.7**. The EHA systems have low and stable chamber pressures during extension of the piston. The conventional system experiences high spikes during no-load operations, as well as a little oscillation at *31-second*.

During the holding stage, the EHA systems continue to run to maintain the position of the piston and as a result, builds pressure in the piston chamber. In the valve-controlled system, the valve spool is closed and fluid flow from the pump is directed to the tank through port T. Hence the reduced chamber pressures during the holding phase.

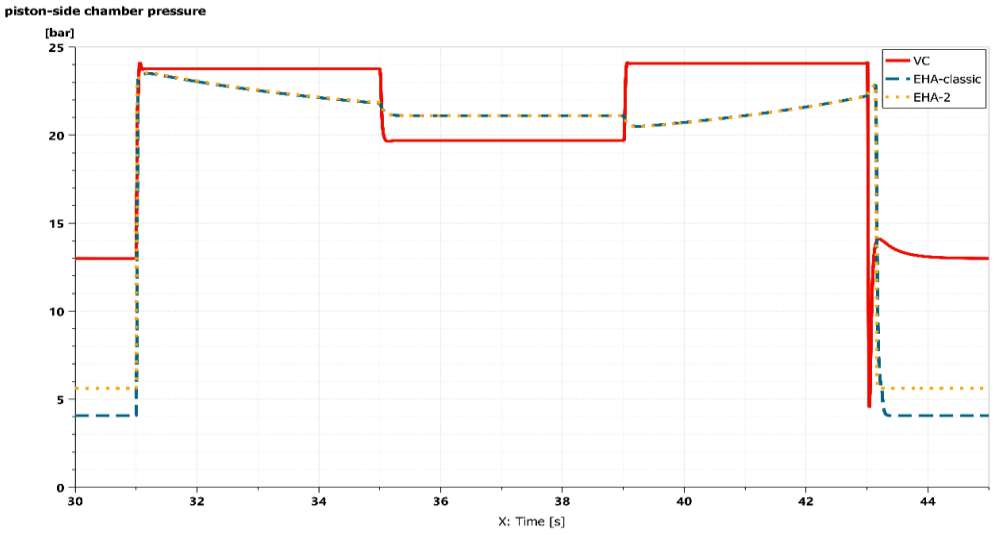

(a)

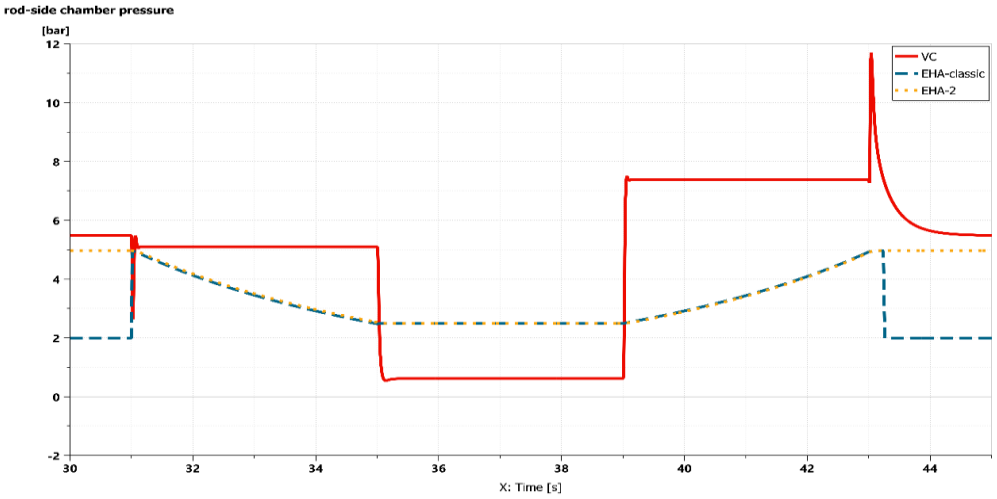

(b)

Figure 5.7: *No-load chamber pressures* ***(a)*** *piston-side chamber* ***(b)*** *rod-side chamber*

5.4.2 150 kg payload

The payload is increased to analyze the pressure dynamics when the system is operated at half-load. **Figure 5.8** presents the results for the operation. A similar dynamic is observed in the half-load condition as was seen in the no-load condition. The main difference observed in Figure 5.8**(a)** is the increased pressure levels in the piston-side chamber. This is a result of the increased static pressure of the load, requiring higher chamber pressure for extension. The rod-side chamber pressure remains similar since the load does not affect this chamber significantly during extension.

A few spikes are observed in the classic EHA with significant oscillations observed at 31 and 43-second. The valve-controlled piston-side chamber pressure dynamics demonstrates high spikes at the beginning and end of each phase during valve switching. The

two-pump EHA experiences lower oscillations at 12-second but has a smoother profile compared to the other two systems, with no spikes observed.

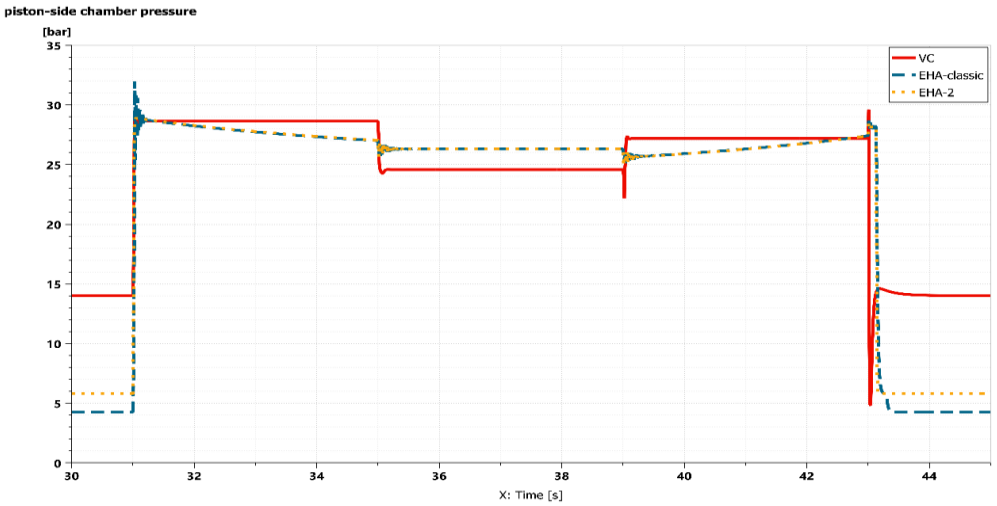

(a)

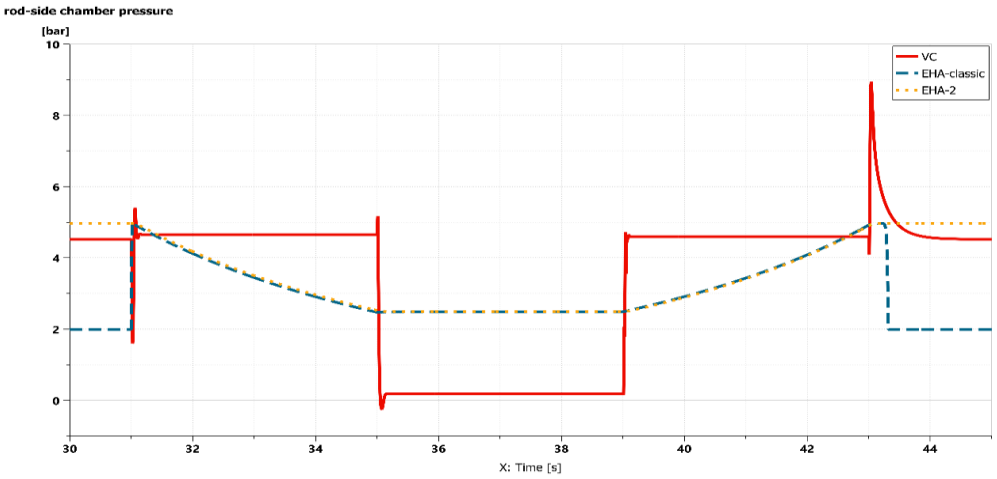

(b)

Figure 5.8: *Half-load chamber pressures* ***(a)*** *piston-side chamber* ***(b)*** *rod-side chamber*

5.4.3 300 kg payload

The effect of load variation is further analyzed by increasing the payload to maximum. The result is demonstrated in **Figure 5.9**. It has been observed that load variations affect the pressure levels significantly in the piston-side chamber but less significantly in the rod-side chamber. Increasing the load also increases the frequency of oscillations in the classic EHA system and valve-controlled system. The phenomenon of pressure spikes and oscillations are more pronounced in the classic EHA system due to the asymmetrical cylinder. Oscillations are reduced in the two-pump EHA system and a lower spike is only observed at the beginning of piston extension phase.

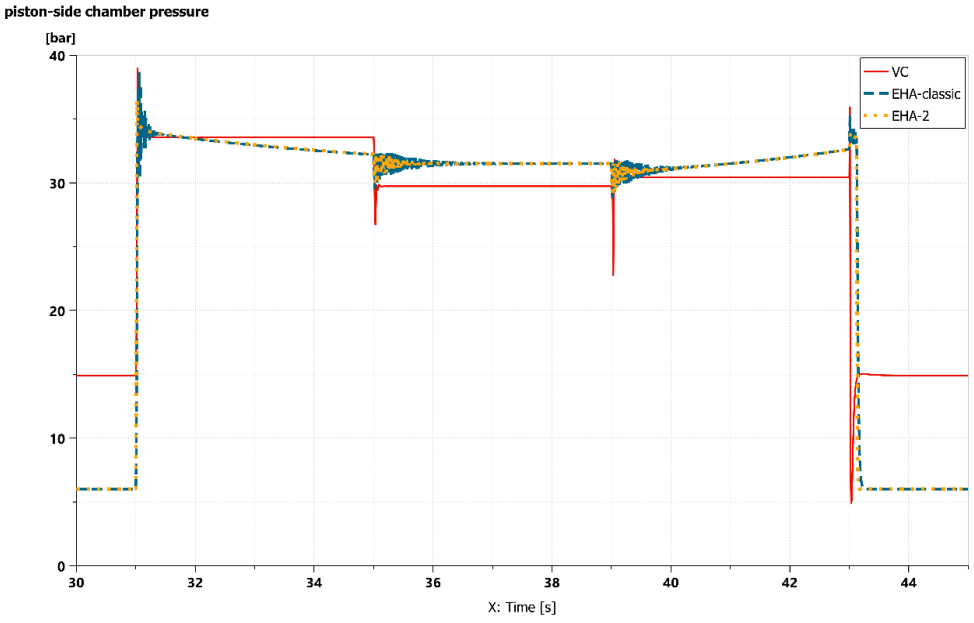

(a)

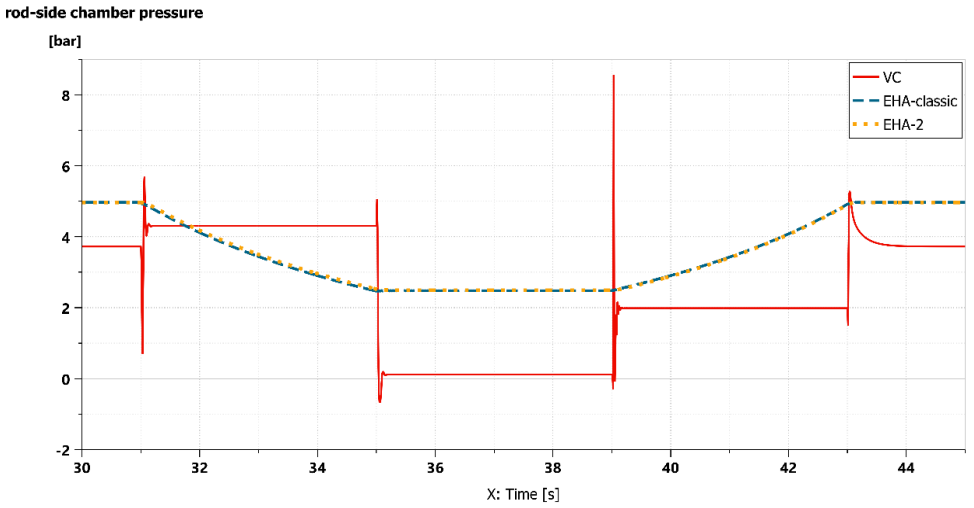

(b)

Figure 5.9: *Maximum-load chamber pressures* ***(a)*** *piston-side chamber* ***(b)*** *rod-side chamber*

5.5 Energy Efficiency at Maximum Payload

This section analyses the principal feature of concern regarding actuation systems in mobile machines. The total energy consumption of the three actuators are studied and thus, their efficiencies are compared.

For this efficiency analysis, the power consumption for the general components common to all the systems are considered here. Power consumption of specific components will

be considered under subsections of the respective systems. To calculate the power consumption at different points in the system, an approach from the motor input power to the cylinder output power is considered.

The electrical input power supply for the system can be calculated as:

$$\boldsymbol{P}_{\boldsymbol{elec}} = \boldsymbol{V} \cdot \boldsymbol{I}\,, \tag{5.1}$$

where V is the voltage supplied and I is the current of the supply. The efficiency of the power inverter has not been considered in the analysis but has rather been given a fixed value of *95%*. The electrical power supplied to the electric motor is then converted to mechanical power at the motor shaft to drive the hydraulic pump. With the motor shaft coupled to the drive shaft of the hydraulic pump, the output power of the motor and input power of the pump is mechanical power given as:

$$\boldsymbol{P}_{\boldsymbol{mech}} = \boldsymbol{T} \cdot \boldsymbol{\omega}\,, \tag{5.2}$$

where T and ω are torque and angular velocity of the rotational shaft, respectively. The mechanical losses between motor shaft and pump drive shaft are assumed to be negligible in this thesis. Hydraulic pumps convert the mechanical power of the drive shaft to fluid power required to drive the actuator. The fluid or hydraulic power in the pump, as a result of generated flow and pressure, is given by the equation:

$$\boldsymbol{P}_{\boldsymbol{h}} = \boldsymbol{Q} \cdot \boldsymbol{p}\,, \tag{5.3}$$

where Q and p are fluid flow and pressure, respectively. The generated power from the pump outlet is directed to the actuating cylinder to overcome pressure induced by the load. The power required to generate the linear movement of the load is calculated by:

$$\boldsymbol{P}_{\boldsymbol{cyl}} = \boldsymbol{F} \cdot \boldsymbol{v}_{\boldsymbol{p}}\,, \tag{5.4}$$

where F is the force exerted by the cylinder piston and v_p is the velocity of the piston.

To obtain the energy consumption in the system or a specific component, the integral of the respective power is taken with respect to time and calculated as:

$$\boldsymbol{E} = \int_{\boldsymbol{0}}^{\boldsymbol{t}} \boldsymbol{P}\, \boldsymbol{dt}\,, \tag{5.5}$$

where P is the power of the component whose energy consumption is to be calculated and t is time.

Finally, efficiency can be calculated as:

$$\eta = \frac{E_{out}}{E_{in}}, \qquad (5.6)$$

where E_{out} is output energy and E_{in} is input energy

The mechanical losses between motor shaft (motor rotational output) and pump drive shaft (pump rotational input) are assumed to be negligible in this thesis and this is shown in **Figure 5.10**. It is worthy of note that in **Figure 5.10**, the negative motor output power and pump input power of the EHAs, between 39 and 43 seconds, implies that the electric motor functions effectively as a generator between this period and presents a potential for energy regeneration.

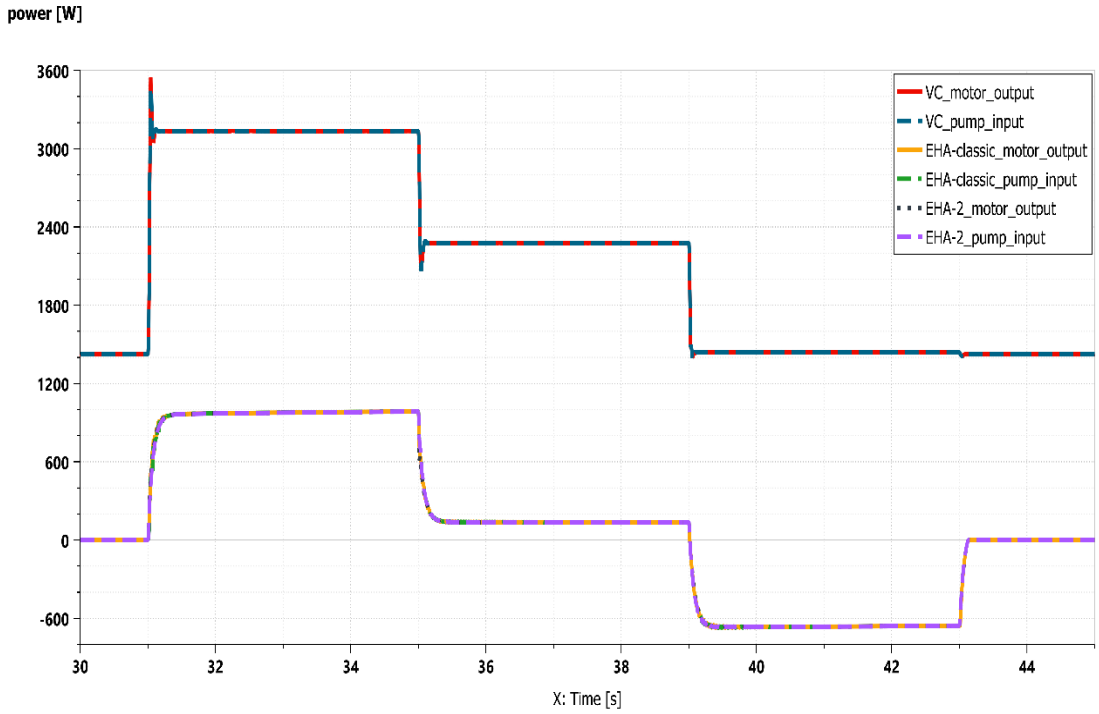

Figure 5.10: *Mechanical losses between motor and pump shaft connection*

To ensure a fair evaluation of the energy consumption, it is necessary to compare the hydraulic output of the actuators for all three systems. **Figure 5.11** proves the hydraulic output power in all the configurations are identical. Also in **Figure 5.11**, a potential for energy recovery is present during the retraction phase of the cylinder piston (39 to 43 seconds) as shown by the negative power levels.

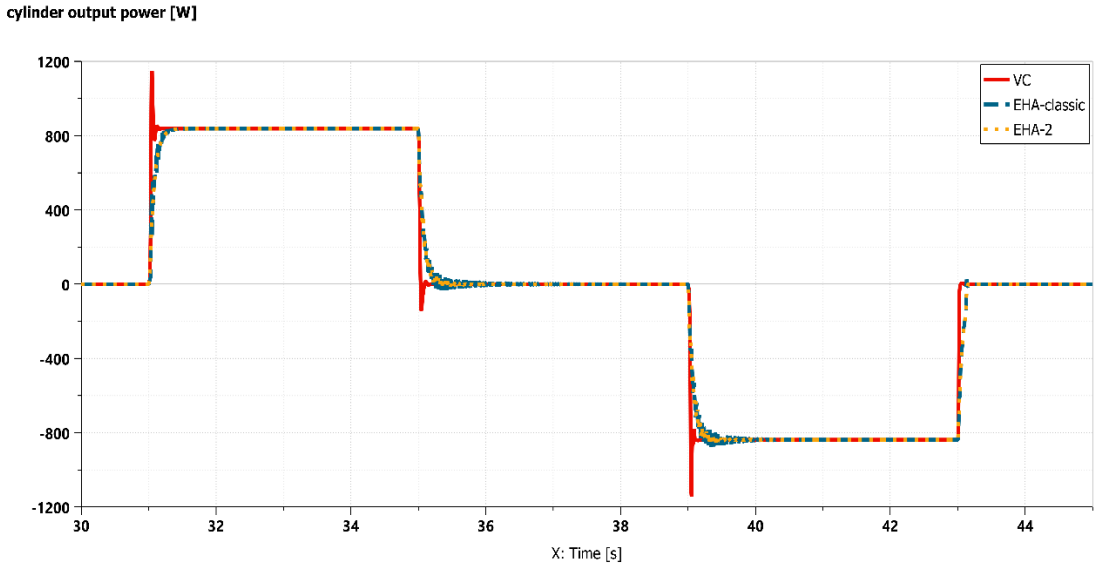

Figure 5.11: *Hydraulic cylinder output power*

Due to the potential of energy regeneration presented in **Figure 5.10** and **Figure 5.11**, the energy efficiency analysis shall be performed separately for the lifting and retraction phases of the working cycle. The forward motion (lifting) shall be considered for 31 to 34 seconds and holding for 34 to 39 seconds. The energy recovered between 39 to 43 seconds shall be considered in the analysis.

Having established a premise for comparison, this section proceeds with the power distribution analysis for each system configuration.

5.5.1 Energy Efficiency Analysis of Conventional Valve-Controlled Actuator System

For this system, the power consumption in these critical components are considered and illustrated in **Figure 5.12**: electric motor, pump, proportional valve and cylinder. Input power (pump_input) to the hydraulic pump is supplied by the electric drive (power_source and motor_input) to generate hydraulic power (pump_output). The hydraulic power output from the pump is considered the same as the valve input power.

The input power of the proportional valve constitutes the flow to the valve through the pressure port (P) and the pressure at the same port (P). The output power is determined depending on the direction of motion of the cylinder. During extraction of the cylinder piston, the output power is the product of the valve out-flow through port A and the pressure at that port. Conversely, the product of the flow through port B and the pressure at port B is the output power during retraction of the piston. The flow from the valve during the holding stage is channelled to tank through port T and the power output is considered at port A, which holds the load in position.

The valve output power (valve_output) is fed to the cylinder to produce mechanical output power (cylinder_output) for linear displacement of piston.

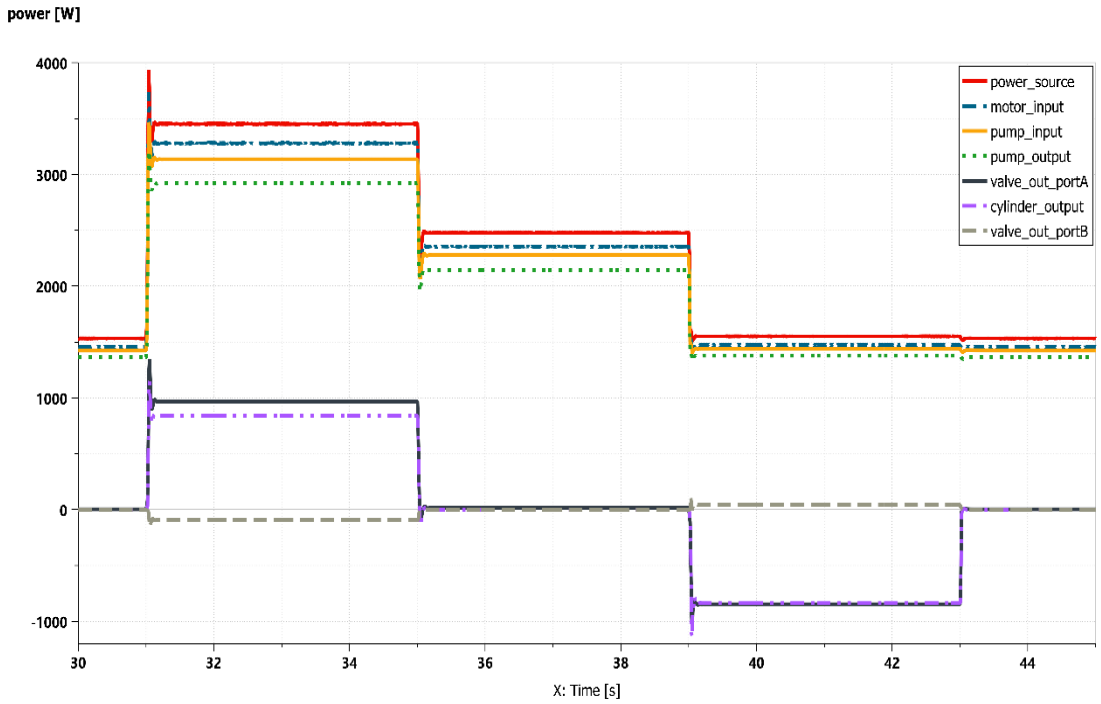

Figure 5.12: *Power distribution in valve-controlled system*

Energy consumption is obtained from the power distribution, as indicated already using Equation **(5.5)**. Results are illustrated for lifting, holding and lowering in **Table 5.7**, **Table 5.8**, and **Table 5.9**, respectively. The energy loss across a component is the difference between the input and output energy of the component.

Table 5.7: *Energy distribution during piston extension and load lifting (valve-controlled system)*

	Source	**Motor**	**Pump**	**Valve**	**Cylinder**
Energy Input (kJ)	13,77	13,09	12,52	11,66	3,86
Energy output (kJ)	13,09	12,52	11,66	3,86	3,33
Energy losses (kJ)	0,68	0,57	0,86	7,80	0,53
Percentage loss (%)	4,94	4,14	6,25	56,64	3,85

Table 5.8: *Energy distribution during load holding (valve-controlled system)*

	Source	Motor	Pump	Valve	Cylinder
Energy Input (kJ)	9,92	9,42	9,12	8,59	0,07
Energy output (kJ)	9,42	9,12	8,59	0,07	0,01
Energy losses (kJ)	0,50	0,30	0,53	8,52	0,06
Percentage loss (%)	5,04	3,02	5,34	85,89	0,60

Table 5.9: *Energy distribution during piston retraction and load lowering (valve-controlled system)*

	Source	Motor	Pump	Valve	Cylinder
Energy Input (kJ)	6,22	5,91	5,78	5,53	0,16
Energy output (kJ)	5,91	5,78	5,53	0,16	-3,33
Energy losses (kJ)	0,31	0,13	0,25	5,37	0,12
Percentage loss (%)	4,98	2,09	4,02	86,33	1,93

The results in the tables prove the huge amount of energy lost (*56-87%*) to throttling in the proportional valve. The remaining losses are distributed among electrical and mechanical losses (less than 10%), pump and hose friction losses (*10%*) and cylinder friction losses (about 4%). Only 24% of the input energy is used for actuation during the lifting phase.

The negative energy output in the cylinder, from the results of **Table 5.9**, represents the total energy recovered during lowering of the load. Energy lost in the cylinder is calculated by subtracting the cylinder output energy from the sum of energy generated and input energy from the valve port B. The output energy from the cylinder is dissipated at the valve in the form of heat energy.

5.5.2 Energy Efficiency Analysis of Classic Electro-hydrostatic Actuator System

Power distribution in the classic EHA system is considered for electric motor, pump cylinder and hydraulic accumulator. The results are demonstrated in **Figure 5.13**. The output of the hydraulic pump (pump_output) is directly supplied to the actuating cylinder to

generate mechanical power output (cylinder_output). The power consumption in the hydraulic accumulator (accumulator) is also presented here.

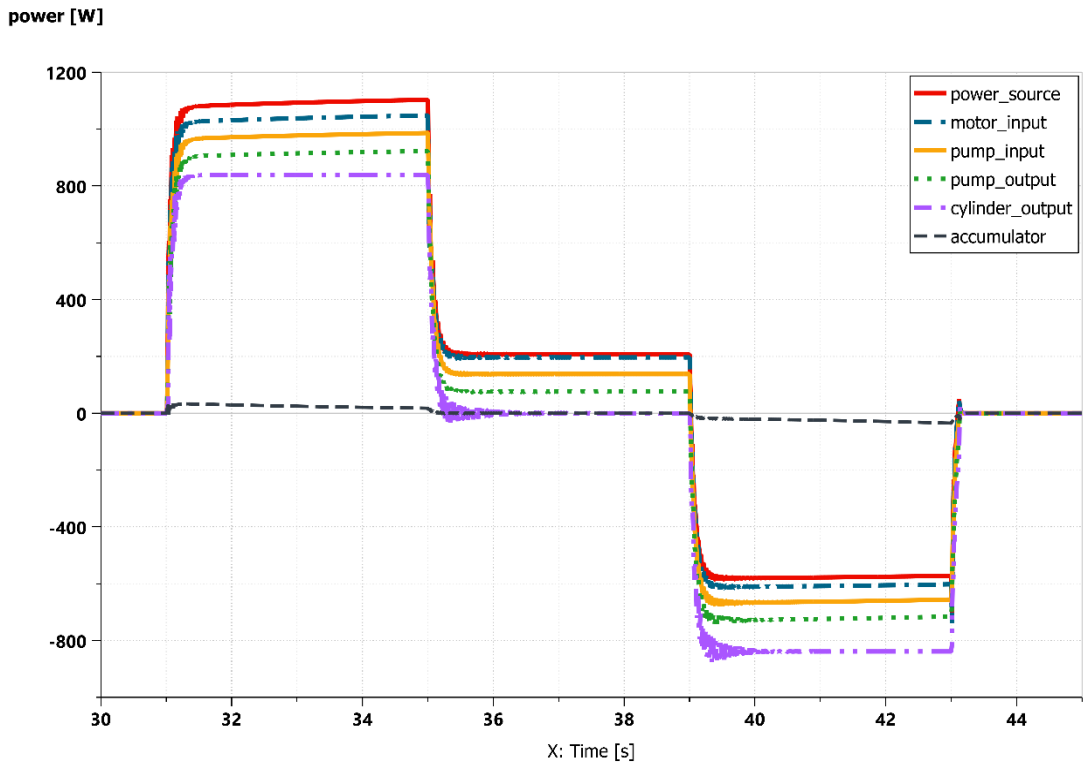

Figure 5.13: *Power distribution in classic electro-hydrostatic actuator system*

The same method is applied to obtain the energy distribution as was done for the conventional system in the previous section **5.5.1**. The results are tabulated below in **Table 5.10**, **Table 5.11** and **Table 5.12**.

Table 5.10: *Energy distribution during piston extension and load lifting (classic EHA system)*

	Source	**Motor**	**Pump**	**Cylinder**	**Accum.**
Energy Input (kJ)	4,30	4,08	3,84	3,59	-
Energy output (kJ)	4,08	3,84	3,59	3,29	0,10
Energy losses (kJ)	0,22	0,24	0,25	0,30	0,10
Percentage loss (%)	5,12	5,58	5,81	6,98	2,33

Table 5.11: *Energy distribution during load holding (classic EHA system)*

	Source	Motor	Pump	Cylinder	Accum.
Energy Input (kJ)	0,88	0,84	0,61	0,36	-
Energy output (kJ)	0,84	0,61	0,36	0,06	10^{-3}
Energy losses (kJ)	0,04	0,23	0,25	0,30	10^{-3}
Percentage loss (%)	4,55	26,14	28,41	34,01	0,14

Table 5.12: *Energy distribution during piston retraction and load lowering (classic EHA system)*

	Source	Motor	Pump	Cylinder	Accum.
Energy input (kJ)	-2,25	-2,37	-2,59	-2,83	
Energy output (kJ)	-2,37	-2,59	-2,83	-3,29	-0,10
Energy losses (kJ)	0,12	0,22	0,26	0,46	-0,10
Percentage loss (%)	3,65	6,69	7,90	13,98	-3,04

76% of the input electrical energy is used for actuation during the lifting phase of the load (**Table 5.10**). The lost energy is distributed among the components and dissipated as heat energy.

There is significant loss in the electric motor and pump during the holding phase (**Table 5.11**) and this could be attributed to the fact that electric motor is inefficient at low speeds. Electric motors are most efficient when operated close to their rated values. During lifting and holding phases, the hydraulic accumulator is discharged to compensate the flow imbalance and energy is dissipated. Energy is stored in the hydraulic accumulator during lowering, hence the negative loss value (**Table 5.12**).

Even though 68% of energy can be recuperated at the electric drive during the lowering stage, the amount of energy regenerated depends also on the efficiency of the regeneration system.

5.5.3 Energy Efficiency Analysis of Two-pump Electro-hydrostatic Actuator System

A similar approach for analyzing the power distribution is adopted for this system as was the case for the previous configurations (sections **5.5.1** and **5.5.2**). The power distribution in the two-pump EHA system is presented in **Figure 5.14**. The pump output power (pump_output) of this system is somehow complicated when compared to the other systems. The main pump operates in pumping mode and the secondary pump operates in motoring mode during piston extension, and vice versa during retraction. For that reason, the pump output power during extension is considered as the main pump output power. For retraction, the secondary pump output power is considered for pump output power.

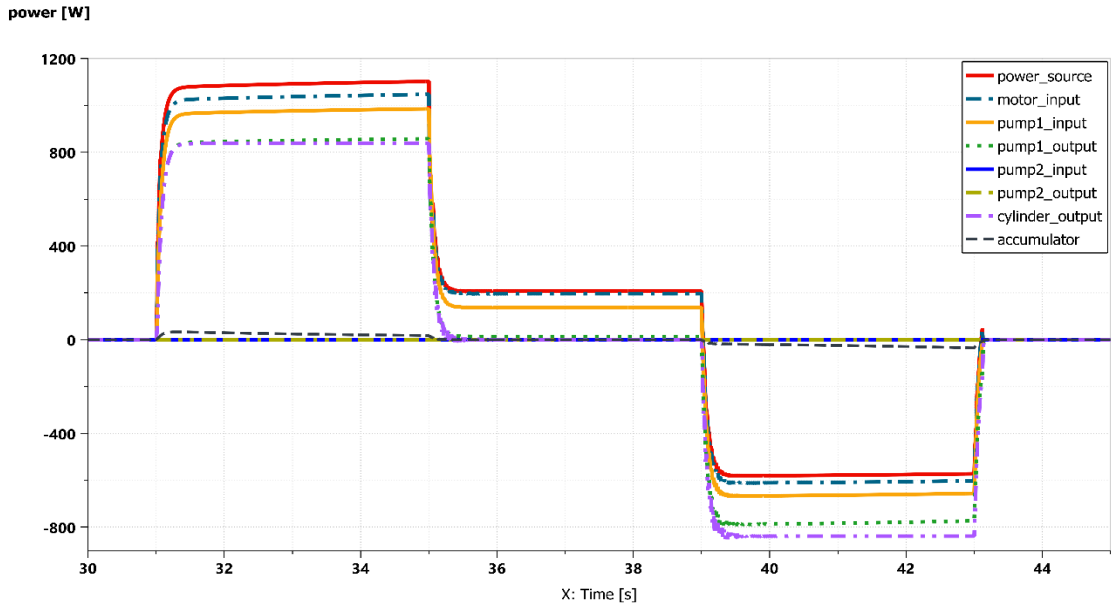

Figure 5.14: *Power distribution in two-pump electro-hydrostatic actuator system*

The other power levels remain the same as explained for the classic EHA system and the energy distribution is tabulated in **Table 5.13**, **Table 5.14** and **Table 5.15**.

Table 5.13: *Energy distribution during piston extension and load lifting (two-pump EHA system)*

	Source	Motor	Pump1	Pump2	Cylinder	Accum.
Energy Input (kJ)	4,30	4,09	3,83	$3{,}1 \cdot 10^{-4}$	3,33	-
Energy output (kJ)	4,09	3,83	3,33	$2{,}8 \cdot 10^{-4}$	3,29	0,10
Energy losses (kJ)	0,21	0,26	0,50	$3 \cdot 10^{-5}$	0,04	0,10
Percentage loss (%)	4,88	6,05	11,63	0,001	0,93	2,33

Table 5.14: *Energy distribution during load holding (two-pump EHA system)*

	Source	Motor	Pump1	Pump2	Cylinder	Accum.
Energy Input (J)	0,88	0,84	0,61	$6 \cdot 10^{-5}$	0,11	-
Energy output (J)	0,84	0,61	0,11	$1 \cdot 10^{-5}$	0,06	0,001
Energy losses (J)	0,04	0,23	0,50	$5 \cdot 10^{-5}$	0,05	0,001
Percentage loss (%)	4,55	26,14	56,82	0,01	5,68	0,11

Table 5.15: *Energy distribution during piston retraction and load lowering (two-pump EHA system)*

	Source	Motor	Pump1	Pump2	Cylinder	Accum.
Energy Input (J)	-2,25	-2,37	-2,59	$-2{,}7 \cdot 10^{-4}$	$3{,}3 \cdot 10^{-4}$	
Energy output (J)	-2,37	-2,59	-2,84	$3{,}3 \cdot 10^{-4}$	-3,29	-0,10
Energy losses (J)	0,12	0,22	0,25	$6 \cdot 10^{-5}$	0,22	-0,10
Percentage loss (%)	3,65	6,69	7,60	$2 \cdot 10^{-3}$	6,69	-3,04

A similar amount of energy is used in this system for the lifting phase compared to the classic EHA system (*4.30 kJ*) even though this configuration involves operating two pumps (**Table 5.13**). From the results, there is much less actuator losses since the cylinder outflow generates power in the secondary pump, operating in motor mode. The result of this is the low electrical consumption, in contrast to an expected increased consumption due to two pumps. The generated power in the secondary pump is proven by the negative torque at its shaft. A similar energy dissipation and storage phenomenon is observed in the hydraulic accumulator as was seen in the classic EHA.

In **Table 5.14**, results shows that 50% more energy is consumed in the main pump during the holding phase as compared to the classic EHA's main pump, whiles the electrical losses remained identical. The increased oscillations observed during the holding stage of the classic EHA cause higher pump output and cylinder input power (Figure 5.9**(a)**), required for the same cylinder output. Consequently, the classic EHA's cylinder efficiency is much lower than the two-pump EHA's cylinder (**Table 5.11**). In effect, both systems produce similar overall energy efficiency as the classic EHA has better pump efficiency and the two-pump EHA has a better cylinder efficiency.

Close to 68% of the energy regenerated during load lowering can be recovered at the electric drive (**Table 5.15**).

5.6 System Comparison and Discussion

5.6.1 Motion Performance

The position tracking performance of the three systems were satisfactory and the error remained within a limit of about 0.*2% - 2.1%*. It was seen that the position-tracking performance in the valve-controlled system was better than the EHA systems. This may not be the case in practical applications and results from other literature [9]. This thesis has not focused on achieving position accuracy with the control system but rather, maintaining the systems within acceptable position error limits to study the energy efficiency. A more accurate tuning of the control could achieve better position accuracy and performance in the EHA systems.

With regards to cylinder chamber pressures, the effect of the asymmetrical cylinder is noticed in the systems by the pressure spikes and oscillations. This anomaly is striking in the classic EHA system as observed in the closed-loop response test in section **5.2** and the load variation tests in section **5.4**. The introduction of the secondary pump eliminates the spikes and reduces the oscillations in the chamber pressures of the two-pump EHA system significantly. It is practically impossible to match cylinder area to pump flow due to pump volumetric efficiency and available manufacturer products, hence, pressure oscillations are still observed. Nevertheless, the two-pump EHA system presents a more stable pressure dynamics through the working cycle.

With the motion tracking performance established as operating within satisfactory limits, the energy efficiency analysis would provide an interesting perspective to the systems.

5.6.2 Energy Efficiency (Without Considering Energy Regeneration)

To analyze the three actuators without energy regeneration, the lifting phase and holding phase of the third cycle (30 to 39 seconds) are considered and illustrated in **Figure 5.15**.

A common feature in all the configurations is the increased pump loses during the holding stage. It is worthy to note that fixed displacement units contribute significantly to system losses and poor energy balance due to their drawback of consuming energy under stationary load and are therefore not recommended for low-speed operations [1]. However, they continuously run to maintain fluid circulation at low speeds for holding load and this renders them very inefficient at the holding phase [8].

Overall, the electrical losses are higher in the EHAs compared to the conventional system due to the fact that the motor in the conventional system is operated closer to its nominal speed whiles the motors in the EHAs are operated usually at lower speeds.

The valve-controlled actuator input seen in **Figure 5.15**, seems to be very high compared to the EHAs and the cylinder output. This is only a representation of an integral, which increases with respect to time. Since the analysis was performed for the third cycle (30 to 45 seconds), the reference of the graph is taken from time *t=30* hence the actual values of energy consumption are given in **Table 5.16**.

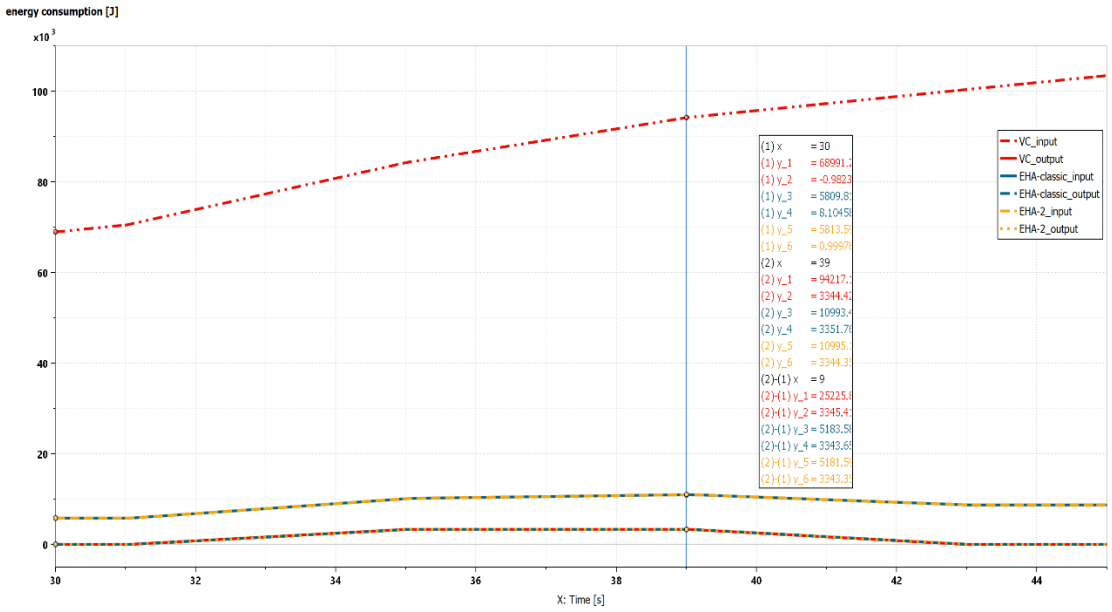

Figure 5.15: *Energy analysis without regeneration*

The numerical results from **Figure 5.15** are summarized in the table below.

Table 5.16: *System energy efficiency without regeneration*

	VC	**EHA-classic**	**EHA-2**
Energy input (kJ)	25,23	5,18	5,18
Energy output (kJ)	3,35	3,34	3,34
Efficiency (%)	13,28	64,51	64,51

The results show that the valve-controlled system is characteristically inefficient compared to the EHA systems (**Table 5.16**). The EHA configurations display an improved efficiency, five times better than the conventional system.

It suffices to say that the secondary pump in a two-pump EHA system can be utilized to achieve a more the stable pressure dynamics than a single-pump EHA, without compromising the efficiency and performance significantly. The downside of the two-pump EHA will obviously be the cost investment and space requirements.

Figure 5.16 demonstrates the Sankey diagrams measured for the three actuators during the lifting and holding stages of the work cycle. The electrical losses in **Figure 5.16** represent the inverter and motor losses. The motor losses constitute iron losses, core losses, winding losses and mechanical losses. The pump losses include the shaft and hydraulic losses, as well as the pipe friction losses incorporated into the system leakages. Cylinder losses are mostly influenced by frictional losses as a result of the seal, temperature and direction of motion. The accumulator losses in the EHA systems are a result of energy dissipated during flow balancing.

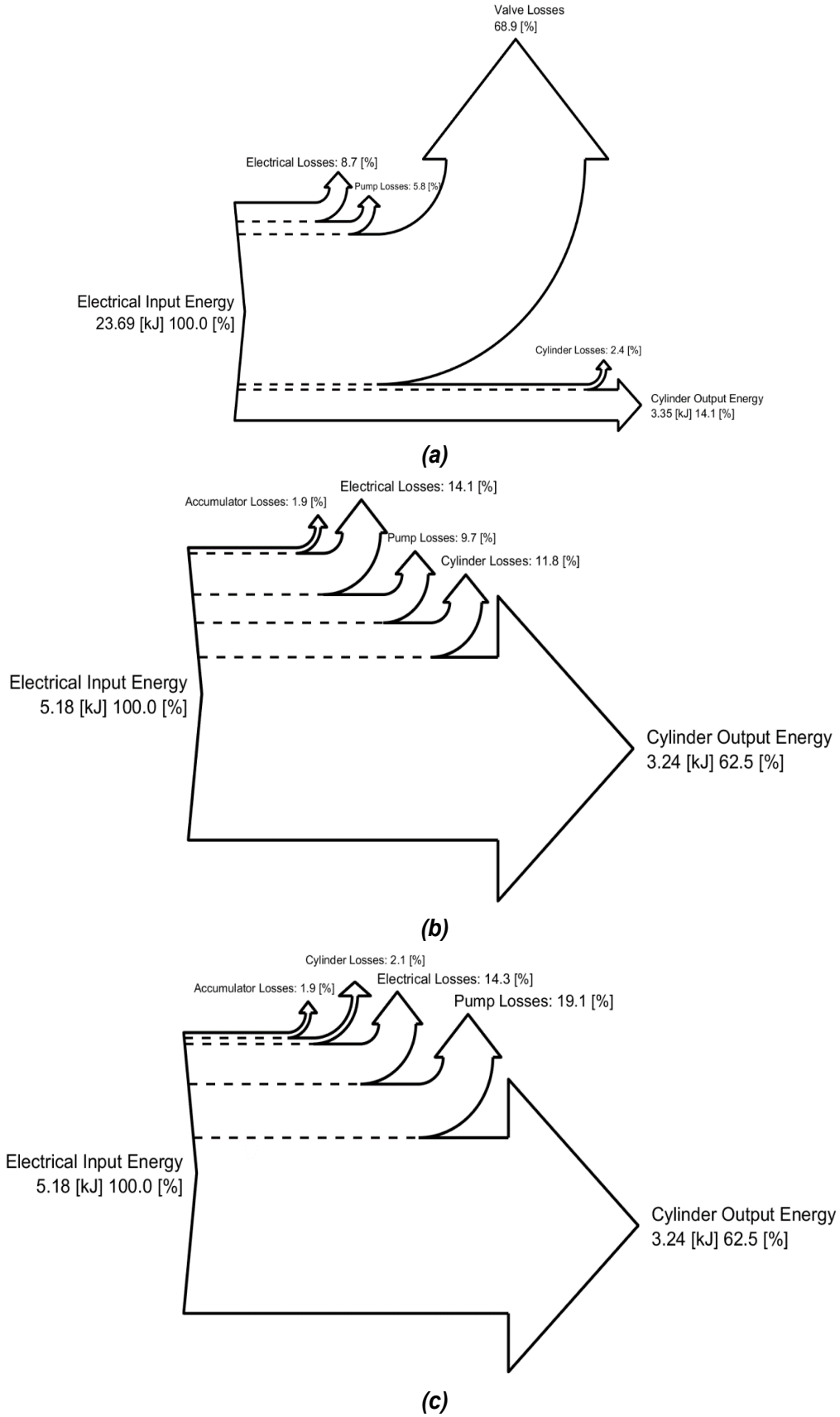

Figure 5.16: *Sankey diagram for lifting and holding stages of the work cycle at maximum load* ***(a)*** *Valve-controlled actuator* ***(b)*** *Classic EHA* ***(c)*** *Two-pump EHA*

5.6.3 Energy Efficiency (Considering Energy Regeneration)

This study has not included energy regeneration systems in the models, yet, the phenomenon of negative power observed in the electric drive compels a study of the energy regeneration capabilities in the systems.

The potential for energy recovery in the valve-controlled system was not observed at the electric drive but only from the actuator during load lowering. For the model used in this system, the recovered energy from the actuator is throttled in the proportional valve and dissipated as heat. To realize a more efficient valve-controlled system, the proposed energy recovery system by Imura et al [17], for example, could be considered to recover a fraction of the energy regenerated in the actuator.

More interesting is the energy recovery potential observed in the EHA systems. The energy recovered in the actuator significantly reduces the overall consumption from the electric motor. This is demonstrated in **Figure 5.17**. From the classic and two-pump EHA plots in **Figure 5.17**, the consumption drops between 39 to 43 seconds (load lowering) and this reduces total consumption at the end of the working cycle. The valve-controlled actuator continuously consume energy from the motor during load lowering.

The effect of the integral is again observed here as explained in section **5.6.2**. The VC energy consumption is seen to be extremely higher than the EHAs, but the actual consumption has reference from time *t=30*.

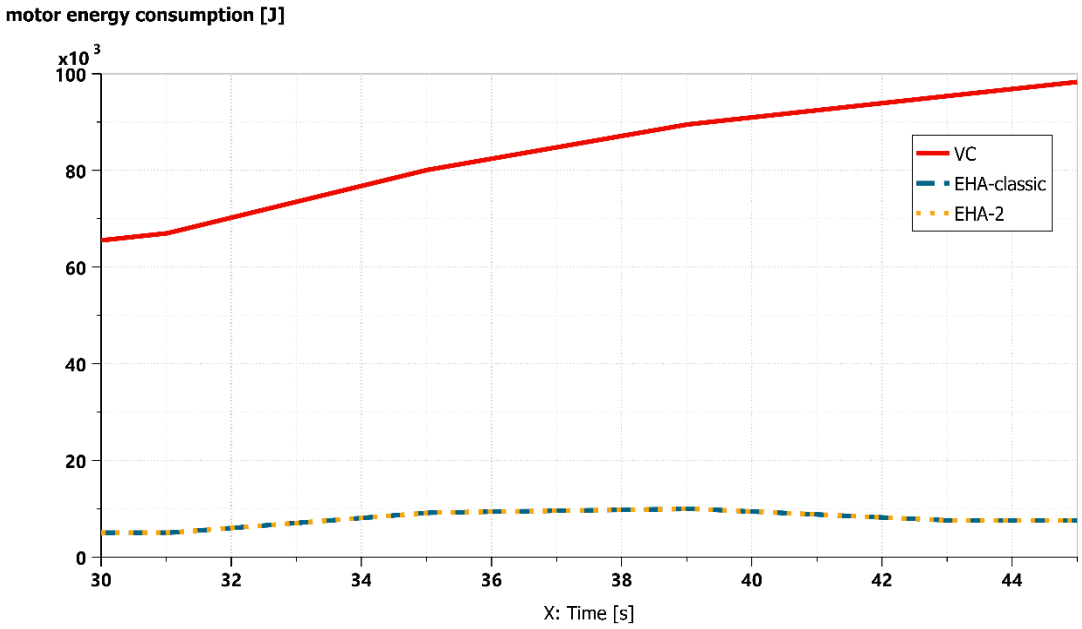

Figure 5.17: *Overall motor consumption during third cycle*

Table 5.17 summarizes the overall consumption of the electric drive during the entire working cycle. The EHA systems consume only 9% of the total energy required by the

valve-controlled system, due to their energy regeneration capabilities(**Table 5.17**). This contributes to significant energy savings and essentially, cost savings during system sizing.

The effective cylinder consumption in **Table 5.17** is due to the regenerative capability of the actuator in a case where energy recuperation is available. In all the systems, the cylinder is capable of regenerating energy close to what it consumes.

Table 5.17: *Effective system input and output energy*

	VC	**EHA-classic**	**EHA-2**
Total System Consumption (kJ)	28,42	2,55	2,55
Overall Cylinder Consumption (kJ)	0,01	0,05	0,05

5.7 Further Analysis of the EHA Systems

Given that the two-pump EHA system operates with two pumps, one would expect the total consumption to be much higher compared to the classic EHA. On the contrary, the simulation results presented so far in this chapter prove otherwise. It was observed that the performance and energy efficiency of the two-pump EHA was similar to the classic EHA system. This phenomenon is specific to the boom crane application operating in two quadrants. As explained in section **4.4**, the piston-side chamber is always the pressurized side and thus, the secondary pump connected to the rod-side chamber operates under low-pressure. Consequently, the efficiency of the secondary pump does not significantly affect the total consumption and system efficiency.

To further build on this phenomenon, the two-pump EHA system model shall be considered under two special cases: four-quadrant operation and cylinder-pump ratio mismatch.

5.7.1 Four-quadrant Operation of EHA systems

To further explore the differences between the classic and two-pump EHA systems, their operation in the third and fourth quadrant are analyzed (**Figure 5.18**). The highlighted quadrants Q3 and Q4, in **Figure 5.18**, are only considered for the analysis in this section. In these quadrants, the load force resists the piston motion during retraction (Q3) and during extension, the load force becomes assistive (Q4). The pressurized side of the

actuator is always the rod-side chamber in these modes of operation, shown by the thicker lines.

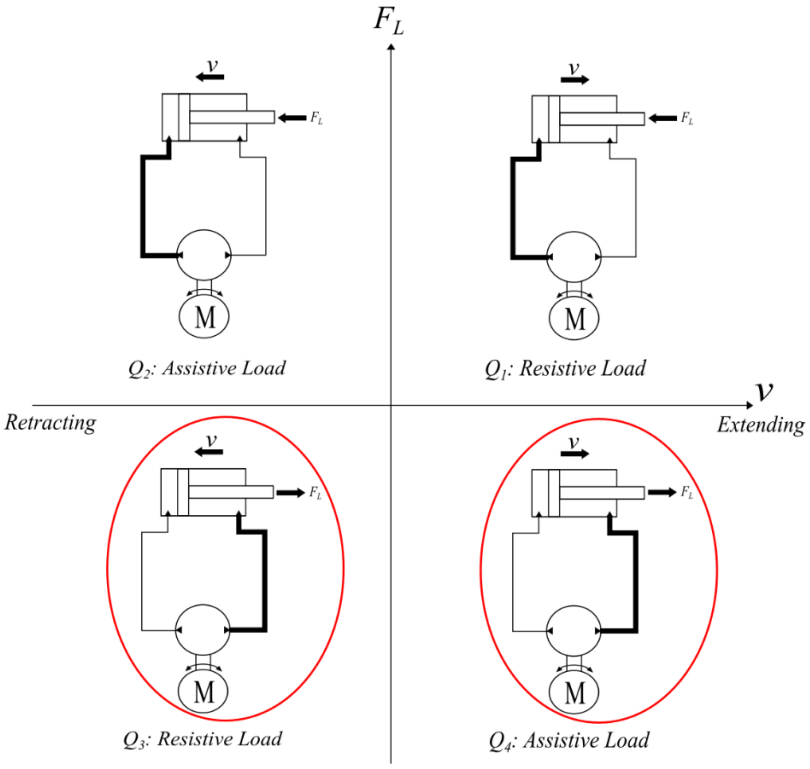

Figure 5.18: *Four-quadrant operation of the EHA systems with analyzed quadrants highlighted*

The following results show simulations performed for the negative load force acting on the cylinder. Figure 5.19**(a)** and **(b)** show the low-pressure piston-side and pressurized rod-side chambers respectively for quadrants 3 and 4, when the load force is negative. The spikes and oscillations are observed in these quadrant operations for the classic EHA system, as was seen in the positive load force condition (section **5.4**).

The position tracking performance of the EHA systems is much improved here for the lifting and holding stages, when compared to the positive load force conditions (Figure 5.19**(c)**). Moreover, the classic EHA system has about 30% better accuracy for these conditions than the two-pump EHA system (**Table 5.18**).

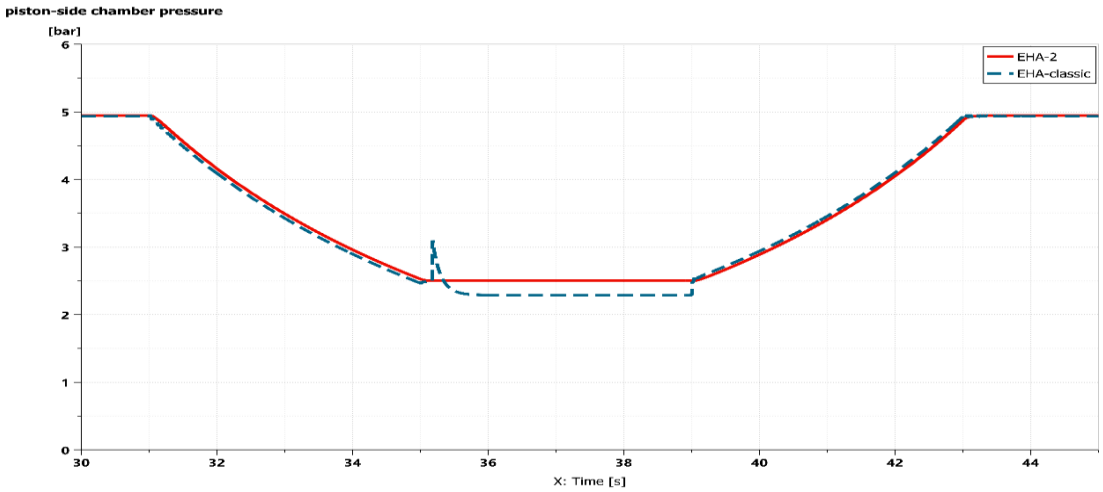

(a)

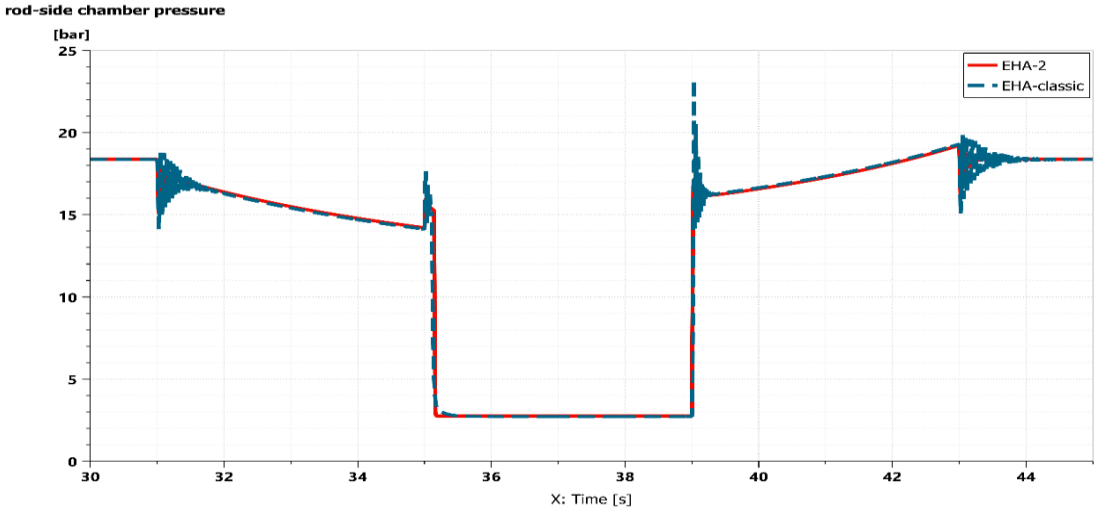

(b)

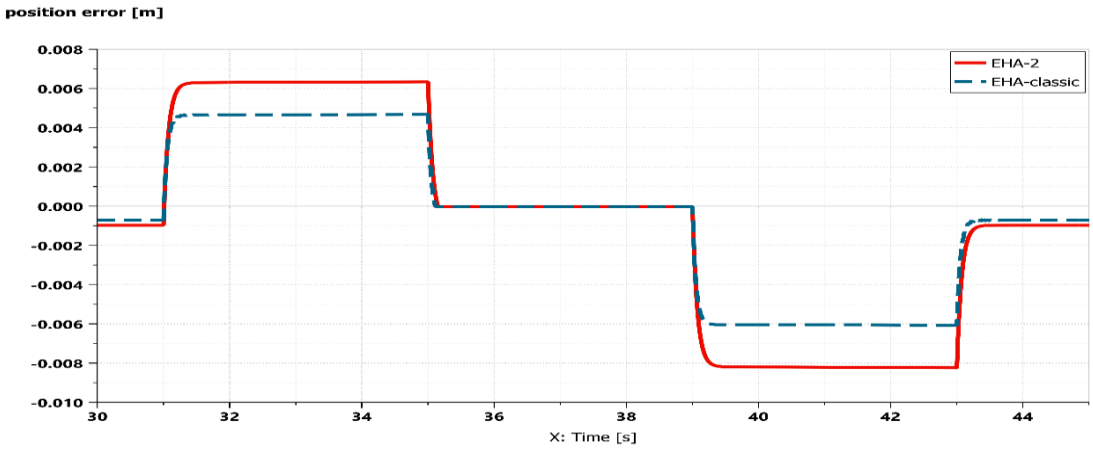

(c)

Figure 5.19: *Motion dynamics of EHA systems for negative load force* ***(a)*** *piston-side chamber pressure* ***(b)*** *rod-side chamber pressure* ***(c)*** *position tracking error*

Table 5.18: *Absolute position error for negative load force condition*

System	Absolute position error at different stages (mm)		
	Lifting	**Holding**	**Lowering**
EHA-classic	4,67	0,00	6,07
EHA-2	6,34	0,00	8,24

In contrast to the positive load force condition, the potential for energy regeneration for negative load force was observed in quadrant 4 when the piston was extending under an assistive load force, between 31 and 35 seconds (**Figure 5.20**). The classic EHA's pump (Figure 5.20**(a)**) and pump2 of the two-pump EHA (Figure 5.20**(b)**) operates in motoring mode to generate energy which can be recovered, hence the negative motor power.

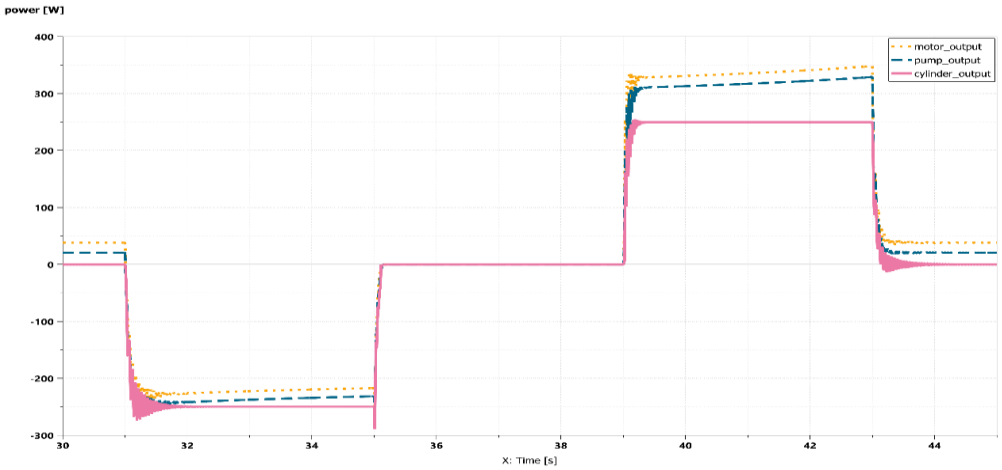

(a)

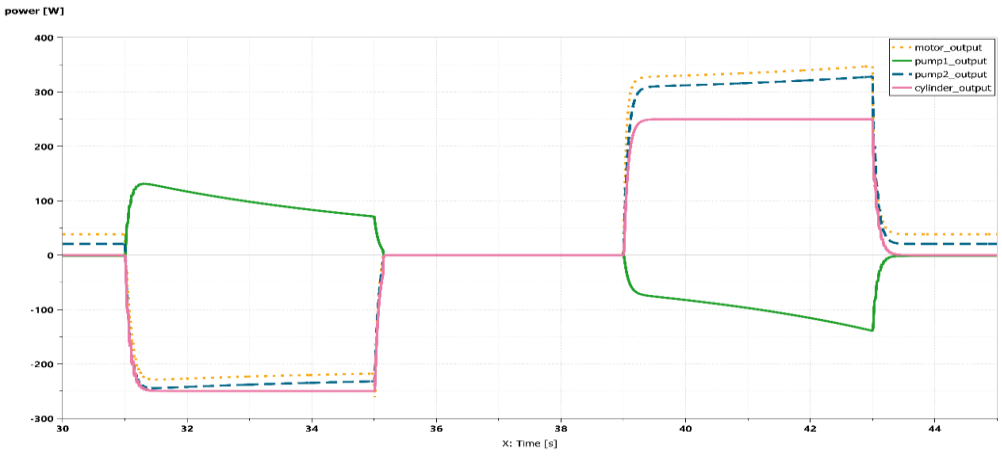

(b)

Figure 5.20: *Power distribution for negative load force (a) classic EHA (b) two-pump EHA*

Figure 5.21 shows the total input and output energy of the classic EHA and two-pump EHA systems. The input energy for the two systems show some obvious differences, contrary to the observation made in the positive load force simulation. The energy consumptions are compared in **Table 5.19**. From the **Figure 5.21**, the input energy appears wide apart from the output energy, as though their difference represents energy loss. Also, the input and output energy appear in the different halves of the graph. But this is only a result of showing the third cycle operation. The reference of the input energies are taken with respect to the initial values at time *t=30*, thus the numerical results are presented in **Table 5.19**.

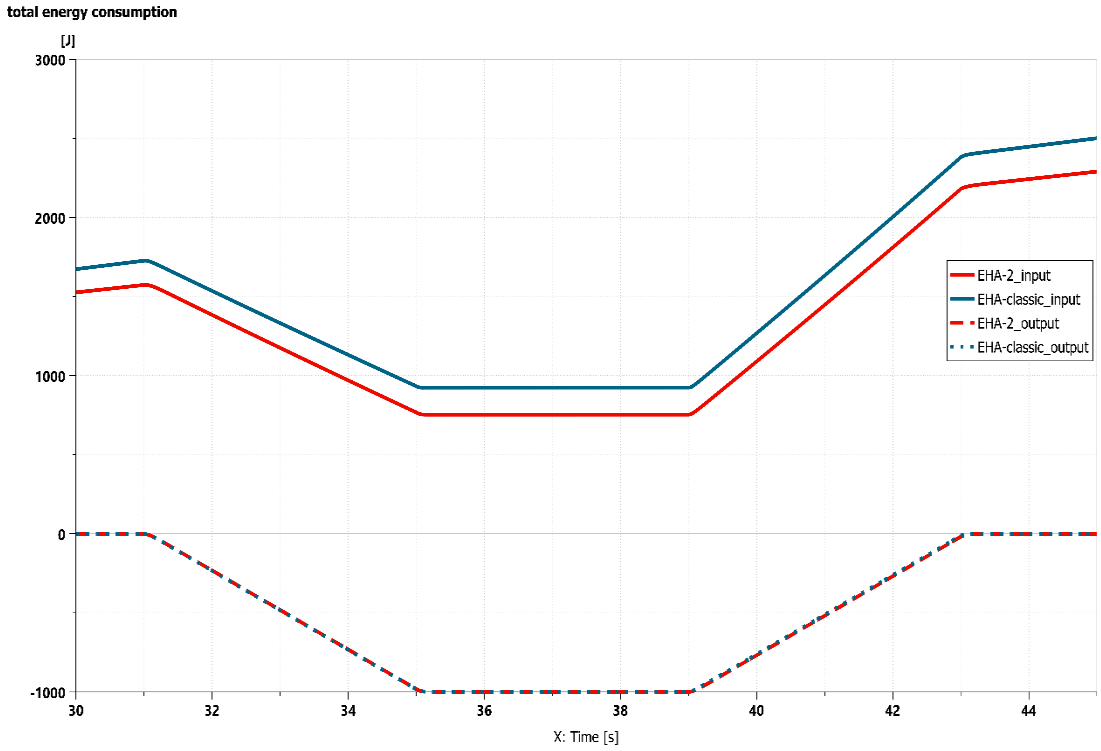

Figure 5.21: *Total energy consumption for negative load force*

The energy consumption for the negative load force condition is about 70% lower than the positive load force conditions for both EHA systems (**Table 5.19**). This is observed partly due to lower pressure in the cylinder chambers for the negative load condition (**Figure 5.19**) compared to the positive load conditions (**Figure 5.9**) at the same load mass. Moreover, the total force acting on the actuator under positive-load conditions is the sum of the boom force and the force exerted by the mass. Whereas in negative-load conditions, the total force on the actuator is the difference between the boom force and force exerted by the mass, resulting in a lower net force. Thus, less torque is generated by the electric motor to move the actuator under negative load conditions. Consequently, lower energy is consumed.

The classic EHA consumes 2.5% more energy than the two-pump EHA, yet it is 1.6% less efficient than the two-pump EHA. This is explained by the dominant operation of the secondary pump in the two-pump EHA under negative-load conditions. For the two-pump EHA working under negative load conditions, the secondary pump on the high-pressure side generates the power needed for motion while the main pump operates under low pressure. Due to the small size of the secondary pump, it is more efficient than the main pump in the classic EHA system, and thus, the efficiency of the two-pump EHA is better than the classic EHA. Moreover, 2% more energy can be recovered in the two-pump EHA system than the classic EHA system.

Table 5.19 represent the actual consumption within the given period (30 to 45 seconds).

Table 5.19: *Comparing energy distribution in classic and two-pump EHA systems*

	EHA-classic	**EHA-2**	**Percentage Difference (%)**
Energy Input during lowering (kJ)	1,58	1,54	2,53
Energy output during lowering (kJ)	0,99	0,99	0,00
Energy Efficiency without regeneration (%)	62,66	64,29	1,63
Energy Regenerated during lifting (kJ)	-0,99	-0,99	0,00
Energy Recovered at electric motor (kJ)	-0,80	-0,82	2,50
Energy recovered (%)	80,81	82,83	2,02

In effect, the classic EHA system has better position tracking accuracy (30%) and marginally worse efficiency (only 2%) than the two-pump EHA system. The better EHA configuration among the two presented in this thesis largely depends on the application in question. For applications which require high accuracy, the classic EHA is obviously the better choice.

Nevertheless, in HDMM applications, accuracy is not of major concern especially since the two-pump EHA system provides a satisfactory level of accuracy as well. Efficiency and cost-savings are among the major determining factors for system configuration selection in HDMM applications. For that matter, in low-pressure applications where a few spikes do not pose high-risk dangers, the classic EHA would be a cost-effective choice. In high-pressure applications, the spikes evident in the classic EHA pressure dynamics might prove hazardous for the system and system operators. As such, the secondary

pump's capability of eliminating pressure spikes in the two-pump EHA system would prove to be a better selection for safety concerns.

5.7.2 Effect of Unbalanced Flows on the Two-pump EHA system as a Result of Cylinder Asymmetry

To further understand the dynamics of the two-pump EHA system, the effect of pump-cylinder ratio is examined by varying the rod size of the cylinder to achieve different chamber area ratios of the cylinder. This analysis is performed to investigate practical applications where exact cylinder-pump ratio cannot be established due to available components. The initial cylinder used so far in this thesis has a chamber area ratio of 0,75 which closely matches the pump displacement ratio of 0,74 (section **4.1.2**). The study is applied to a scenario where cylinder ratio is 20% more and 20% less of the simulated two-pump EHA system. The piston rod is sized to achieve three cylinder ratio cases compared to the 0.74 pump displacement ratio: overmatched system with cylinder ratio of 0.9, ideal system with cylinder ratio of 0.75 and undermatched system with 0.6 cylinder ratio. The response of the overmatched and undermatched systems was investigated and compared to the results obtained for the two-pump EHA with ideal ratios.

Due to the increased asymmetrical flow induced by the increased piston rod area in the case of the undermatched cylinder system, the hydraulic accumulator volume of the model was increased to compensate the increased flow imbalance adequately. This was necessary to prevent low-pressures in the rod-side chamber during the holding stage. The hydraulic accumulator volume was increased to the same volume in all the three cases to ensure a fair comparison.

The pressure response in the ideal system was most stable through the work cycle. The overmatched system displayed a higher chamber pressures during the lifting stage (31 to 35 seconds) due to the decrease rod area (Figure 5.22**(a)** and **(b)**). During the lowering stage between 39 to 43 seconds, piston and rod-side chamber pressures are both higher in the undermatched system compared to the other two systems mainly because of the increased unbalanced flow (Figure 5.22**(a)** and **(b)**). The rod-side pressure is significantly 65% higher during the lowering stage in the undermatched system mainly because of reduced rod-side chamber area (Figure 5.22**(b)**). The undermatched cylinder system maintained about 1% better position accuracy than the ideal and overmatched cylinder system through the working cycle (Figure 5.22**(c)**). The overmatched system position accuracy was less than 1% worse compared to the ideal system for both lifting and holding stages. **Table 5.20** summarizes the effect of cylinder chamber ratio on the position performance of the two-pump EHA system.

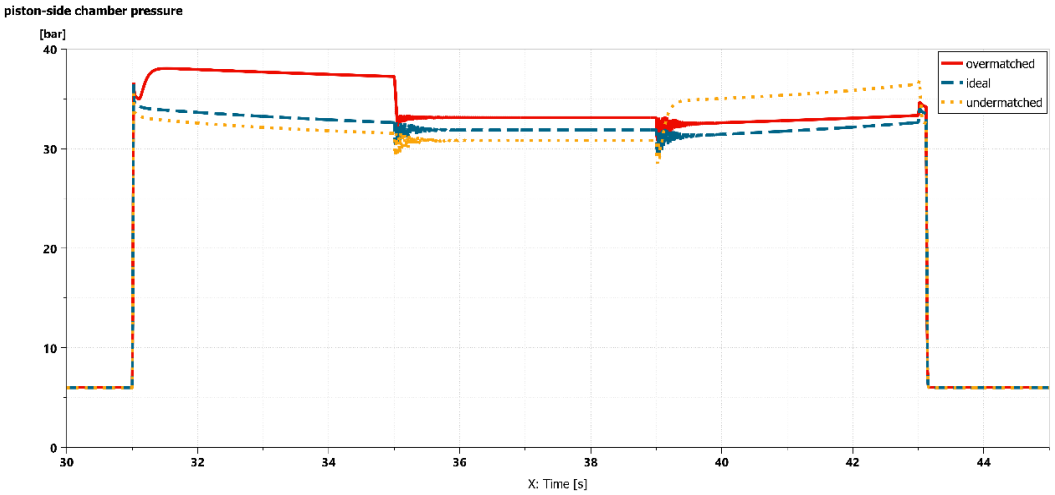

(a)

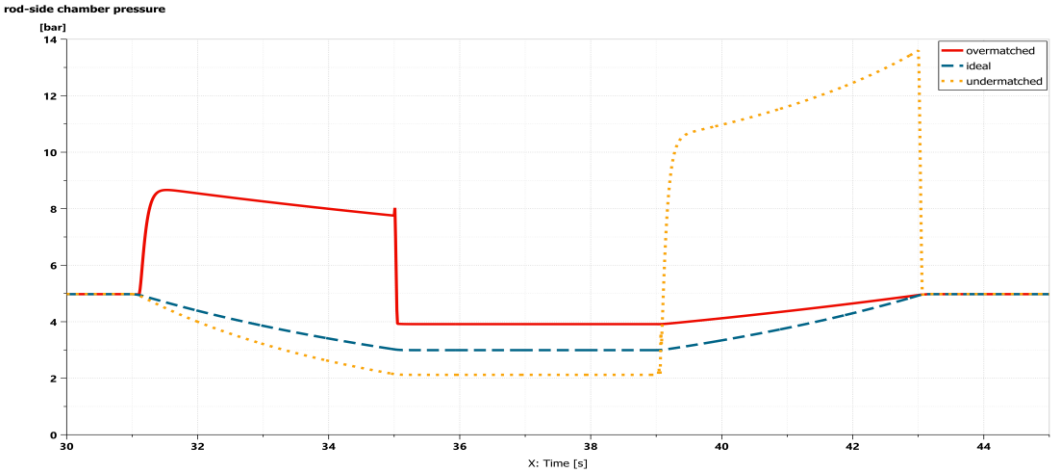

(b)

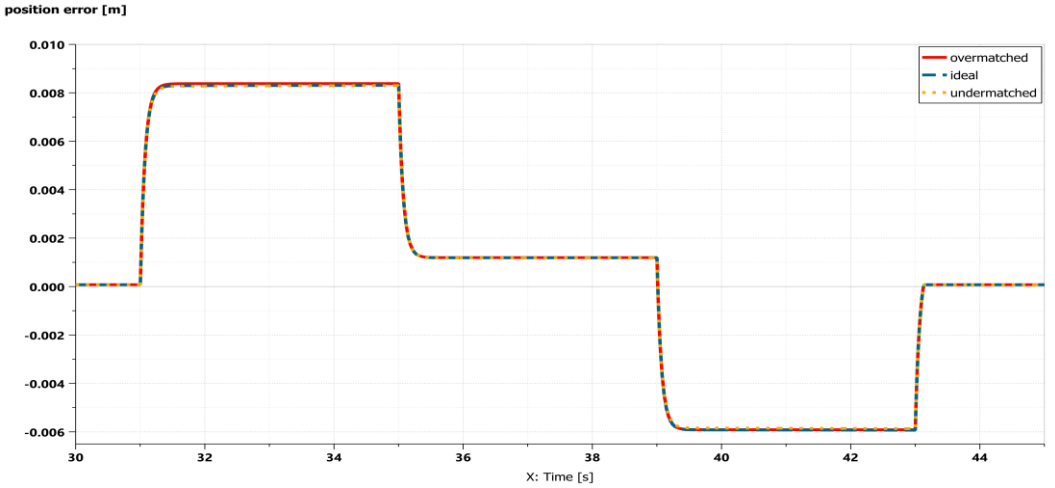

(c)

Figure 5.22: *Effects of chamber area ratio on motion dynamics of two-pump EHA system (a) piston-side chamber pressure (b) rod-side chamber pressure (c) position tracking error*

Table 5.20: *Absolute position of mismatched cylinder chamber ratio*

System	Absolute position error at different stages (mm)		
	Lifting	**Holding**	**Lowering**
Overmatched Cylinder	8,38	1,20	5,91
Ideal Cylinder	8,31	1,19	5,93
Undermatched Cylinder	8,30	1,18	5,87

In **Figure 5.23**, the power distribution for the motor, pumps and cylinder are presented for the three different cylinder ratio cases. The secondary pump (pump2) works in motoring mode during lifting and holding stages. The main pump (pump1) in the overmatched system operates close to the power level of the motor output as a result of higher power generated in pump2 (Figure 5.23**(a)**). The increased flow from the rod-side chamber due to the larger area contributes to a higher generated power when pump2 operates as a motor, which increases the power delivered to pump1. The pump2 in the ideal and undermatched system generate lower power in motoring mode.

However, the pump output from the ideal and undermatched system is efficiently utilized as shown by the cylinder output power (Figure 5.23 **(b)** and **(c)**)This is also attributed to the lower power generated in pump2, resulting in lower power delivered to pump1 and consequently lower pump1 output compared to the overmatched system.

In Figure 5.23**(c)**, pump2 output power is highest in the undermatched system due to increased pressure caused by the smaller rod-side area. The effect of this is seen in the increased pump1 power generated during motoring mode (39 to 43 seconds).

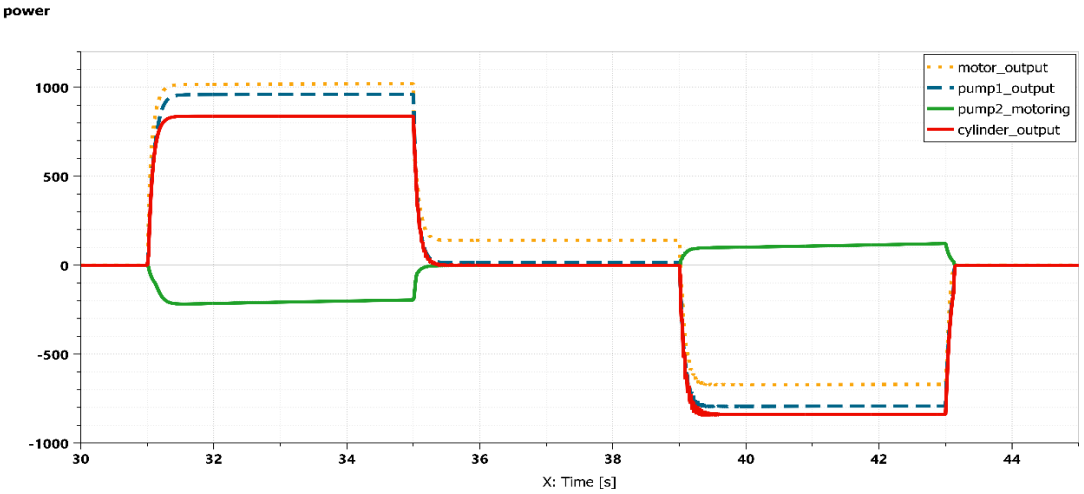

(a)

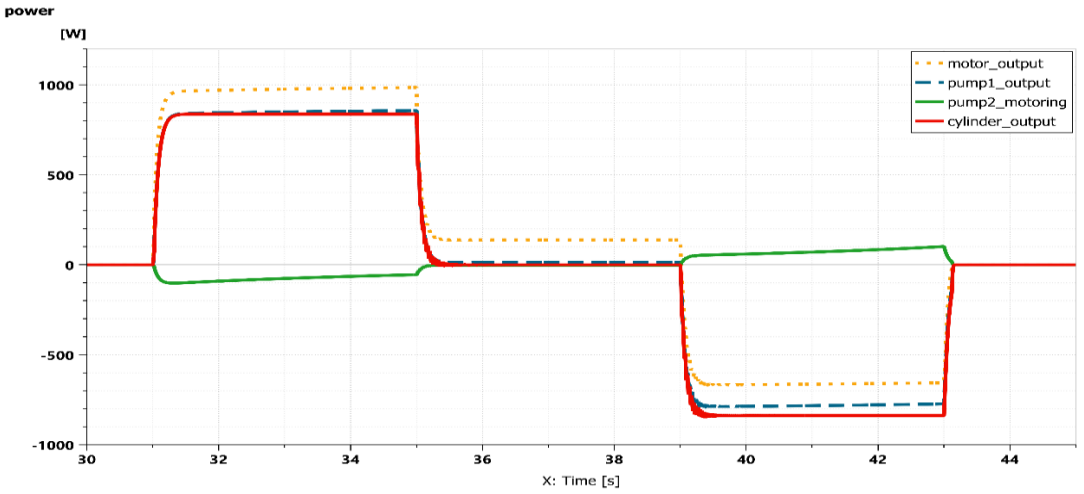

(b)

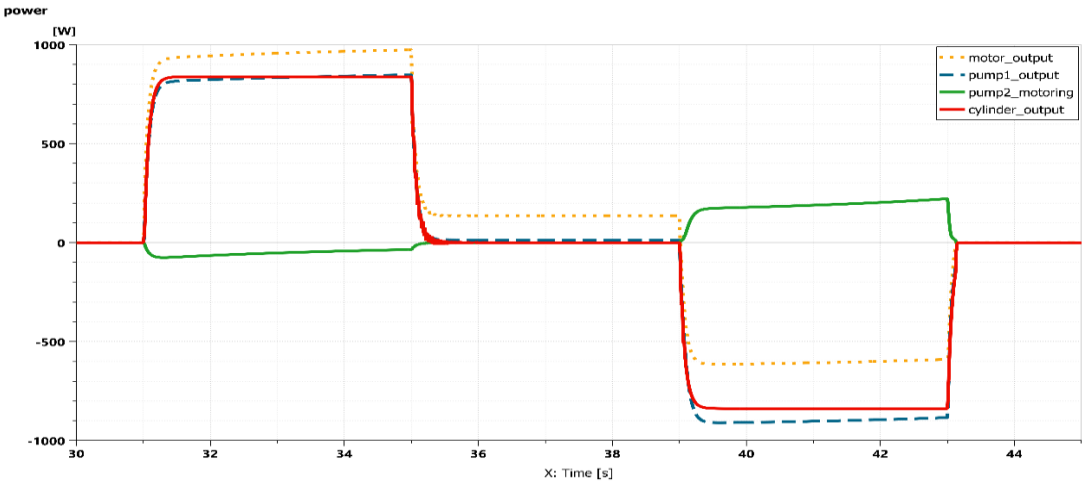

(c)

Figure 5.23: *Effects of chamber area ratio on power distribution (a) overmatched cylinder (b) ideal cylinder (c) undermatched cylinder*

The undermatched cylinder system shows less than 2% better energy efficiency than the ideal and overmatched system during lifting and holding (**Figure 5.24**). However, over 5% more energy is recovered in the ideal and overmatched system during the lowering stage, than the undermatched system. Overall, the efficiency of the ideal system is the best among the three systems when energy regeneration is considered (**Table 5.21**).

The difference between the input and output energies seen in **Figure 5.24** do not exactly represent the system losses. The input and output energies are integrals and their reference, when considered from time *t=30*, provide the accurate energy consumptions summarized in **Table 5.21**.

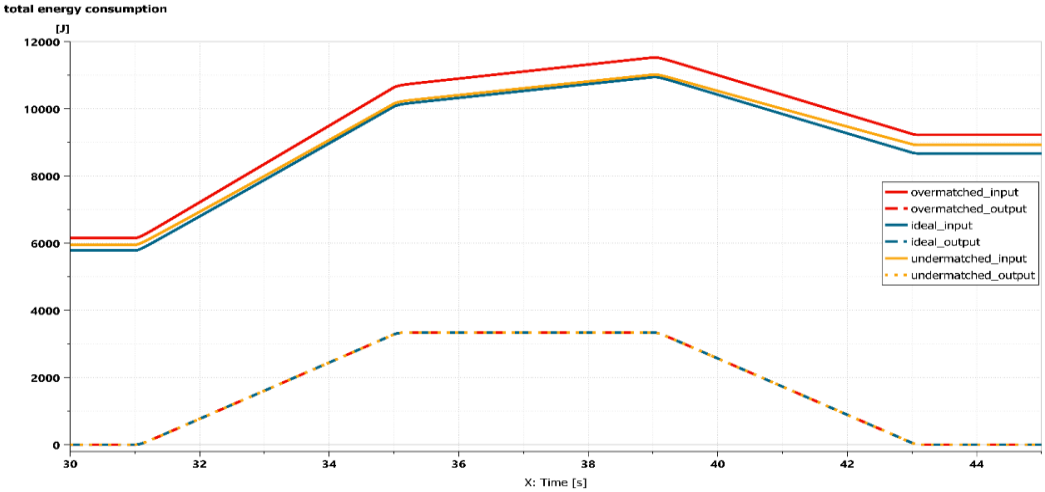

Figure 5.24: *Effects of chamber area ratio on total energy consumption in two-pump EHA systems*

Table 5.21: *Comparing energy distribution in a matched and mismatched area ratio for two-pump EHA system*

	Overmatched Cylinder	Ideal Cylinder	Undermatched Cylinder
Energy Input during lifting and holding (kJ)	5,38	5,16	5,07
Energy Output during lifting and holding (kJ)	3,34	3,34	3,34
Energy Efficiency without regeneration (%)	62,08	64,73	65,88
Energy Regenerated during lowering (kJ)	-3,29	-3,29	-3,29
Energy Recovered at electric motor (kJ)	-2,28	-2,25	-2,07
Energy recovered (%)	69,30	68,39	62,92

The better efficiency observed in the undermatched system can be explained when the energy dissipation in the hydraulic accumulator is considered. **Figure 5.25** shows the gas volume of the hydraulic accumulator discharged to compensate the unbalanced flow. It is seen that a high volume is discharged in the undermatched system to compensate the unbalanced flow due to the larger rod-side chamber area. The high flow from the hydraulic accumulator boosts the energy efficiency of the undermatched system significantly, thus, the improved efficiency shown in the results.

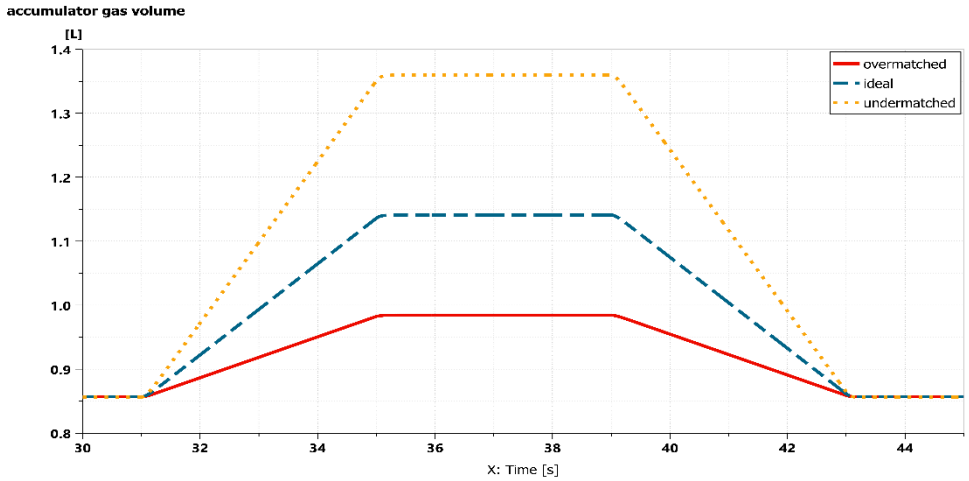

Figure 5.25: *Hydraulic accumulator gas volume discharged for flow compensation during work cycle*

Practically, this means that the hydraulic accumulator utilized in ideal and overmatched systems can be significantly downsized to achieve similar energy efficiency achieved in the undermatched system.

The analyses of the two-pump EHA systems provided in this section **5.7.2** has shown that, an ideal matching of the cylinder area ratio and pump displacement ratio produces a better pressure response in the system, with comparable energy efficiency and better energy regeneration capabilities.

6. CONCLUSIONS

The closed-loop position tracking performance and energy efficiency of three different actuators as applied to a mobile boom crane have been studied in this thesis. The actuators studied in this thesis were valve-controlled, classic one-pump and two-pump electro-hydrostatic actuators. The systems consist of hydraulic, electrical and mechanical components which have been modified and parameterized based on an existing experimental test rig, available product data and information found in literature.

The system configurations have been modelled and studied in Simcenter AMESIM. The model verification was considered with static load, with the pressure and displacement results being identical to mathematical data.

It was observed from the simulation results that, the motion performance was satisfactory for all the three actuator systems, with 2% maximum tracking error. The conventional valve-controlled system maintained a better tracking accuracy (less than 1% maximum tracking error) in all load conditions compared to both EHAs.

The classic EHA system exhibited more prominent chamber pressure spikes and oscillations compared to the two-pump EHA system. The effect of the secondary pump in the two-pump system for flow balancing has been justified in this study since the oscillations are significantly reduced in the cylinder chambers. Spikes were also observed in the chamber pressure dynamics of the conventional system. Overall, the two-pump EHA presented better pressure dynamics than the classic EHA and conventional system. This means the two-pump EHA system is better suited for high-pressure applications where pressure spikes pose risks for system operations and operators.

The efficiency analysis strongly underlines the inefficiency of the valve-controlled actuator, mainly due to throttling losses. Pump-controlled systems, with two different configurations, were studied and both showed much improved energy efficiency and a significant reduction in energy consumption compared to their valve-controlled counterpart. What this means is that, the prime mover of the actuator can be significantly downsized to as low as 20% of that required by the valve-controlled system for the same application where energy regeneration is not considered, resulting in significant cost-savings.

For the boom crane applications explored in this thesis, the two pump-controlled systems did not exhibit much differences due to the two-quadrant operation of boom cranes. A four-quadrant analysis was further performed for the EHAs to study their differences in

detail. The classic EHA system demonstrated 30% better position accuracy, and yet a marginal 2% worse energy efficiency than the two-pump EHA system.

Finally, even though these pump-controlled solutions provide improved energy efficiency compared to the current state-of-the-art actuators for mobile machine applications, results show significant losses in pumps, actuating cylinder and hoses. These losses offer a potential for energy savings, which motivate further research into more efficient systems. Considering the electrical losses in the actuator system (constituting only about 10% of total system energy) and efficiency of the EHAs during a lifting phase (64% of total system energy), the remaining percentage energy lost in the system is attributed to hydraulic losses. Moreover, significantly higher hydraulic losses were recorded during the holding phase (close to 65%). For that matter, electromechanical actuators would offer a potential for eliminating these hydraulic losses and further improving the system efficiency provided they can match the power density of hydraulic actuators.

6.1 Future Work

In order to obtain a more practical and viable system, the simulation models could be improved to capture more details about system performance and repeatability. Simulation tests were performed with a static load and thus, experimentation with dynamic load would be recommended to represent practical operational conditions. The simulation model did not take into account thermal effects and a more accurate friction model. The control system employed could also be developed to ensure robustness and better accuracy. Better system pressure dynamics could be achieved if the control system is designed with pressure feedback.

Different configurations of the electro-hydrostatic actuator system could be studied, and their dynamics evaluated. For instance, a two-pump-two-motor configuration can increase the flexibility of the system, especially in terms of controllability as it employs separate electric drives for each pump. Obviously, increased components would also mean high investment cost and a less compact system in terms of production. Nevertheless, different configurations would be worth a study.

REFERENCES

[1] J. Lodewyks and P. Zurbrügg, “Decentralized energy-saving hydraulic concepts for mobile working machines,” *10th Int. Fluid Power Conf.*, pp. 79–90, 2016.

[2] W. Cao, B. C. Mecrow, G. J. Atkinson, J. W. Bennett, and D. J. Atkinson, “Overview of electric motor technologies used for more electric aircraft (MEA),” *IEEE Trans. Ind. Electron.*, vol. 59, no. 9, pp. 3523–3531, 2012, doi: 10.1109/TIE.2011.2165453.

[3] J. C. Maré and J. Fu, “Review on signal-by-wire and power-by-wire actuation for more electric aircraft,” *Chinese J. Aeronaut.*, vol. 30, no. 3, pp. 857–870, 2017, doi: 10.1016/j.cja.2017.03.013.

[4] H. Çalışkan, T. Balkan, and B. E. Platin, “A Complete Analysis for Pump Controlled Single Rod Actuators,” *10th Int. Fluid Power Conf.*, no. March, pp. 119–132, 2016, doi: 10.13140/RG.2.2.13163.75046.

[5] “Volvo CE Unveils 100% Electric Compact Excavator Prototype.” https://www.volvoce.com/global/en/news-and-events/press-releases/2017/volvo-ce-unveils-100-percent-electric-compact-excavator-prototype/ (accessed Sep. 11, 2020).

[6] M. G. Antonelli, G. Bucci, F. Ciancetta, and E. Fiorucci, “Automatic test equipment for avionics Electro-Mechanical Actuators (EMAs),” *Meas. J. Int. Meas. Confed.*, 2014, doi: 10.1016/j.measurement.2014.08.005.

[7] J. Fu, J. C. Mare, L. Yu, and Y. Fu, “Multi-level virtual prototyping of electromechanical actuation system for more electric aircraft,” *Chinese J. Aeronaut.*, vol. 31, no. 5, pp. 892–913, 2018, doi: 10.1016/j.cja.2017.12.009.

[8] K. Søren, D. Padovani, T. O. . Andersen, M. K. Ebbesen, and L. Schmidt, “Classification and Review of Pump-Controlled Differential Cylinder Drives,” pp. 1–27, 2019, doi: 10.3390/en12071293.

[9] D. Hagen, D. Padovani, and M. Choux, “A Comparison Study of a Novel Self-Contained Electro-Hydraulic Cylinder versus a Conventional Valve-Controlled Actuator—Part 1: Motion Control,” *Actuators*, vol. 8, no. 4, p. 79, 2019, doi: 10.3390/act8040079.

[10] Z. Quan, L. Quan, and J. Zhang, “Review of energy efficient direct pump controlled

cylinder electro-hydraulic technology," *Renew. Sustain. Energy Rev.*, vol. 35, pp. 336–346, 2014, doi: 10.1016/j.rser.2014.04.036.

[11] S. Zhang, T. Minav, M. Pietola, H. Kauranne, and J. Kajaste, "The effects of control methods on energy efficiency and position tracking of an electro-hydraulic excavator equipped with zonal hydraulics," *Autom. Constr.*, vol. 100, no. December 2018, pp. 129–144, 2019, doi: 10.1016/j.autcon.2019.01.003.

[12] N. Alle, S. S. Hiremath, S. Makaram, K. Subramaniam, and A. Talukdar, "Review on electro hydrostatic actuator for flight control," *Int. J. Fluid Power*, vol. 17, no. 2, pp. 125–145, 2016, doi: 10.1080/14399776.2016.1169743.

[13] T. A. Minav, J. E. Heikkinen, and M. Pietola, "Electric-driven Zonal Hydraulics in Non-Road Mobile Machinery," in *New Applications of Electric Drives*, M. Chomat, Ed. Rijeka: IntechOpen, 2015.

[14] L. Schmidt, D. Roemer, H. Pedersen, and T. Andersen, *Speed-Variable Switched Differential Pump System for Direct Operation of Hydraulic Cylinders*. 2015.

[15] A. Lajunen, P. Sainio, L. Laurila, J. Pippuri-Mäkeläinen, and K. Tammi, "Overview of powertrain electrification and future scenarios for non-road mobile machinery," *Energies*, vol. 11, no. 5, 2018, doi: 10.3390/en11051184.

[16] A. Lajunen, J. Suomela, J. Pippuri, K. Tammi, T. Lehmuspelto, and P. Sainio, "Electric and hybrid electric non-road mobile machinery - Present situation and future trends," *EVS 2016 - 29th Int. Electr. Veh. Symp.*, vol. 8, pp. 172–183, 2016.

[17] S. Imura, H. Satake, K. Ishikawa, S. Hijikata, and T. Kaneta, "Patent Application Publication (10) Pub. No.: US 2015/0247305 A1," vol. 1, no. 19, 2015.

[18] A. Bonavolontà, C. Dolcin, P. Marani, E. Frosina, and A. Senatore, "Comparison of energy saving and recovery systems for hydraulic mobile machines," *AIP Conf. Proc.*, vol. 2191, no. December, 2019, doi: 10.1063/1.5138758.

[19] M. Huova, A. Aalto, M. Linjama, K. Huhtala, T. Lantela, and M. Pietola, "Digital hydraulic multi-pressure actuator–the concept, simulation study and first experimental results," *Int. J. Fluid Power*, vol. 18, no. 3, pp. 141–152, 2017, doi: 10.1080/14399776.2017.1302775.

[20] Q. Zhang, X. Kong, B. Yu, K. Ba, Z. Jin, and Y. Kang, "Review and development trend of digital hydraulic technology," *Appl. Sci.*, vol. 10, no. 2, 2020, doi: 10.3390/app10020579.

[21] H. C. Pederson, L. Schmidt, T. O. Anderson, and M. H. Brask, "Investigation of

New Servo Drive Concept Utilizing Two Fixed Displacement Units," *JFPS Int. J. Fluid Power Syst.*, vol. 8, no. 1, pp. 1–9, 2014, doi: 10.5739/jfpsij.8.1.

[22] J. Huang, H. Zhao, L. Quan, and X. Zhang, "Development of an asymmetric axial piston pump for displacement-controlled system," *Proc. Inst. Mech. Eng. Part C J. Mech. Eng. Sci.*, vol. 228, pp. 1418–1430, May 2013, doi: 10.1177/0954406213508385.

[23] G. Ren, G. K. Costa, and N. Sepehri, "Position control of an electro-hydrostatic asymmetric actuator operating in all quadrants," *Mechatronics*, 2020, doi: 10.1016/j.mechatronics.2020.102344.

[24] K. G. Cleasby and A. R. Plummer, "A novel high efficiency electrohydrostatic flight simulator motion system," *Proc. ASME/BATH Symp. Fluid Power Motion Control*, no. Fpmc 2008, pp. 437–449, 2008.

[25] G. Vael, P. Achten, and J. Potma, *Cylinder Control with the Floating Cup Hydraulic Transformer*. 2003.

[26] R. Rahmfeld, "Development and Control of Energy Saving Hydraulic Servo Drives for Mobile Systems," TUHH, 2002.

[27] T. G. Ling, M. F. Rahmat, and A. R. Husain, "ANFIS modeling of electro-hydraulic actuator system," *Proc. - 2012 IEEE 8th Int. Colloq. Signal Process. Its Appl. CSPA 2012*, pp. 89–92, 2012, doi: 10.1109/CSPA.2012.6194697.

[28] T. Minav, L. Papini, A. Jarf, K. Tammi, and M. Pietola, "Direct Driven Hydraulics: What can possibly go wrong? -A thermal analysis," *Proc. - 2016 22nd Int. Conf. Electr. Mach. ICEM 2016*, pp. 1618–1624, 2016, doi: 10.1109/ICELMACH.2016.7732740.

[29] L. Kai, L. Zhong, L. Kun, and Y. Ping, "Thermal-hydraulic modeling and simulation of piston pump in electro-hydrostatic actuator system," *Proc. 2015 Int. Conf. Fluid Power Mechatronics, FPM 2015*, pp. 1097–1101, 2015, doi: 10.1109/FPM.2015.7337282.

[30] A. Järf, T. Minav, and M. Pietola, "Nonsymmetrical Flow Compensation Using Hydraulic Accumulator in Direct Driven Differential Cylinder Application." Oct. 26, 2016, doi: 10.1115/FPNI2016-1516.

[31] T. Minav, J. E. Heikkinen, and A. V. Devyatkin, "Modes of failure in zonal hydraulics for construction machinery," *Proc. 2018 IEEE Conf. Russ. Young Res. Electr. Electron. Eng. ElConRus 2018*, vol. 2018-Janua, pp. 928–931, 2018, doi: 10.1109/EIConRus.2018.8317241.

[32] P. C. Palavicino, W. Lee, B. Sarlioglu, and T. Minav, “On Faults and Diagnostics in Electrified Hydraulic Actuator Systems,” *2018 20th Eur. Conf. Power Electron. Appl. EPE 2018 ECCE Eur.*, p. P.1-P.9, 2018.

[33] S. Danaee, T. Minav, and M. Pietola, “Sensorless Position Control for Electro-Hydraulic System-A technological status review,” *2018 Glob. Fluid Power Soc. PhD Symp. GFPS 2018*, pp. 1–6, 2018, doi: 10.1109/GFPS.2018.8472381.

[34] “Electrohydrostatic.” https://www.moog.com/products/actuators-servoactuators/actuation-technologies/electrohydrostatic.html (accessed Feb. 21, 2020).

[35] “Mecalac E12: A 100%-Electric Excavator for Urban Building Sites.” https://www.mecalac.com/en/e12-electric-wheel-excavator.html (accessed Sep. 13, 2020).

[36] “Yanmar Unveils its Exciting New eFuzion Concept at bauma.” https://www.yanmar.com/global/construction/news/2019/04/10/53748.html (accessed Sep. 13, 2020).

[37] J. Wang, Z. Yang, S. Liu, Q. Zhang, and Y. Han, “A comprehensive overview of hybrid construction machinery,” *Adv. Mech. Eng.*, vol. 8, no. 3, pp. 1–15, 2016, doi: 10.1177/1687814016636809.

[38] T. S. Kwon *et al.*, “Power control algorithm for hybrid excavator with supercapacitor,” *IEEE Trans. Ind. Appl.*, vol. 46, no. 4, pp. 1447–1455, 2010, doi: 10.1109/TIA.2010.2049815.

[39] H. Yao and Q. Wang, “Control strategy for hybrid excavator swing system driven by electric motor,” *IFAC Proc. Vol.*, vol. 46, no. 5, pp. 109–115, 2013, doi: 10.3182/20130410-3-CN-2034.00065.

[40] C. Bonato, “Position Control and Overall Efficiency of Electro-Hydraulic System,” Aalto University, 2014.

[41] A. Järf, “Flow compensation using hydraulic accumulator in direct driven hydraulic differential cylinder application and effects on energy effciency,” Aalto University, 2016.

[42] C. Bonato, T. A. Minav, P. Sainio, and M. Pietola, “Position Control of Direct Driven Hydraulic Drive.” Jun. 11, 2014, doi: 10.1115/FPNI2014-7823.

[43] Vivoil Oleodinamica, “Reversible Motors - XV Series,” 2009. https://www.vivoil.com/files/vivoil_m_en.pdf (accessed May 10, 2020).

[44] Emerson Industrial Automation, “Technical Data Unimotor fm and hd High performance AC brushless servo motors,” 2011. https://acim.nidec.com/drives/control-techniques/products/servo-drives/ac-servo-motors/unimotor-fm (accessed Mar. 25, 2020).

[45] Pikapaja Oy, “Miro Hydraulisylinterit,” 2009. http://www.pikapaja.fi/MIRO_cylinders_FIN+SWE.pdf (accessed May 10, 2020).

[46] Duplomatic Motion Solutions, “Hydraulic Cylinders HC2 Series 20,” 2014. https://www.duplomatic.com/assets/SchedeTecniche/GB/71000.pdf (accessed Mar. 20, 2020).

[47] Bosch Rexroth, “Hydraulic cylinder tie rod design CDT3 ... Z-3X.” https://www.boschrexroth.com/fi/fi/tuotteet/tuoteryhmaet/teollisuushydrauliikka/cylinders/tie-rod-cylinders/cd-single-rod-cylinder/cdt3-z-3x (accessed Mar. 20, 2020).

[48] X. Ding, J. Su, J. Lai, Q. Peng, and C. Zhou, “A Position Estimate Method for PMSM,” *Proc. - 2018 IEEE Int. Power Electron. Appl. Conf. Expo. PEAC 2018*, 2018, doi: 10.1109/PEAC.2018.8590442.

[49] A. Navatha, K. Bellad, S. S. Hiremath, and S. Karunanidhi, “Dynamic Analysis of Electro Hydrostatic Actuation System,” *Procedia Technol.*, vol. 25, no. Raerest, pp. 1289–1296, 2016, doi: 10.1016/j.protcy.2016.08.223.

[50] O. Erol, M. Aktaş, and Y. Altun, “Obtaining of PI Control Parameters for Vector Controlled PMSM,” *Int. Conf. Hydraul. Pneum. Tools, Seal. Elem. Fine Mech. Specif. Electron. Equip. Mechatronics– HERVEX 2017*, no. November 2017, pp. 233–237, 2017, [Online]. Available: http://www.fluidas.ro/hervex/proceedings2017/pp.233-237.pdf.

[51] R. G. Kanojiya, “Method for Speed Control of DC Motor,” *Int. Conf. Adv. Eng. Sci. Manag.*, pp. 117–122, 2012.

APPENDIX A: MANUFACTURER DATASHEET SPECIFICATIONS FOR COMPONENTS

APPENDIX A - I: *Component parameters selected from design specifications*

Component	Specifications
Electric motor (PMSM)	Model: Unimotor 115U2C Rated voltage: 400V Stall current: 5.9 A Rated torque: 8.1 Nm Rated speed: 3000 rpm Rated power: 2.54 kW Inertia: 9.0 $kgcm^2$ R (ph-ph): 2.02 Ω L (ph/ph): 13.27 mH
Hydraulic pump/motor 1	Model: Vivoil XV-2M/22 Displacement : 22.8 cm^3/rev Max inlet pressure: 240 bar Max speed: 3000 rpm Max power: 3.23 kW Max torque: 30.84 Nm
Hydraulic pump/motor 2	Model: Vivoil XV-2M/17 Displacement : 16.8 cm^3/rev Max inlet pressure: 270 bar Max speed: 3500 rpm Max power: 2.38 kW Max torque: 22.73 Nm
Cylinder	Model: MIRO C-10-60 Piston diameter: 60 mm Shaft diameter: 30 mm Stroke: 400 mm

APPENDIX B: SIMULATION MODELS IN AMESIM

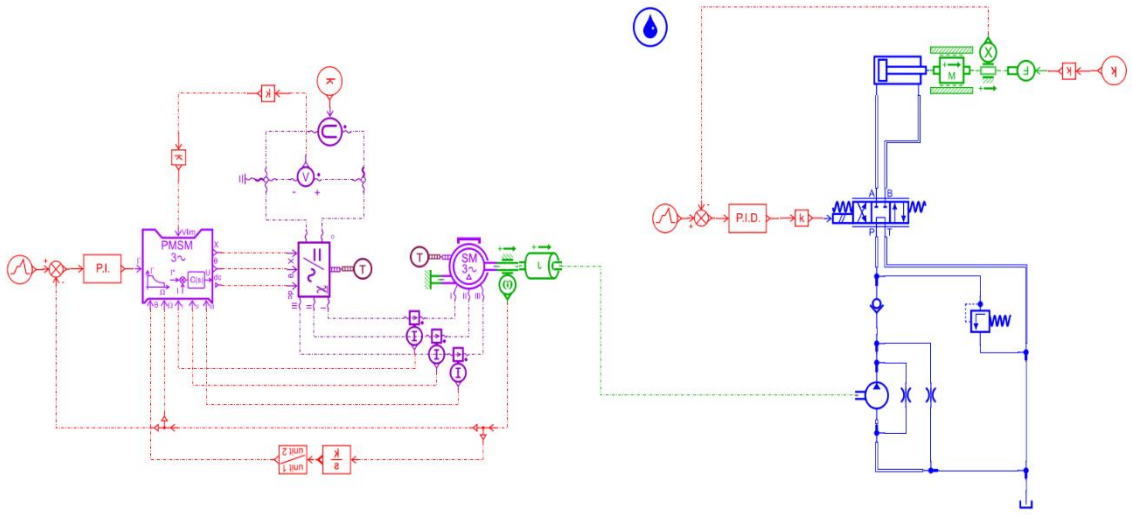

APPENDIX B - I: *AMESIM Simulation Model of Conventional Valve-Controlled Actuator System*

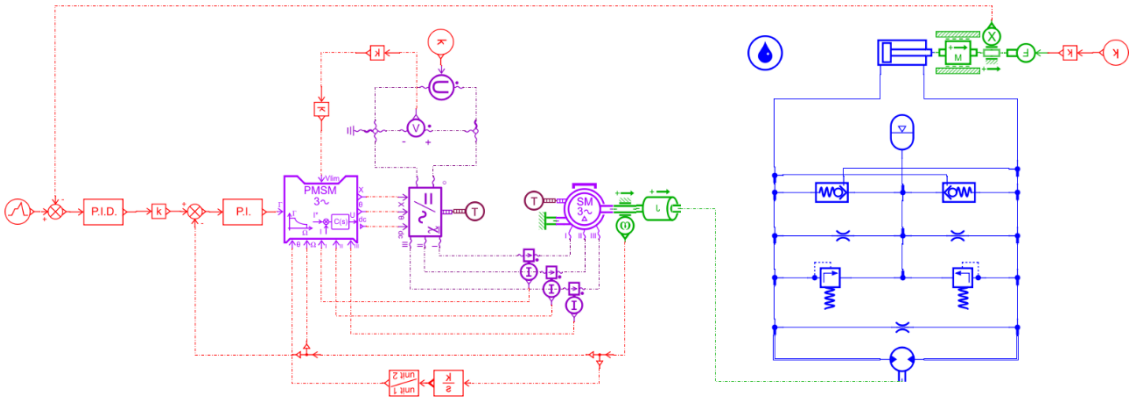

APPENDIX B - II: *AMESIM Simulation Model of Classic Electro-hydrostatic Actuator System*

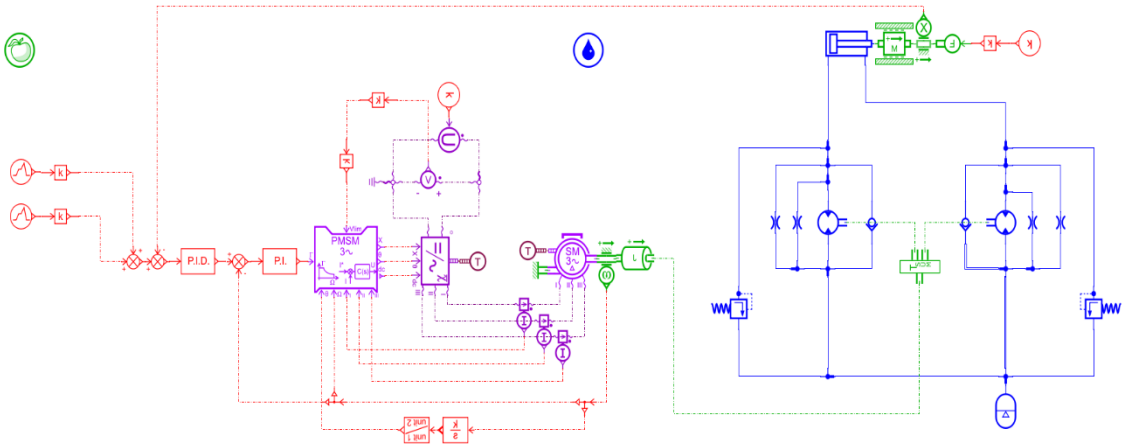

APPENDIX B - III: *AMESIM Simulation Model of Two-pump Electro-hydrostatic Actuator System*

APPENDIX C: MODEL PARAMETERS IN AMESIM

Name	Title	Value	Unit
p	pole pairs	**3**	
mFvisc	viscous friction on motor shaft	0.0002	Nm/(rad/s)
Phif	machine permanent magnet flux linkage	0.531	Wb
Rs	machine stator resistance	2.02	Ohm
Ls	machine stator cyclic inductance	0.013273	H
Lsd	machine stator cyclic inductance d	Ls*0.9	H
Lsq	machine stator cyclic inductance q	Ls*1.1	H
Taud	d axis PI time constant	0.01	s
Tauq	q axis PI time constant	0.01	s
Imax	Maximum rms current	5.9	A
w	angular velocity	3000	rev/min
Udc	DC load voltage	400	V
connectType	winding connection	**delta**	

APPENDIX C - I: *Electric Motor Model Parameters*

Title	Value	Unit	Tags	Name
ⓟ pressure at port 1	0	bar		p1
ⓟ pressure at port 2	0	bar		p2
index of hydraulic fluid	0			indexf
use initial displacement	yes			usedispl
#displacement of piston	0	m		xact0
piston diameter	**60**	mm		diamp
rod diameter	**30**	mm		diamr
length of stroke	**0.4**	m		stroke
dead volume at port 1 end	50	cm**3		dead1
dead volume at port 2 end	50	cm**3		dead2
viscous friction coefficient	**2000**	N/(m/s)		visc
leakage coefficient	**0.01**	L/min/bar		leak
spring rate at endstops	100000	N/mm		k
damping coefficient on endstops	100000	N/(m/s)		cdamp
deformation on endstops at which damping rate is f...	0.001	mm		distdef

APPENDIX C - II: *Hydraulic Cylinder Model Parameters*

Parameters of accumulator [HA001-1]

Title	Value	Unit	Tags	Name
# pressure at port 1	**5**	bar		pout
index of hydraulic fluid	0			indexf
isothermal initialization (0) or adi...	1			init
gas precharge pressure	**2**	bar		gaspc
accumulator volume	1	L		accvol
polytropic index	1.4	null		gamma

APPENDIX C - III: *Hydraulic Accumulator Model Parameters*

Parameters of hsv_3pos4port_03 [HSV34_03-1]

Title	Value	Unit	Tags	Name
valve rated current	40	mA		irate
▾ valve dynamics				
dynamics	**1st order**			spooldyn
# initial fractional spool po...	0	null		cx
valve time constant	**0.01**	s		tau
▾ pressure drop characteristic				
ports P to A characteristic fl...	**10**	L/min		qpa
ports P to A corresponding...	1	bar		ppa
ports P to A critical flow nu...	1000	null		lcpa
ports B to T characteristic fl...	**10**	L/min		qbt
ports B to T corresponding ...	1	bar		pbt
ports B to T critical flow nu...	1000	null		lcbt
ports P to B characteristic fl...	**10**	L/min		qpb
ports P to B corresponding ...	1	bar		ppb
ports P to B critical flow nu...	1000	null		lcpb
ports A to T characteristic fl...	**10**	L/min		qat
ports A to T corresponding...	1	bar		pat
ports A to T critical flow nu...	1000	null		lcat
ports P to T characteristic fl...	**10**	L/min		qpt
ports P to T corresponding ...	1	bar		ppt
ports P to T critical flow nu...	1000	null		lcpt
fluid properties for pressur...	at reference conditions			userfp

APPENDIX C - IV: *Proportional Valve Model Parameters*